

## ABSTRACT

Title of Document: PHOTOINDUCED ELECTRON TRANSFER  
IN IONIC MEDIA

Rebecca Cristine Vieira, Doctor of Philosophy,  
2008

Directed By: Dr. Daniel E. Falvey, Department of Chemistry  
and Biochemistry

The goal of this research was to explore the use of room temperature ionic liquids (RTILs) and ionic liquids crystals (ILCs) as reaction media for photoinduced electron transfer (PET) processes.

Photoinduced electron transfer in two room-temperature ionic liquids, 1-butyl-3-methylimidazolium hexafluorophosphate (BMIM-PF<sub>6</sub>) and 1-octyl-3-methylimidazolium hexafluorophosphate (OMIM-PF<sub>6</sub>) has been investigated using steady-state fluorescence quenching of 9,10-dicyanoanthracene (DCA) with a series of single electron donors. From these fluorescence quenching rates, reorganization energy values and  $k_{diff}$  values can be derived from a Rehm-Weller analysis. In many cases, these fluorescence quenching reactions occur at rates larger than what would be expected based on the Smoluchowski equation. In addition, reorganization energy values of 10.1 kcal/mol and 16.3 kcal/mol for BMIM-PF<sub>6</sub> and OMIM-PF<sub>6</sub>, respectively, have been determined.

The dynamics of electron transfer reactions in butyl pyridinium bis(trifluoromethanesulfonyl)imide (**3.1**) and other solvents have been explored using laser flash photolysis. In these experiments, benzophenone (BP), duroquinone (DQ), and 9-cyanoanthracene (9CA) were used as excited-state acceptors, 1,4-diazabicyclo[2.2.2]octane (DABCO) and hexamethylbenzene (HMB) were used as ground-state donors, and methyl viologen ( $MV^{2+}$ ) was used as a probe molecule. Analysis of kinetic and spectroscopic data from these experiments shows that electron transfer from photoreduced acceptors to the probe occurs via one or more solvent ions in cases where the acceptor anion radical has a reduction potential that is more negative than the solvent ions ( $BP^{\bullet-}$  and  $9CA^{\bullet-}$  in BuPyr-NTf<sub>2</sub>). Mediated electron transfer was demonstrated to significantly enhance quantum efficiencies of photoinduced electron transfer in cases where back electron transfer would otherwise predominate.

In addition to RTILs, a pyridinium and imidazolium ILC were used as reaction media in LFP experiments. In these experiments, BP and a pyrromethene dye were used as excited-state acceptors, DABCO and DMB were used as ground-state donors, and  $MV^{2+}$  was used as a probe molecule. In these experiments it was determined that the pyridinium ILC was able to mediate electron transfer with both BP and PM such that quantum efficiencies ( $\Phi$ ) using both acceptors are improved significantly. Additionally, a rate enhancement for PET is observed using the pyridinium ILC as opposed to the imidazolium ILC for the BP system.

PHOTOINDUCED ELECTRON TRANSFER IN IONIC MEDIA

By

Rebecca Cristine Vieira

Dissertation submitted to the Faculty of the Graduate School of the  
University of Maryland, College Park, in partial fulfillment  
of the requirements for the degree of  
Doctor of Philosophy  
2008

Advisory Committee:

Professor Daniel Falvey, Chair

Professor Jeff Davis

Professor Philip DeShong

Professor Steven Rokita

Professor Srinivasa Raghavan (Dean's Representative)

© Copyright by  
Rebecca Cristine Vieira  
2008

## Dedication

For Mom and Dad. Without you, none of this would have been possible.

## Acknowledgements

I would like to first and foremost thank my advisor, Dr. Daniel E. Falvey, for acting as my boss and mentor for the past five odd years. Thank you for trusting me with new project and allowing me to find my own way with it. I have become a more inquisitive, independent, thorough and thoughtful scientist thanks to your patient guidance.

I also owe a debt of gratitude to my dissertation committee. To Dr. Jeff Davis, for being an excellent teacher during my first year of graduate school, and for being a good “down the hall” boss. To Dr. Phil DeShong, for being a mentor, and providing me with other professional opportunities. To Dr. Steve Rokita, for being a kind and understanding boss during the time that I was his discussion TA, and for writing countless letters of recommendation. And to Dr. Srinivasa Raghavan, for acting as my Dean’s Rep and allowing me to use his rheometer (with the help of Aimee Ketner!)

During my graduate school years, I have been inordinately lucky to meet many people that have helped make the years more bearable. First to my groupmates, present and former, Drs. Chitra Sundararajan, Andrew Kung, Selina Thomas, Arthur Winter, Yu Tang, Hojae Choi, Wei-Hao Huang, Ms. Rebecca Pease, Mr. Brian Borak, Mr. Raffael Perrotta, Ms. Megan Pierson, and Mr. Giovanni Greaves. Shout out to Andy, Selina, Art, Rebecca(traitor!) and Brian, with whom I spend most of my lab time, I couldn’t have asked for any better people to work with on a daily basis. To my batchmates, particularly Showme, Regan and Lingy for starting with me in

August of 2003 and keeping me in check since then. To Will, for putting up with me, Monday or otherwise, and to the Davis group for adopting me as one of their own. To Dr. Susanna Lopez-Sola and Dr. Monica Melegari, for visiting and injecting their bright personalities into the mix. And to the countless others that I have met along the way, you are what have helped make my graduate career fun.

I would be remiss if I did not extend a word of thanks to the support staff of the UMD Chemistry Department. I would like to particularly thank Dr. Yu-Fai Lam and Dr. Yinde Wang for providing excellent NMR facilities and support.

And finally, to my family. My family has always been supportive of me in whatever path I have chosen for my life, even when that choice has kept me away from them for extended periods of time. Graduate school has been a wild ride, and it's almost over. Thank you for always being there.

# Table of Contents

Dedication.....	ii
Acknowledgements.....	iii
Table of Contents.....	v
List of Tables.....	vii
List of Figures.....	viii
List of Schemes.....	xi
Chapter 1: Introduction.....	1
1.1 Photoinduced Electron Transfer.....	1
1.2 Room Temperature Ionic Liquids.....	13
1.3 Ionic Liquid Crystals.....	21
Chapter 2: Photoinduced Electron Transfer in Two RTILS <sup>‡</sup> .....	25
<sup>‡</sup> Excerpts of this chapter have been previously published as Vieira, R.C.; Falvey, D.E. <i>J. Phys. Chem. B</i> , 2007, 111, 5023 – 5029.....	25
2.1 Introduction and Background.....	25
2.2 Results and Discussion.....	27
2.3 Conclusions.....	48
Chapter 3: Solvent-Mediated Photoinduced Electron Transfer in a Pyridinium Ionic Liquid <sup>‡</sup> .....	50
<sup>‡</sup> Excerpts from this chapter have previously been published as: Vieira, R.C.; Falvey, D.E. <i>J. Am. Chem. Soc.</i> , 2008, 130, 1552-1553.....	50
3.1 Introduction and Background.....	50
3.2 Results and Discussion.....	54
3.3 Conclusions.....	69
Chapter 4: A Continuation: Solvent-Mediated Photoinduced Electron Transfer in Ionic Liquid Crystals.....	71
4.1 Introduction and Background.....	71
4.2 Results and Discussion.....	75
4.3 Conclusions.....	91
Chapter 5: Conclusions.....	92
Chapter 6: Experimental.....	95
6.1 General Experimental Information.....	95
6.2 Lifetime Measurements.....	95
6.3 Viscosity Measurements.....	97
6.4 Fluorescence Quenching Experiments.....	97

6.5 General Procedures for Laser Flash Photolysis Experiments .....	98
6.6 Data Analysis .....	100
6.6.1 Methods used in Chapter 2 .....	100
6.6.2 Methods used in Chapter 3 .....	100
6.6.3 Methods used in Chapter 4 .....	103
6.6 Synthesis .....	105
Appendices.....	116
Bibliography .....	120

## List of Tables

<b>Table 2.1</b> Fluorescence lifetimes ( $\tau$ , ns) of 9,10-dicyanoanthracene ( <b>2.3</b> ) in the two RTILs, as well as viscosity measurements ( $\eta$ , Pa s, 25°C) for the corresponding RTIL.....	35
<b>Table 2.2:</b> Oxidation Potentials ( $E_{ox}$ , V) and $k_q$ ( $M^{-1} s^{-1}$ ) values for Fluorescence Quenching Experiments of DCA with Various Electron Donors in <b>2.1</b> and <b>2.2</b> measured at $20 \pm 1^\circ C$ .....	39
<b>Table 2.3</b> Electron Transfer Parameters Derived from Rehm-Weller Analysis of Fluorescence Quenching Data.....	46
<b>Table 3.1</b> Rate constants for PET Reactions.....	68
<b>Table 4.1</b> Rate Constants and Quantum Yields for reactions using <b>3.2</b> measured at $20 \pm 1^\circ C$ .....	84
<b>Table 4.2.</b> Rate Constants and Quantum Yields for all PET Reactions measured at $20 \pm 1^\circ C$ .....	89

## List of Figures

<b>Figure 1.1.</b> A graphical representation of classical Marcus theory of electron transfer.....	3
<b>Figure 1.2.</b> Model of Reorganization Energy. I depicts a loosely solvated neutral complex. Immediately after excitation the initial a loosely solvated, separated ion pair (II) is formed. Finally, III is the final closely solvated ion pair.....	5
<b>Figure 1.3:</b> A potential energy surface representations explaining Marcus theory.....	7
<b>Figure 1.4.</b> A graphical representation of the data obtained by Rehm and Weller. The black indicates the trend they observed, while the blue is the predicted (but not observed) Marcus Inverted region.....	10
<b>Figure 1.5.</b> Acceptor-Steroid-Donor System studied by Miller and Closs.....	11
<b>Figure 1.6.</b> Common cations and anions used in RTILs.....	15
<b>Figure 1.7</b> A representative of three of the potential mesophases of RTILs.....	22
<b>Figure 1.8</b> Examples of different ILCs.....	24
<b>Figure 2.1</b> The two RTILS used in these experiment 1-butyl-3-methyl-imidazolium hexafluorophosphate (BMIM-PF <sub>6</sub> , <b>2.1</b> ) and 1-octyl-3-methylimidazolium hexafluorophosphate (OMIM-PF <sub>6</sub> , <b>2.2</b> ) .....	32
<b>Figure 2.2</b> Absorption spectra of neat <b>2.1</b> (—) and neat <b>2.2</b> (--) in a 10 mm cuvette.....	32
<b>Figure 2.3</b> Stern Volmer Analysis of Fluorescence Quenching Data From Two Amine Donors in <b>2.1</b> . .....	38

<b>Figure 2.4</b> Stern Volmer Analysis of Fluorescence Quenching Data From Two Amine Donors in <b>2.2</b> .....	38
<b>Figure 2.5</b> Rehm-Weller Analysis of the experimental data with $\Delta G$ offset for <b>2.1</b> .....	45
<b>Figure 2.6</b> Rehm-Weller Analysis of the experimental data with $\Delta G$ offset for <b>2.2</b> .....	45
<b>Figure 3.1</b> Transient absorption spectra of <b>3.2/3.6/ 3.7<sup>2+</sup></b> in CH <sub>3</sub> CN.....	59
<b>Figure 3.2</b> Transient absorption spectra of <b>3.2/3.6/ 3.7<sup>2+</sup></b> in <b>3.1</b> with inset of waveform at 610 nm .....	60
<b>Figure 3.3</b> Transient absorption spectra of <b>3.3/3.6/ 3.7<sup>2+</sup></b> <b>3.1</b> with inset of waveform at 610 nm.....	60
<b>Figure 3.4</b> Waveforms at 540 nm depicting the quenching of <b>3.2<sup>-</sup></b> by <b>3.1</b> .....	61
<b>Figure 3.5</b> . Waveform at 610 nm of <b>3.2/3.6/3.7<sup>2+</sup></b> in MeCN with corresponding fit from Copasi.....	64
<b>Figure 3.6</b> . Waveform at 610 nm of <b>3.3/3.6/3.7<sup>2+</sup></b> in MeCN with corresponding fit from Copasi.....	65
<b>Figure 3.7</b> Waveform at 610 nm of <b>3.2/3.6/3.7<sup>2+</sup></b> in <b>3.1</b> with corresponding fit from Copasi.....	65
<b>Figure 3.8</b> . Waveform at 610 nm of <b>3.3/3.6/3.7<sup>2+</sup></b> in <b>3.1</b> with corresponding fit from Copasi.....	66
<b>Figure 3.9</b> . Waveform at 610 nm of <b>3.4/3.5/3.7<sup>2+</sup></b> in <b>3.1</b> with corresponding fit from Copasi.....	66

<b>Figure 3.10.</b> Waveform at 545 nm of <b>3.2/3.6/3.7<sup>2+</sup></b> in <b>2.2</b> with corresponding fit from Copasi.....	67
<b>Figure 4.1</b> Potential ILC mediated PET pathway.....	73
<b>Figure 4.2</b> Cartoon depiction of the S <sub>M</sub> A mesophase.....	74
<b>Figure 4.2.</b> Transient absorption spectra of <b>3.2/4.4/3.7<sup>2+</sup></b> in a <b>4.1</b> .....	80
<b>Figure 4.3.</b> Transient absorption spectra of <b>3.2/4.4/3.7<sup>2+</sup></b> in <b>4.2</b> .....	81
<b>Figure 4.4.</b> Selected waveforms from transient absorption spectra of <b>3.2/4.4/3.7<sup>2+</sup></b> in <b>4.1</b> .....	82
<b>Figure 4.5.</b> Selected waveforms transient absorption spectra of <b>3.2/4.4/3.7<sup>2+</sup></b> in <b>4.2</b> .....	82
<b>Figure 4.6.</b> Waveform at 610 nm ( <b>3.7<sup>2+</sup></b> ) in imidazolium ILC (●) and pyridinium ILC (●).....	86
<b>Figure 4.7.</b> Waveforms at 610 nm for <b>4.3/3.7<sup>2+</sup></b> in various solvents.....	91
<b>Figure 5.1</b> An RTIL (a.) and ILC (b.) acting as charge shuttles in a PET reaction...	93

## List of Schemes

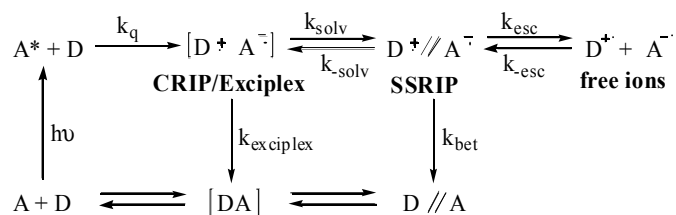
<b>Scheme 1.1.</b> Common pathways in photoinduced electron transfer (PET) in non-viscous solvents.....	1
<b>Scheme 1.2.</b> Fluorescence quenching.....	8
<b>Scheme 1.3.</b> Photoinduced Electron Transfer by Triplet Quenching.....	12
<b>Scheme 1.4.</b> Triplet Quenching via Donor Excitation Motif.....	12
<b>Scheme 1.5</b> Reaction of methyl p-nitrobenzenesulfonate with halides.....	20
<b>Scheme 2.1</b> General Reaction Scheme For Synthesis of Quaternary Nitrogen Based RTILS.....	28
<b>Scheme 2.2.</b> Final Optimized Reaction Conditions For Imidazolium Based RTILS (and other quaternary nitrogen comprising species.).....	30
<b>Scheme 3.1</b> The role of a conventional molecular solvent in PET.....	54
<b>Scheme 3.2</b> The potential role of an RTIL in PET.....	54
<b>Scheme 3.3</b> Triplet Mediated PET using Benzophenone as a Triplet Acceptor.....	56
<b>Scheme 3.4</b> Singlet Mediated PET using 9-Cyanonanthracene as a Singlet Acceptor.....	57
<b>Scheme 4.1</b> Synthesis of <b>4.1</b> .....	75
<b>Scheme 4.2</b> Synthesis of <b>4.2</b> .....	76

# Chapter 1: Introduction

## 1.1 Photoinduced Electron Transfer

One of the most basic reactions studied in organic chemistry is photoinduced charge or electron transfer (PET.) In PET, an electron rich donor (**D**) or an electron deficient acceptor (**A**) undergoes excited state electron transfer with another acceptor or donor. (Scheme 1.1) This generates the anion radical of the acceptor and the cation radical of the donor, which can result in the formation of a contact radical ion pair (CRIP), which is also known as an exciplex. Depending on other factors, such as interaction with the solvent, the ion pair can undergo solvation to become a solvent separated radical ion pair (SSRIP) or can directly undergo back electron transfer in the exciplex form. The SSRIP can then undergo back electron transfer, which will result in the ground-state acceptor and donor, or undergo the more desired process of undergoing solvent cage escape which generates the free radical ions in solution.

**Scheme 1.1.** Common pathways in photoinduced electron transfer (PET) in non-viscous solvents



There are many occasions when a high yield of free radical ions in solution is warranted. However, this is often impeded by the overall efficiency of back electron transfer. A high yield of free radical ions is especially desired for applications in biomimetic systems<sup>1</sup> and molecular electronic devices<sup>2,3</sup> where long lived charge separation is likely to improve the overall efficiency of the operation.

The free energy associated with PET can be described by the following equation:

$$\Delta G_{ct} = 23.06 \left( E_{ox}^D - E_{red}^A - \frac{q^2}{\epsilon r} \right) - E_{oo} \quad (1)$$

where is  $E_{ox}^D$  the oxidation potential of the donor,  $E_{red}^A$  is the reduction potential of the acceptor,  $q^2/\epsilon r$  is a coulombic interaction term, and  $E_{oo}$  is the excited state energy of the acceptor. The  $E_{oo}$  term can be approximated by the equation:

$$E_{oo} (kcal / mol) = \frac{28600}{\lambda_{oo}} \quad (2)$$

where  $\lambda_{oo}$  is the wavelength at which the excitation and emission spectra of the acceptor overlap.

The driving force dependence of PET can be predicted by Marcus theory which describes this dependence as a quadratic free energy relationship.<sup>4,5</sup> Instead of

the commonly observed linear free energy relationship (LFER), where the rate of reaction continues to increase as the driving force becomes more and more favorable, a quadratic free energy relationship predicts that the rate of a reaction will reach a maximum at a specific driving force, and then will decrease again at more favorable driving forces in a parabolic manner (Figure 1.2). Region I depicts the normal region where the rate of electron transfer increases commensurate to the increase in driving force. Region II describes the reorganization energy ( $\lambda$ ), the point at which the exothermicity reaches a maximum rate and is where  $\Delta G = \lambda$ . Region III is the inverted region, where the rate begins to decrease as a function of driving force.

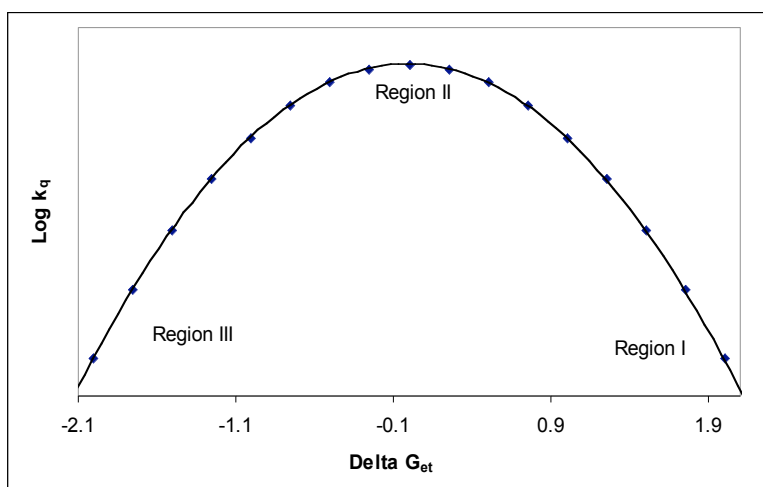


**Figure 1.1.** A graphical representation of classical Marcus theory of electron transfer.

Overall, classical Marcus theory holds that  $\Delta G_{et}^\ddagger$  is dependent on the driving force and the reorganization energy ( $\lambda$ ) with the following relationship:

$$\Delta G_{et}^\ddagger = \frac{\lambda}{4} \left( 1 + \frac{\Delta G_{et}}{\lambda} \right)^2 \quad (3)$$

Reorganization energy is a parameter that describes the ability of the solvent and the reactants to adapt as the reaction progresses.<sup>6,7</sup> In order for electron transfer to occur, both the solvent and the reactants must change their overall orientations. Total reorganization energy is comprised of both of these factors, and can be summarized by the following:

$$\lambda = \lambda_s + \lambda_i \quad (4)$$

Internal reorganization energy ( $\lambda_i$ ) involves the energy required to change bond lengths, orientations and geometries of the reactants. These are changes that must occur in order to conform to the new orientation reached during electron transfer. Solvent reorganization energy ( $\lambda_s$ , Figure 1.3) involves the energy needed for the solvent to orient around a charged radical ion pair from its original neutral state.  $\lambda_s$  is partially dependent upon solvent polarity. To this effect, it is known that  $\lambda_s$  values for polar solvents are relatively high, which would suggest that polar solvents undergo substantial changes to adjust to the newly generated charged state. On the other hand,  $\lambda_s$  values for non-polar solvents are low and would indicate that non-polar solvents do

not need to greatly realign to stabilize and accommodate the newly charged state generated during the reaction.

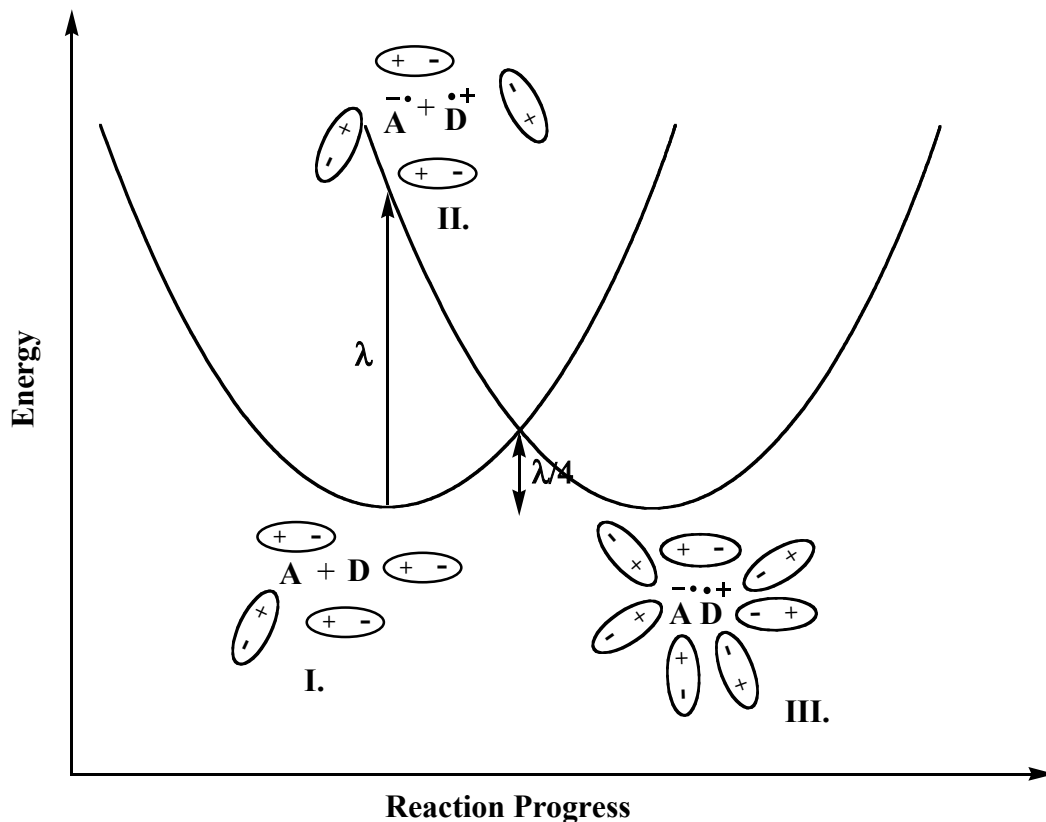


**Figure 1.2.** Model of Reorganization Energy. I depicts a loosely solvated neutral complex. Immediately after excitation the initial a loosely solvated, separated ion pair (II) is formed. Finally, III is the final closely solvated ion pair.

A theoretical model proposed by Marcus can potentially be used to predict values for  $\lambda_s$  (equation 6),

$$\lambda_s = \frac{(\Delta e)^2}{4\pi\epsilon_o} \left( \frac{1}{d_A} + \frac{1}{d_{D^+}} - \frac{1}{R_{AD^+}} \right) \left( \frac{1}{n^2} - \frac{1}{\epsilon} \right) \quad (4)$$

where  $\Delta e$  is electronic charge being transferred,  $\epsilon_0$  is the permittivity of free space,  $n$  and  $\epsilon$  are the solvent refractive index and dielectric constant respectively,  $d_A$  and  $d_{D^+}$  are the diameters for the reduced acceptor and the oxidized donor, and  $R_{A-D^+}$  is the center to center separation of the donor and acceptor.<sup>4</sup> This model can be only used with the following two assumptions; that a dielectric constant can be measured for solvent in question and that the donor-acceptor system being studied is spherical in nature. These are assumptions that can be made for some chemical systems but not all. Thus on occasion eq. 4 can provide a somewhat flawed interpretation of reorganization energy, as there are occasions when the reactants are not completely spherical in nature or when the dielectric constant of the solvent can not be measured. It is in these cases the eq. 4 provides an insufficient picture of solvent reorganization during PET, and thus is an experiment exploration of  $\lambda_s$  must be done.

The parabolic nature of Marcus theory can be understood from an explanation of Figure 1.3.

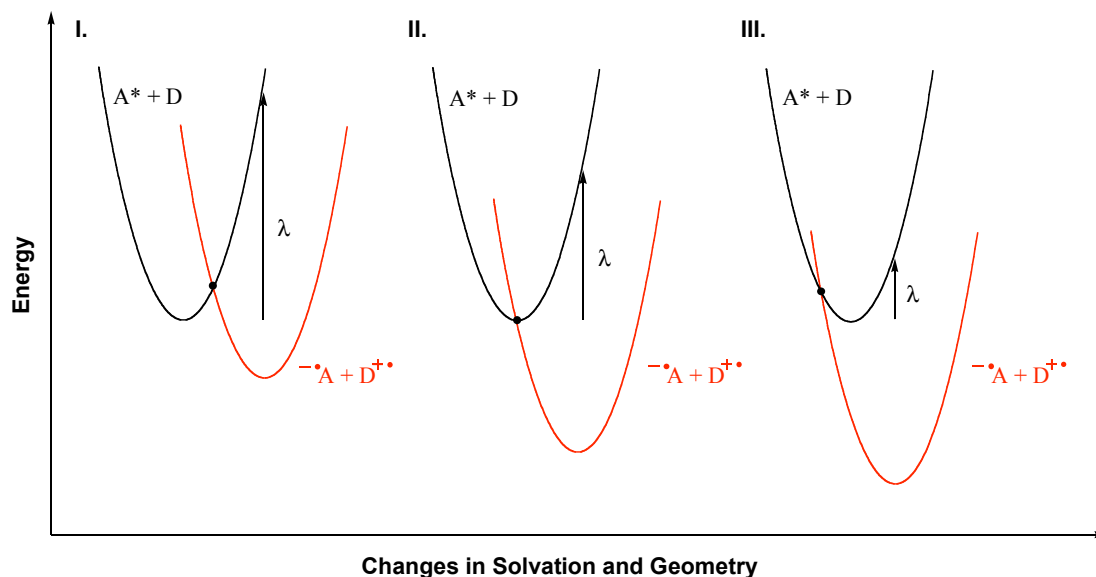
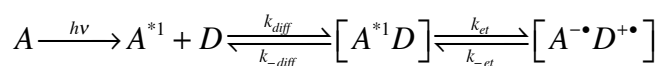


**Figure 1.3:** A potential energy surface representations explaining Marcus theory

Parabola I depicts an area where the reaction profiles cross in a place in which the  $\Delta G_{\text{et}}$  is less than the reorganization energy and  $\Delta G^\ddagger$  is greater than zero. As the exothermicity of the reaction increases, so too does the rate of the reaction, which will increase until  $\Delta G_{\text{et}}$  is roughly equivalent to the reorganization energy. This is depicted by parabola II and is the normal region. The Marcus inverted region, parabola III, is observed as the exergonicity of the reaction increases to greater levels, a rate decrease will be observed, and  $\Delta G_{\text{et}}$  is greater than the solvent reorganization energy. This counter-intuitive phenomenon is based on the fact that reactions which occur at higher driving forces have a considerable amount of energy that needs to be dissipated as driving force increases. This energy dissipation causes a rate decrease.

In 1970 Rehm and Weller probed fluorescence quenching in over 60 donor-acceptor pairs.<sup>8,9</sup> Fluorescence quenching is one example of PET. (This process in Scheme 1 would take one through to the step where the exciplex is formed, at the rate of  $k_q$ .) In the process of fluorescence quenching, **A** absorbs a photon, reaches its singlet excited state (**A\***) and then accepts an electron from **D**. Much like what is described above, **A\*** then collides with **D** at a rate of  $k_{diff}$  to form the encounter complex. (Scheme 1.2) This complex then undergoes the electron transfer process to form the successor complex. The successor complex can then undergo back electron transfer, ( $k_{bet}$ ) which converts the excited state complex into the individual ground state molecules, can undergo solvation to form free ions, or can undergo further chemistry to generate new products. Fluorescence quenching can also occur in an alternative scheme, where the donor is excited directly and then donates an electron to a ground state acceptor.

**Scheme 1.2.** Fluorescence quenching



There are two basic types of fluorescence quenching; static quenching and dynamic quenching. Static quenching implies that **A** and **D** are preassociated in solution before excitation of **A**, while dynamic quenching implies that **A** and **D** are not preassociated, and that after excitation, they must undergo diffusion to form an encounter complex. The rate of fluorescence quenching can be derived from Scheme

1.2 when the steady state approximation is applied to the encounter complex and the successor complex.

Therefore we find that

$$k_q = \frac{k_{diff}}{1 + \frac{k_{diff}k_{-diff}}{k_{et}k_{diff}}} \quad (5)$$

By substituting

$$K_{diff} = \frac{k_{diff}}{k_{-diff}} \quad (6)$$

and employing the Eyring equation (equation 7)

$$k_{et} = \wp k_{max} \exp\left(\frac{-\Delta G_{et}^\ddagger}{RT}\right) \quad (7)$$

where  $\wp$ , the transmission coefficient, is equal to 1 for adiabatic processes and  $k_{max}$  is the frequency factor, we find that  $k_q$  can be summarized as

$$k_q = \frac{k_{diff}}{1 + \frac{k_{diff}}{k_{max}K_{diff}} \exp\left(\frac{-\Delta G_{et}^\ddagger}{RT}\right)} \quad (8)$$

The free energy for the overall reaction can be predicted by the following equation:

$$\Delta G_{et}^\ddagger = \frac{\Delta G_{et}}{2} + \left[ \left( \frac{\Delta G_{et}}{2} \right)^2 + \left( \frac{\lambda}{4} \right)^2 \right]^{1/2} \quad (9)$$

Unfortunately, the Marcus inverted region was not observed in the bimolecular quenching studies performed by Rehm and Weller. Instead, what was observed was a relationship where the rate of the electron transfer reaches a plateau at high driving forces (Figure 1.4).

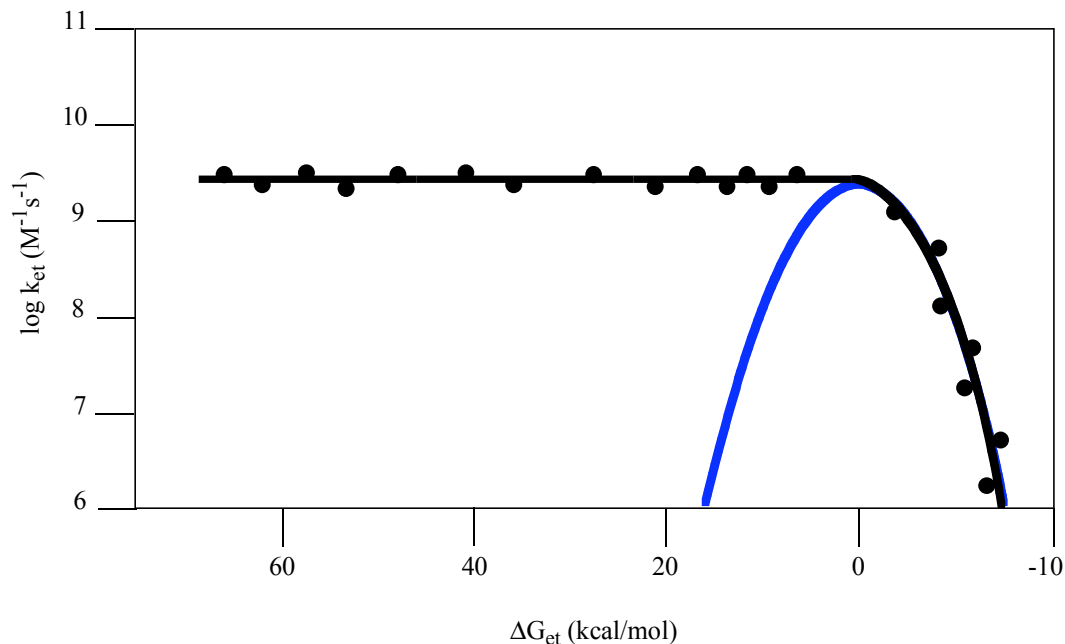


**Figure 1.4.** A graphical representation of the data obtained by Rehm and Weller. The black indicates the trend they observed, while the blue is the predicted (but not observed) Marcus Inverted region.

There are several arguments as to why a Marcus inverted region is not observed in forward bimolecular electron transfer. These include the argument that actual rates of electron transfer are much faster than the rates at which diffusion occurs.<sup>5</sup> Thus, for diffusion controlled reactions such as bimolecular electron transfer, it would be expected that a Marcus inverted region would not be observed.

The Marcus inverted region proved to be elusive until the work of Miller and Closs was reported twenty years after the initial publication of Marcus' theory.<sup>4</sup> In this work, electron transfer of a rigid linked system (Figure 1.5), comprised of various electron donors and a biphenyl acceptor separated by a steroid bridge was studied by pulse radiolysis.<sup>10</sup> Thus, no longer would the electron transfer reaction be ruled by diffusion kinetics, and a Marcus inverted region might be observed.

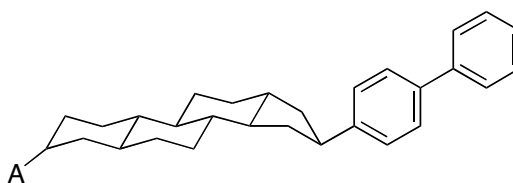


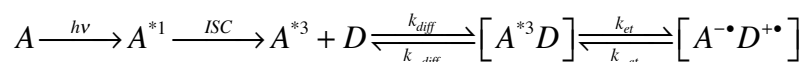
**Figure 1.5.** Acceptor-Steroid-Donor System studied by Miller and Closs

It was observed that rates for highly exergonic intramolecular electron transfers conformed to the Marcus inverted region. The Marcus inverted region was also observed when Gould and Farid studied the kinetics of bimolecular back electron transfer in several donor/acceptor pairs.<sup>11-13</sup>

Photoinduced electron transfer can also occur in a triplet motif. In contrast to fluorescence quenching in triplet PET, the acceptor (A) absorbs a photon of light, reaches its excited state and rapidly undergoes intersystem crossing. Intersystem crossing is a process in which a high energy singlet excited state is converted into a lower energy triplet excited state due to a spin flip of one of the unpaired orbital electrons of the excited state species. The newly generated triplet state then goes on to react with a ground state electron donor much in a similar fashion to what occurs

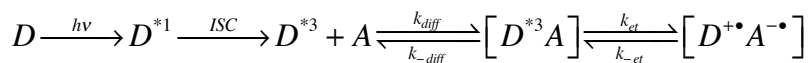
during fluorescence quenching. One of the advantages to studying PET in a triplet motif is that back electron transfer is a spin forbidden process. A spin forbidden process is one which occurs at a much slower rate than normal.

**Scheme 1.3.** Photoinduced Electron Transfer by Triplet Quenching



Additionally much like fluorescence quenching, triplet quenching or PET can occur through a mechanism wherein the donor is the chromophore. Thus the donor undergoes direct excitation to the excited singlet state and subsequently intersystem crossing to the triplet after which the photoexcited donor gives one of its electron to a electron deficient ground state acceptor.

**Scheme 1.4.** Triplet Quenching via Donor Excitation Motif



There are a multitude of methods to study, detect and quantify PET reactions. PET that occurs through a fluorescence quenching mechanism can be easily quantified by the use of a simple fluorimeter. One can observe the initial fluorescence of a sample of acceptor and then monitor how that fluorescence is attenuated as increasing amounts of donor is added to that solution. Monitoring PET that occurs via

a triplet regime is more difficult as it is difficult to detect phosphorescence through direct spectroscopic means.

One of the most common methods for the detection of triplet PET is laser flash photolysis (LFP.) LFP is an excellent technique to detect short-lived transient species such as those generated in PET experiments. A pulse from an excitation source (in our case a Nd:YAG laser) can generate the desired triplet state that can then proceed to do other chemistry, including PET. All the transient species (including the triplet) can be detected by a probe beam (UV-Vis xenon lamp,  $\lambda = 200\text{-}800\text{ nm}$ ) which monitors the generation of these new transients via a change in optical density as a function of time at a specific wavelength (known as a waveform.) This information can then be plotted as  $\Delta\text{OD}$  vs. wavelength to give what is known as a transient spectrum. Thus rates of PET can be determined by monitoring a variety of transient species. For example, in a sample containing an acceptor (A) and donor (D) one can monitor rates of PET by either the decay of  $A^{*3}$  or the growth of  $A^{\bullet}$  or  $D^{+\bullet}$ .

## **1.2 Room Temperature Ionic Liquids**

Room temperature ionic liquids (RTILs) have garnered much interest within the past five years due to their utility as “green” alternatives to conventional organic solvents. RTILs, which are similar to molten salts, are organic cations bonded electrostatically with weakly binding anions, and are generally based off of nitrogen containing heterocycles. While research in the field of RTILs has increased

exponentially in the past few years, much is still unknown about many of the properties of these interesting materials.

Ionic liquids were initially introduced to the world as “molten salts”. These were materials that contained both an inorganic cation and anion. Unlike contemporary RTILs, molten salts were not always liquid at room temperature. They were in fact generally in amalgam form and were “molten” above 100°C. The necessity of high temperature naturally limited their use in industrial applications.

The first true RTIL, reported in 1948, was comprised of a chloroaluminate anion and an ethyl pyridinium counter ion, and was used as a solution for electroplating aluminum.<sup>14</sup> In 1970s, the popularity of these chloroaluminate-based RTILs grew due to the work of the Osteryoung and Wilkes groups.<sup>15-17</sup> These chloroaluminate RTILs were employed for a multitude of uses, but mostly for electrochemical manipulation. Unfortunately, the chloroaluminate RTILs are highly reactive with air and moisture which limits their practical use. Thus if widescale use of RTILs was to be warranted, a combination of cations and anions were robust and water stable needed to be developed.

Most of the RTILs currently being investigated are based off of tetravalent nitrogen containing compounds (Figure 1.6). They can be synthesized readily following basic literature procedures from the corresponding chloride salts.<sup>18-21</sup> Thus, different series of RTILs can be generated through a simple counter-anion exchange.

This “plug and play” feature of RTILs suggests an easy of use and modification that is not commonly accessible with molecular solvents .

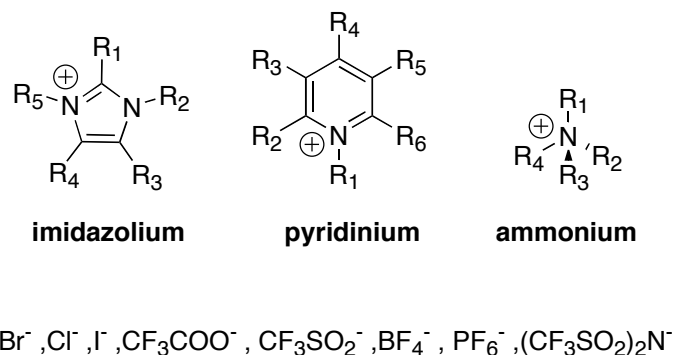


**Figure 1.6.** Common cations and anions used in RTILs

RTILs have several interesting and unique properties when compared to typical molecular solvents. One physical property that makes RTILs most attractive as “green” alternatives to conventional organic solvents is the fact that RTILs have a virtually immeasurable vapor pressure and low flammability. Their thermal stability is quite high and in most cases RTILs are reported to decompose at temperatures of 400 °C or higher.<sup>22</sup>

One of the most interesting characteristics of RTILs is their viscosity. The imidazolium RTIL series have reported viscosities of 450 cP (dried BMIM-PF<sub>6</sub>) and 585 cP (dried OMIM-PF<sub>6</sub>),<sup>23</sup> comparable to 0.3 cP for CH<sub>3</sub>CN. The high viscosities of RTILs have generally been attributed to increased van der Waals forces between the anionic and cationic component.<sup>24</sup> It had also been observed that the viscosities of

the several classes of RTILs is dependant on the strength of the hydrogen bond between the C<sub>2</sub> hydrogen and the counter anion.<sup>25</sup> Finally, symmetry and size of the counter anion can have an affect on viscosity as well, as a trend has been observed that viscosity decreases with the following order Cl<sup>-</sup> > PF<sub>6</sub><sup>-</sup> > BF<sub>4</sub><sup>-</sup> > NTf<sub>2</sub><sup>-</sup>.<sup>23,26,27</sup>

A result of these large viscosities is that the diffusion constant ( $k_{diff}$ ) for the RTILs is substantially smaller ( $\sim 10^7$  M<sup>-1</sup>s<sup>-1</sup>) that what is predicted for less viscous solvents such as CH<sub>3</sub>CN, MeOH and CH<sub>2</sub>Cl<sub>2</sub> ( $\sim 10^{10}$  M<sup>-1</sup>s<sup>-1</sup>). The diffusion constant ( $k_{diff}$ ) for a solvent can be calculated using the Smoluchowski-Stokes-Einstein equation (Equation 1), where R is the ideal gas constant (in J K<sup>-1</sup> mol<sup>-1</sup>), T is temperature (K), and  $\eta$  is viscosity in Pa s<sup>-1</sup>

$$k_{diff} (M^{-1}s^{-1}) = \frac{8000RT}{3\eta} \quad (10)$$

High viscosities and subsequently low diffusion constants for solvents can have consequences on rates and occasionally efficiencies of reactions. Remarkably, there have been many instances of reactions that traditionally are considered diffusion limited reactions occur at faster rates in RTILs than would be predicted by their estimated  $k_{diff}$ .<sup>28-32</sup> These phenomena will be discussed in further detail in Chapter 2.

Relative polarities of various RTILs have been quantified by a several methods. The first experiment that investigated polarities of RTILs using solvatochromic dyes was performed by Carmichael et al.<sup>33</sup> These experiments used

the imidazolium class of RTILs with a neutral probe molecule, the fluorescent dye, Nile Red. Through these solvatochromic studies it was determined that the imidazolium RTILs had polarities that were similar to short chain alcohols. Studies done in RTILs by Gordon et al using solvatochromic probes have show that BMIM-PF<sub>6</sub> has a polarity similar to methanol and acetonitrile in the E<sub>T</sub> scale.<sup>34</sup> EPR studies which compare the isotropic hyperfine EPR coupling constants of <sup>14</sup>N in nitroxide radicals (considered to be the a<sub>N</sub> scale) in organic solvents and RTILs, have also confirmed that the polarity of several RTILs in the a<sub>N</sub> scale are between that of acetonitrile and methanol.<sup>35</sup>

Most of the quantification of RTIL polarities have been performed by photochemical and solvatochromic measurements. These types of studies provide a basis from which the polarity of each of the RTILs can be approximated. However, as when considering polarities of molecular solvents, one must regard the values critically. Polarities can be used as a rule of thumb but not as an absolute when evaluating properties that are often related to polarity such as solubility and solvent reorganization energy.

Solvatochromic studies have been employed in the study of polarity of RTIL solvents as well as solvation dynamics. While polarity is considered a property that remains static and is generally attributed to the bulk solvent, solvation dynamics is an investigation of how the microscopic dynamics of the solvent can change during the course of a reaction. Recently Samanta et al and Maroncelli et al. explored solvation

dynamics of several imidazolium RTILs using a series of time-resolved fluorescence experiments with neutral donor-acceptor dye molecules.<sup>36-40</sup> Time resolved fluorescence measurements are appropriate in the study of solvation dynamics as the changes in the fluorescence spectra of the dyes are a direct result of relaxation of the fluorescence of the dye which is solvent induced. What was observed in these experiments was that the rotational times of the probe molecules occurred at slower times in RTILs than in polar molecular solvents, presumably due to the fact that RTILs have a much higher viscosity than conventional molecular solvents. In addition to this observation Samanta and Maroncelli observed biphasic dynamics that occurred at a picosecond and nanosecond time scale. The Samanta and the Maroncelli studies have two different explanations for this phenomena. Samanta believes that the picosecond motion is due to dye solvation by the anions of the RTILs, while the nanosecond motion can be attributed to the dual motion of anions and cations.<sup>36-38</sup> Maroncelli believes that both components are due to translational movement of both the cations and anions of the solvent as they work to solvate the dye molecules.<sup>39,40</sup>

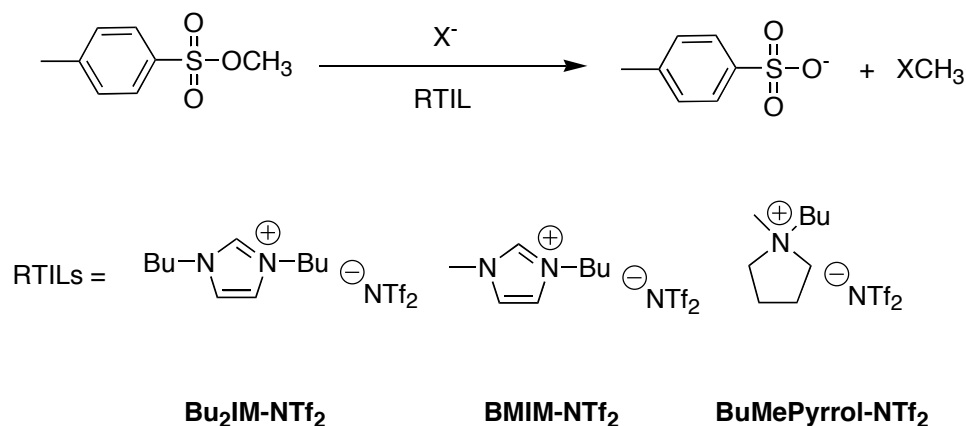
Maroncelli extended his work to a series of non-imidazolium RTILs and found that the picosecond solvation component that had been observed in imidazolium series was no longer manifesting itself when the same experiments were performed with other non-imidazolium RTILs.<sup>40,41</sup> This phenomena was attributed to the fact that the imidazolium cation can have “small-amplitude” movement as it comes in contact with the dye molecules. Additionally, Maroncelli proposed that the

solvation of the dye is dependant on the slowest moving component of the solvent, which in these cases is the bulky organic cation.

Since their growing rise in popularity, there have been a vast number of applications for which RTILs have been employed. RTILs have found great favor as solvents for organic and inorganic synthesis.<sup>42-46</sup> In many cases, RTILs are ideal solvents because they can be cleaned of any additional organic substrate and recycled as a solvent in a subsequent reaction. Many RTILs are immiscible in non-polar solvents such as diethyl ether and hexanes. These conventional organic solvents can therefore be used to extract any remaining organic impurities, which might result from unreacted starting material or unwanted side reactions, cleaning the RTIL for subsequent use. Additionally, to remain completely “green”, supercritical CO<sub>2</sub> can be utilized in place of volatile organic solvents as the method of extraction.

In addition to the fact that RTILs are easily recycled, they are also attractive alternatives to conventional organic solvents in organic synthesis due to their innate charged nature. This feature can be exploited to stabilize a vast number of reactive intermediates that form during chemical reactions. For instance, the nucleophilicity of Cl<sup>-</sup>, Br<sup>-</sup> and I<sup>-</sup> in a S<sub>N</sub>2 reaction with methyl p-nitrobenzenesulfonate in a series of RTILs has recently been investigated.<sup>47</sup>

**Scheme 1.5** Reaction of methyl p-nitrobenzenesulfonate with halides.



In aprotic polar solvents, nucleophilicity is known to adopt the trend Cl<sup>-</sup>, Br<sup>-</sup>, I<sup>-</sup> and while in protic solvents, it is known that the nucleophilicity of halides is I<sup>-</sup>, Br<sup>-</sup> and Cl<sup>-</sup> (due to deactivation of the smaller nucleophiles due to solvation by the protic solvent.) In the BuMePyrrol-NTf<sub>2</sub>, a trend in nucleophilicity similar to aprotic solvents and gas phase calculations is observed, while in BMIM-NTf<sub>2</sub>, the protic solvent nucleophilicity trend is observed. Finally, in Bu<sub>2</sub>IM-NTf<sub>2</sub>, the trend in nucleophilicity is observed to be Cl<sup>-</sup>, I<sup>-</sup> and Br<sup>-</sup>. These data would indicate that while the pyrrolidinium RTIL interacts with each halide ion equally, the BMIM and Bu<sub>2</sub>IM RTILs have specific interactions with the halide ions. In addition to nucleophilicity, studies that investigate competing S<sub>N</sub>1 and S<sub>N</sub>2 pathways<sup>48</sup> as well as studies that explore electrophilic addition reactions and Diels-Alder reactions have also been performed.<sup>49</sup>

In addition to their use in synthetic applications, RTILs have found a place in analytical chemistry applications. Rogers et al reported the first use of an RTIL in separations chemistry in 1998. In this case, they used an RTIL as part of a biphasic liquid system to extract  $^{14}\text{C}$  labeled aromatic amines and other substituted benzene compounds in an imidazolium/water biphasic system.<sup>50</sup> More recently, there have been accounts of task specific RTILs that can be used for heavy metal ion extraction from water.<sup>51</sup> In gas chromatography applications, triflate-imidazolium RTILs have been used as stationary phases and affect a efficient separations with great tolerance for high column temperatures (i.e. stationary phase will not decompose below 260 °C.)<sup>52,53</sup> RTIL stationary phases have been found particularly useful with the separations of alkanes and isomeric compounds of alcohols, aromatics, and polychlorinated biphenyls (PCBs).<sup>53</sup> Finally, RTILs have become attractive in electrochemistry as well. RTILs have wide electrochemical windows and high conductivities and have been used in series of basic electrochemical investigations.<sup>54</sup>

### **1.3 Ionic Liquid Crystals**

Liquid crystals (LCs) are a unique and interesting class of compounds whose physical properties are considered to be between those of the solid and liquid phase. Most liquid crystals contain a neutral mesogen, which is the structural motif that that induces crystalline order and phase behavior. Ionic liquid crystals (ILCs) are unique from LCs due to the fact that the central mesogen is charged.<sup>55</sup> This charged nature, much like that of RTILs, dictates that ionic liquid crystals have unique physical properties from their neutral counterparts. However, unlike their RTIL cousins, the

literature documentation of ILCs is extremely limited. (60 articles that contain the term “ionic liquid crystals” in Scifinder as of later 2008.)

ILCs display a multitude of mesophases. A mesophase is the liquid crystalline phase that is determined by positional, orientational, short range and long range order of the ILC molecules in assembly.

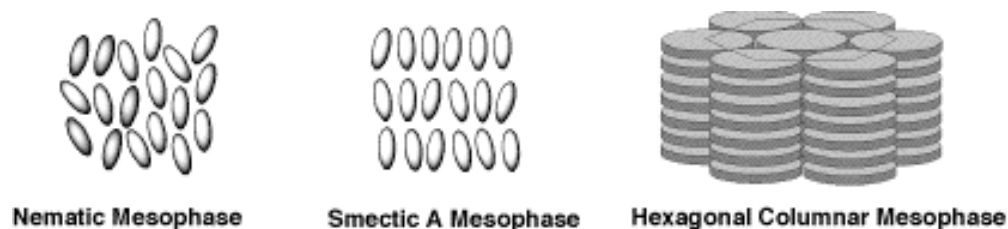


**Figure 1.7** A representative of three of the potential mesophases of RTILs.

There are several distinct types of mesophases that can be adopted by an ILC which are made up of molecules that are either rod-like (calamitic) or disc-like (discotic) in nature.<sup>55</sup> For calamitic ILCS, the least common mesophase, and most disordered is the nematic phase (Figure 1.7). The nematic phase has short-range one dimensional orientational order but lacks the long range positional that makes up the more sophisticated mesophases. The Smectic phases have order that is oriented in layers. The smectic A (SmA) phase (Figure 1.7) is the least ordered of the smectic phases, and is arranged in long one-dimensional layers. However, there is generally no level of organization between layers. The Smectic B phase is a more highly ordered mesophase that has interlayer orientation, but has small losses in translational order within a few bond distances.

Discotic ILCs can also adopt several mesophases. The least ordered discotic phase is the nematic discotic phase. Here, much like the calamitic nematic phase, each molecule adopts a different orientation in space. In the columnar nematic phase, the disc-like molecules form several columns of molecules that have no long-term orientation to one another. The hexagonal columnar phase (Figure 1.7) is the most ordered of all the mesophases. In this mesophase columns of the disc-like molecules are stacked together in a hexagonal motif that has both a large degree of long range order.

ILCS have been based off of several ionic motifs. There are examples of ammonium, imidazolium, viologen, pyrylium ILCs in the literature.<sup>55</sup> Additionally there ILCs that incorporate a metal center as part of their mesogen.

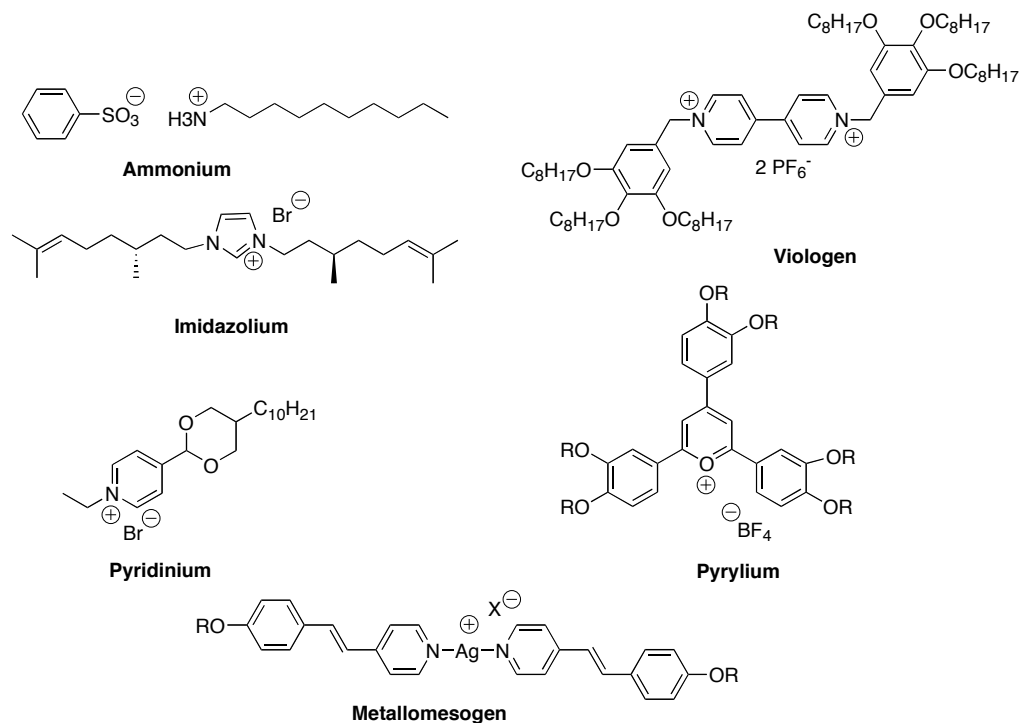


**Figure 1.8** Examples of different ILCs

ILCs have found to be applicable in a few arenas. ILCs have proven excellent materials as materials for ion conduction due to their structural organization and ionic nature. Kato et al performed extensive work on this subject<sup>56-60</sup> and have shown that an hexagonal columnar imidazolium ILC displays good ionic conductivity parallel to the columnar axis. ILCs have also been used as ordered reaction media, although to date only a few studies on this subject exist. Specifically, Lin et al. observed that a liquid crystalline imidazolium RTIL could affect the stereoselectivity of a Diels Alder reaction between cyclopentadiene and diethylmalonate. In this case, the exo product was preferred over the endo product with a 54:46 percent ratio<sup>61</sup>, whereas this same reaction carried out in ethanol gave an exo/endo ratio of 12:88, indicating that the LC mesophase had a strong influence on the selectivity of the reaction.

## Chapter 2: Photoinduced Electron Transfer in Two RTILS<sup>‡</sup>.

<sup>‡</sup>Excerpts of this chapter have been previously published as Vieira, R.C.; Falvey, D.E. *J. Phys. Chem. B*, **2007**, *111*, 5023 – 5029

### 2.1 Introduction and Background

Room temperature ionic liquids (RTILs) have garnered much interest within the past five years due to their utility as “green” alternatives to conventional organic solvents. There have been several examples which demonstrate the effectiveness of RTILs as solvents for various synthetic reactions.<sup>42-46,62</sup> It would be ideal if synthetic chemists could choose RTILs that best suit a given reaction. Due to the charged nature of the RTILs, it is widely believed that they can be used as reaction media to stabilize charged intermediates that are generated in various organic reactions. However, currently, the application of various RTILs to synthetic procedures is determined largely by empirical, rather than fundamental considerations. There is a need for more quantitative and systematic information on how RTILs influence the rates of fast reactions, particularly those that result in the formation of charged species.

One of the most elementary reactions in organic chemistry is photoinduced electron transfer (PET) which generates a radical cation and radical anion species from two neutral species. PET reactions in molecular solvents, such as CH<sub>3</sub>CN and CH<sub>3</sub>OH have been extensively documented.<sup>4,5,9-11,13,63</sup> There have been several studies

of electron transfer reactions in RTILs.<sup>21,30-32,64-67</sup>, very few of these examples involve PET reactions.<sup>66,67</sup> Using BMIM-PF<sub>6</sub> (2.1) as a solvent, Pandey et al. observed that when several polycyclic aromatic hydrocarbons and nitromethane were used in a fluorescence quenching study efficiencies of fluorescence quenching were decreased when 1-butyl-3-methylimidazolium hexafluorophosphate (BMIM-PF<sub>6</sub>, **2.1**) was used as a solvent rather than CH<sub>3</sub>CN.<sup>66</sup> McLean et al. observed using laser flash photolysis that fluorescence quenching between Ru(bpy)<sub>3</sub><sup>2+</sup> and methyl viologen in BMIM-PF<sub>6</sub> (**2.1**) occurred rate that was estimated by the diffusion limit of the solvent, while the generation of cage escape radical ions was higher than expected.<sup>68</sup> Roth et al. studied the differences in environment when using BMIM-PF<sub>6</sub> (**2.1**) and zeolite Y as media for PET reactions and found that both the zeolite and RTIL environment fostered the generation of long lived charged intermediates.<sup>69</sup>

Despite the fact that Roth et al above describes how the RTIL environment affects the rate of reaction, this instance is by no means representative of every case. To this point, it is not widely known how rates of bimolecular PET will be affected by the solution environment provided by the RTILs. In general, rates of bimolecular PET reactions with favorable  $\Delta G_{et}$  values occur at higher rates than ground-state electron transfer reactions with unfavorable  $\Delta G_{et}$  values. It is well known that while rates of most PET reactions are governed by the relationship proposed by Marcus,<sup>4,5,63</sup> however, the rates of bimolecular PET follow Rehm-Weller behavior.<sup>8,9</sup>

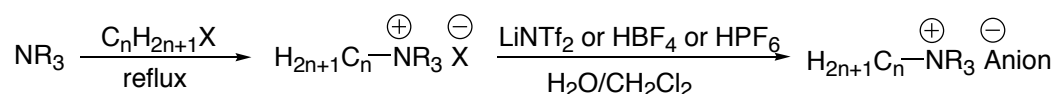
Herein we described a series of fluorescence quenching experiments to designed to determine  $k_q$ ,  $k_{diff}$  and reorganization energy ( $\lambda$ ) for the PET reactions occurring in the RTILs 1-butyl-3-methylimidazolium hexafluorophosphate (BMIM-PF<sub>6</sub>, **2.1**) and 1-octyl-3-methylimidazolium hexafluorophosphate (OMIM-PF<sub>6</sub>, **2.2**). It was found that fluorescence quenching rates for the PET reactions that were most exergonic proceed with rate constants ca. 100-fold larger than what is predicted by the Smoluchowski-Stokes-Einstein equation and that from the fitting parameters, all the reactions studied were more exergonic than initially predicted by equation 1. It was also found that the experimentally determined values for  $\lambda$  were lower than expected when compared to molecular solvents of similar polarities. Using  $\eta$  values previously reported,<sup>23</sup>  $k_{diff}$  values of  $1.47 \times 10^7 \text{ M}^{-1}\text{s}^{-1}$  and  $1.14 \times 10^7 \text{ M}^{-1}\text{s}^{-1}$  are predicted for **2.1** and **2.2** respectively. Despite their high viscosities and predicted  $k_{diff}$ , several accounts of reactions which occur at a rate higher than the diffusion limit of the solvent in RTILs have been reported.<sup>29,30,70,71</sup> This is an interesting feature of the solvent type and merits further exploration. (It has also been reported that that oxygen has low solubility in RTILs.<sup>67</sup>) However, due to the fact that general behaviors of RTILs are not widely known, it is necessary to study a series of reactions to characterize the properties of each RTIL.

## 2.2 Results and Discussion

RTILs can be purchased from conventional sources such as Sigma-Aldrich and Merck but at a great cost and of questionable purity. Alternatively, most RTILs can be obtained synthetically from relatively inexpensive starting materials and via two

step synthetic routes. The first of these is a S<sub>N</sub>2 reaction employing the desired tertiary amine and an alkyl halide, while the second a simple anion metathesis reaction performed under aqueous conditions.

**Scheme 2.1** General Reaction Scheme For Synthesis of Quaternary Nitrogen Based RTILS



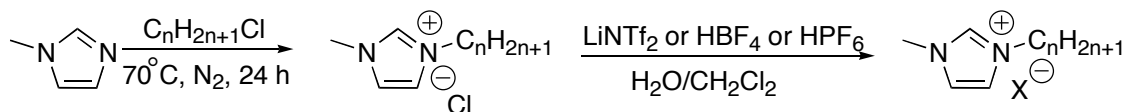
Our first concern in the use of RTILs as solvents for photochemistry was to ensure that the RTILs were as free from impurities and as “spectroscopically pure” (i.e. absorbing no light greater than 300 nm.) While these two prerequisites do not initially seem daunting, achieving either is not a trivial undertaking. Impurities that are generated during the formation of the initial halide-imidazolium salt cause strong discoloration of the RTIL. These impurities can cause the RTIL to adopt a light yellow to a deep orange tone which is unacceptable in a solvent that will be used for photochemical applications. These impurities, which are most likely caused by halide oxidation<sup>72</sup>, are undetectable by all conventional spectroscopic methods, including NMR.

As RTILs are difficult to purify after synthesis due to the fact that unlike conventional molecular solvents they are nearly to impossible to distill. Thus, it is imperative that any impurities generated during initial synthetic steps be removed during the aqueous reaction workup or never generated during synthesis altogether.

During our initial attempt at synthesis of imidazolium RTILs, we found that literature procedures were deceptively simple. Following literature procedures directly yielded highly colored, highly viscous halide salts that were never employed in the subsequent anion metathesis reaction. After this, we knew that in order for the imidazolium RTILs to be used in photochemical reactions, the literature procedure would have to be optimized to achieve our goal of “colorless” and impurity free RTILs.

Several attempts later, we discovered an optimized set of conditions that afforded “colorless” and impurity free RTILs in reasonable yields and reaction times. These conditions apply mainly to the first step of the reaction and are as follows. First, all starting material must be rigorously purified via known methods i.e. vacuum distillation (in the case of the amine component) or extraction (in the case of the alkyl halide component.) Secondly and most importantly, reaction temperatures of no higher than 70°C must be employed. Finally, it is suggested that the reaction be performed under inert (N<sub>2</sub>) conditions. Following the conditions described we were able to generate spectroscopically transparent imidazolium RTILs and were also able to apply these conditions to RTILs incorporating alternative tertiary amine cores (i.e. pyridinium.)

**Scheme 2.2.** Final Optimized Reaction Conditions For Imidazolium Based RTILS (and other quaternary nitrogen comprising species.)



At the time this research was performed there was a dearth of literature that encompassed obtaining RTILs that were spectroscopically pure. Samanta et al observed that a sample of neat **2.1** had prominent UV absorption above 300 nm that tailed into the 400 nm region.<sup>73,74</sup> In addition to this UV absorption, it was also observed that the same sample had a marked fluorescence spectrum at an excitation wavelength of 280, 300, 320, 340, 360, 370, 380, 400, and 420 nm. The fluorescence was attributed to energetically unique species of imidazolium ion in the bulk RTIL.<sup>73</sup> These results were in direct contradiction to what we were able to observe. As evidence from Figure 1.1, the synthetic procedure detailed in this chapter afforded us two imidazolium RTILS (one, BMIM-PF<sub>6</sub> as studied by Samanta) that did not absorb above 300 nm. Additionally when neat RTILs were studied by fluorescence using an excitation wavelength of 420 nm (which we subsequently used in the fluorescence quenching experiments) the signal observed was indistinguishable from fluorescence observed with air. Thus we were confident that the RTILs we produced were spectroscopically pure.

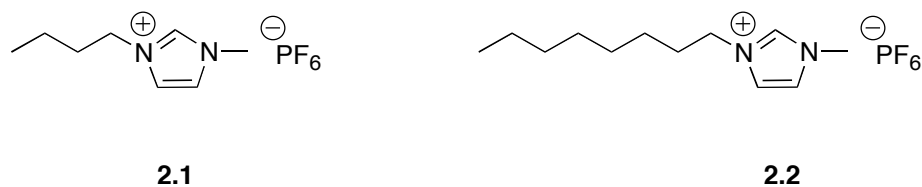


**Figure 2.1** The two RTILS used in these experiment 1-butyl-3-methyl-imidazolium hexafluorophosphate (BMIM-PF<sub>6</sub>, **2.1**) and 1-octyl-3-methylimidazolium hexafluorophosphate (OMIM-PF<sub>6</sub>, **2.2**)

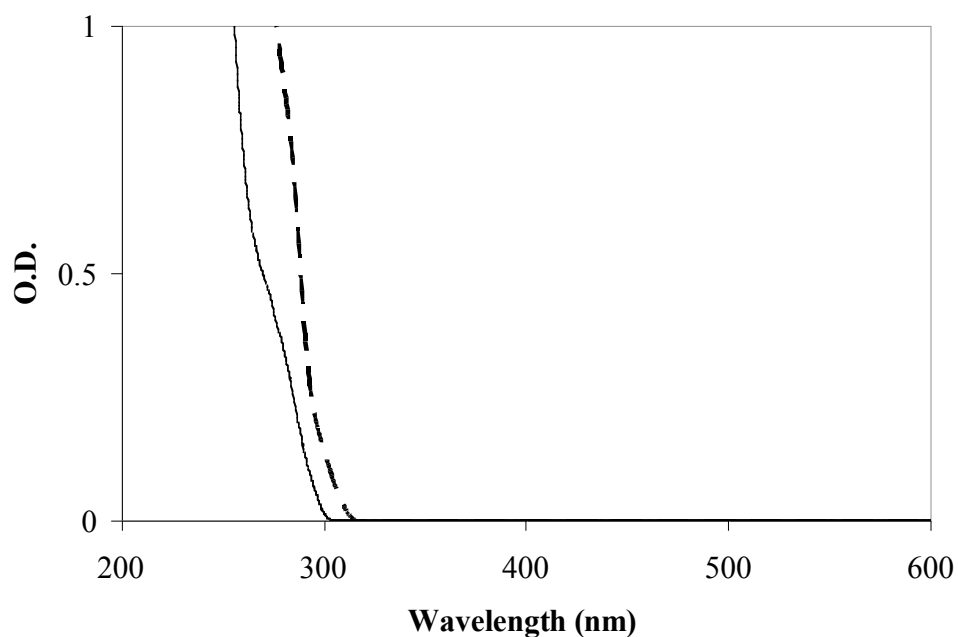


**Figure 2.2** Absorption spectra of neat **2.1** (—) and neat **2.2** (--) in a 10 mm cuvette

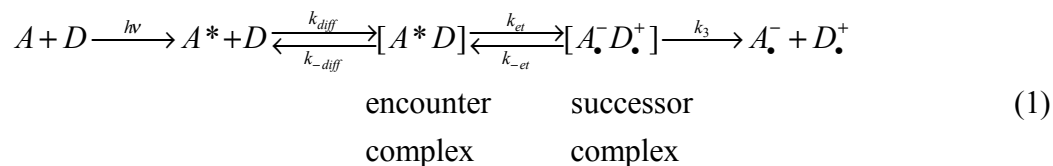
In addition to coloration, impurities in RTILs also cause changes to viscosity of the liquid.<sup>72</sup> This is particularly evident in ionic liquids that no longer possess a halide counter ion (i.e. **2.1**) but still contain small amounts of halide ions (i.e. Cl<sup>-</sup>) due to

lack of complete halide ion removal after a aqueous work up procedure following anion metathesis. It was observed that when increasing quantities of  $\text{Cl}^-$  was added to a sample of BMIM- $\text{BF}_4$  the viscosity increased from 66.5 mPa s to 92.4 mPa s.<sup>72</sup> We used a silver nitrate test to asses contamination of non-chloride containing RTILs with chloride impurities. In all cases the chloride ion concentration was found to be below the 10 ppm limit of detection determined for this test.  $^{31}\text{P}$  NMR experiments were carried out to assay for any phosphate ion impurities. Only  $\text{PF}_6^-$  (-143.6 ppm, septet) could be detected. Any other phosphate species were below the limit of detection.

The RTILs employed in this study have been previously shown to absorb atmospheric moisture.<sup>72,75,76</sup> This can be significant because even small amounts of water (~1%) can have a measurable effect on the viscosity ( $\eta$ ) of the RTILs, as well as the solvation dynamics in RTILs.<sup>77</sup> In principle, employing rigorous dry-box techniques could avoid this problem. However, we reasoned that more meaningful results could be obtained under conditions where the RTILs are likely to be used in applications, i.e. where water absorption is minimized but not eliminated through storing the solvent under vacuum and carrying out measurements under a positive pressure of  $\text{N}_2$ . Under these conditions we obtain the viscosities shown in Table 2.1 (Although there has been some conflict in the reporting of the viscosity of **2.1**, the viscosities measured for the **2.1** and **2.2**, measured at 25°C, fall within the range of the values reported.<sup>23,72,76,78</sup>) To ensure reproducible results the fluorescence measurement were carried out using solutions that fell into the range of viscosities

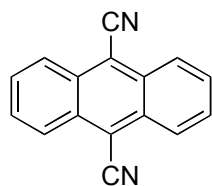
reported. In a few cases batches of the RTILs became cloudy and evolved an acrid gas. We assume that the latter is HF which results from the hydrolysis of the PF<sub>6</sub> anion. In any case, these samples were discarded and not used in the experiments.

Armed with spectroscopically pure RTILs, we were then able to begin the fluorescence quenching experiments. The process of fluorescence quenching can proceed through multiple pathways that lead to the generation of several different species and photoproducts. One of the most common pathways for fluorescence quenching is the process of electron or charge transfer. If one considers the excited state molecule to be *A* and the quencher to be *D*, fluorescence quenching through electron transfer is as follows:

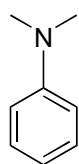


Steady state fluorescence quenching of 9,10-dicyanoanthracene (DCA, **2.3**) using a series of single electron donors (**2.4-2.23**), having higher singlet energies than **2.3**, a good range of oxidation potentials, and a lower wavelength absorption (such that the donors would not absorb light higher than 400 nm) was performed using the final purified, dried, and colorless RTILs as a solvent.

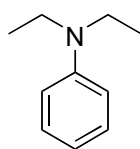
**CHART 2.1** : 9,10-Dicyanoanthracene (**2.3**) and Various Electron Donors Used in the Fluorescence Quenching Experiments



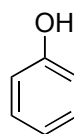
**2.3**



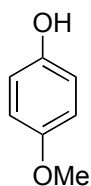
**2.4**



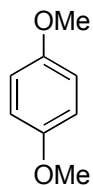
**2.5**



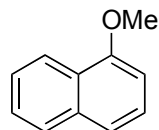
**2.6**



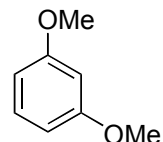
**2.7**



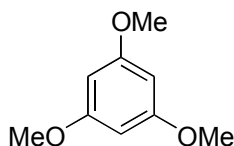
**2.8**



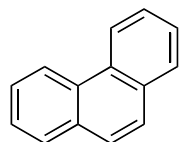
**2.9**



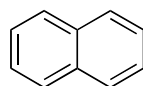
**2.10**



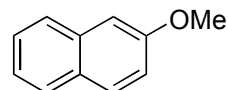
**2.11**



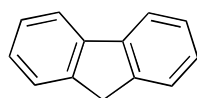
**2.12**



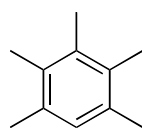
**2.13**



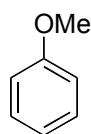
**2.14**



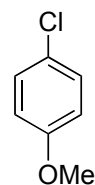
**2.15**



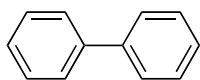
**2.16**



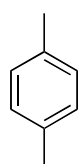
**2.17**



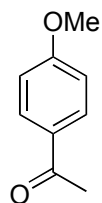
**2.18**



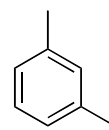
**2.19**



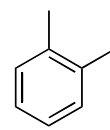
**2.20**



**2.21**



**2.22**



**2.23**

Specifically, **2.3** ( $E_{red}^A = -0.98 \text{ V}$ )<sup>79</sup> was excited at 420 nm, and its fluorescence emission, monitored at 439 nm, was determined in the presence of varying donor concentrations.

Before the steady state fluorescence quenching experiments were accomplished, it was necessary to complete two measurements. First, the fluorescence lifetime ( $\tau$ ) of **2.3** was measured in both of the RTILs using TCSPC. While  $\tau$  for **2.3** in common molecular solvents is well known (14.9 ns in  $\text{CH}_3\text{CN}$ <sup>13</sup>), it is the first time that the fluorescence lifetime has been measured in a RTIL. The value of  $\tau$  was also necessary for proper determination of  $k_q$  as dictated by equation 1. The  $\tau$  values presented in Table 2.1 demonstrate that the fluorescence lifetimes for **2.3** in RTILs does not differ greatly from lifetimes that have been reported for  $\text{CH}_3\text{CN}$ .

**TABLE 2.1** Fluorescence lifetimes ( $\tau$ , ns) of 9,10-dicyanoanthracene (**2.3**) in the two RTILs, as well as viscosity measurements ( $\eta$ , Pa s, 25°C) for the corresponding RTIL.

ionic liquid	$\tau$ of <b>2.3</b> (ns)	$\eta$ (Pa s)
<b>2.1</b>	13.0	0.45
<b>2.2</b>	12.0	0.68

It was also necessary to measure the viscosity ( $\eta$ ) of the RTIL samples. The diffusion limit for a specific solvent can be approximated using Smoluchowski equation (equation 3) and this limit is directly related to  $1/\eta$ . PET reactions are known

to be diffusion limited reactions, thus it is important to obtain proper viscosity values such that a valid limiting  $k_{diff}$  for the solvent can be calculated. The viscosities obtained did not differ greatly from those previously reported.<sup>23</sup>

A stock solution of 9,10-dicyanoanthracene (**2.3**) in the desired RTIL was made such that the absorbance at the excitation wavelength (420 nm) was between 0.1 and 0.2 AU. A 2 mL sample of the stock solution was then transferred into a quartz cuvette. A stock solution of quencher (if quencher was a solid) in RTIL was prepared by dissolving approximately 1 mmol of quencher in 1 mL of RTIL, followed by sonication and use of a vortexer until all of the quencher had dissolved. Neat quencher was added directly to the solution of **2.3** in the RTIL if the quencher was a liquid. The resulting solution was then degassed with N<sub>2</sub> for 15 minutes to eliminate the presence of dissolved O<sub>2</sub> in the RTIL, and to homogenize the sample. Finally, the solution was allowed to rest until all the bubbles had disappeared from the sample. The initial fluorescence of the stock sample was monitored and then the resulting fluorescence was recorded, this value would be regarded as  $\Phi_o$ . After the subsequent addition of an aliquot of quencher solution, the fluorescence of the sample was recorded again. Several aliquots of quencher were added to obtain multiple data points, which were then utilized in determining the fluorescence quenching rate constant ( $k_q$ ).

The fluorescence quenching rate constant ( $k_q$ ) was calculated using the Stern-Volmer Equation using 8-10 different concentrations of a given quencher.:

$$\frac{\Phi_o}{\Phi} = 1 + k_q \tau [Q] \quad (2)$$

where  $\Phi_o$  is the fluorescence of the sample without quencher,  $\Phi$  is the fluorescence of the sample in the presence of quencher,  $\tau$  is the fluorescence lifetime of 9,10-dicyanoanthracene, and  $[Q]$  is the concentration of quencher in molarity.  $\tau$  was obtained from TCSPC measurement was determined to be 13 ns in **2.1** and 12 ns in **2.2**. By plotting  $[Q]$  vs.  $\Phi_o/\Phi$ , the slope ( $k_q \tau$ ) can be determined, and from this  $k_q$  can easily be calculated. All of the Stern-Volmer plots obtained were linear with an average  $R^2$  value of 0.95, indicating good linearity and Stern-Volmer behavior. To address concerns about variability in our RTIL preparations, duplicate Stern-Volmer quenching measurements were carried out for each quencher. The reported values are the average of these determinations and the experimental uncertainty in Table 2.2 reflects the range between these duplicate runs.

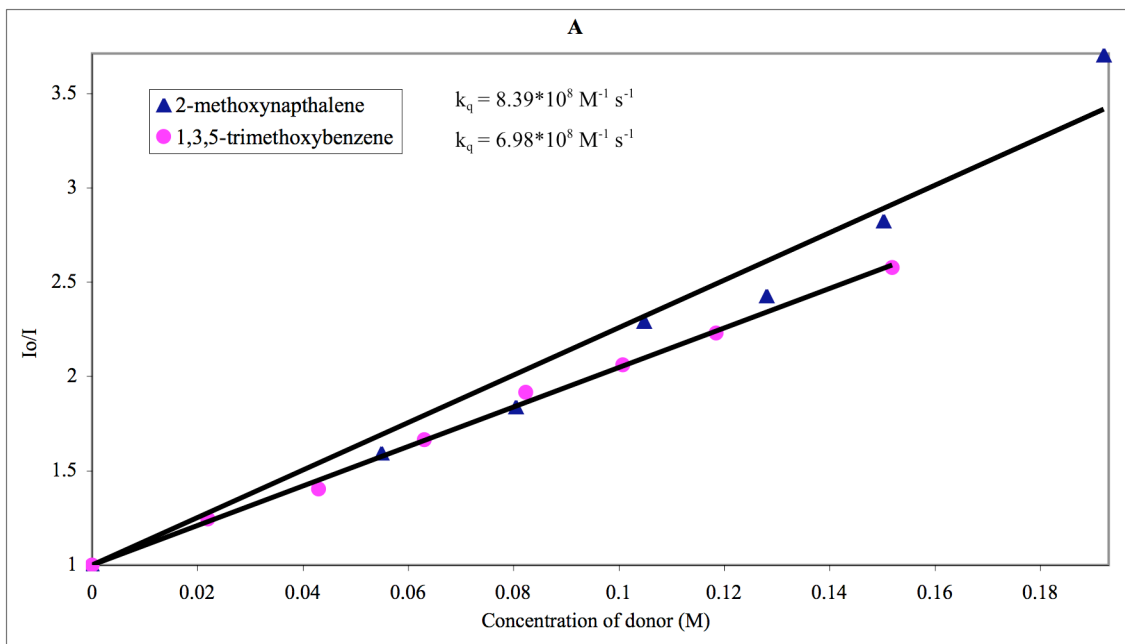


**Figure 2.3** Stern Volmer Analysis of Fluorescence Quenching Data From Two Amine Donors in 2.1.

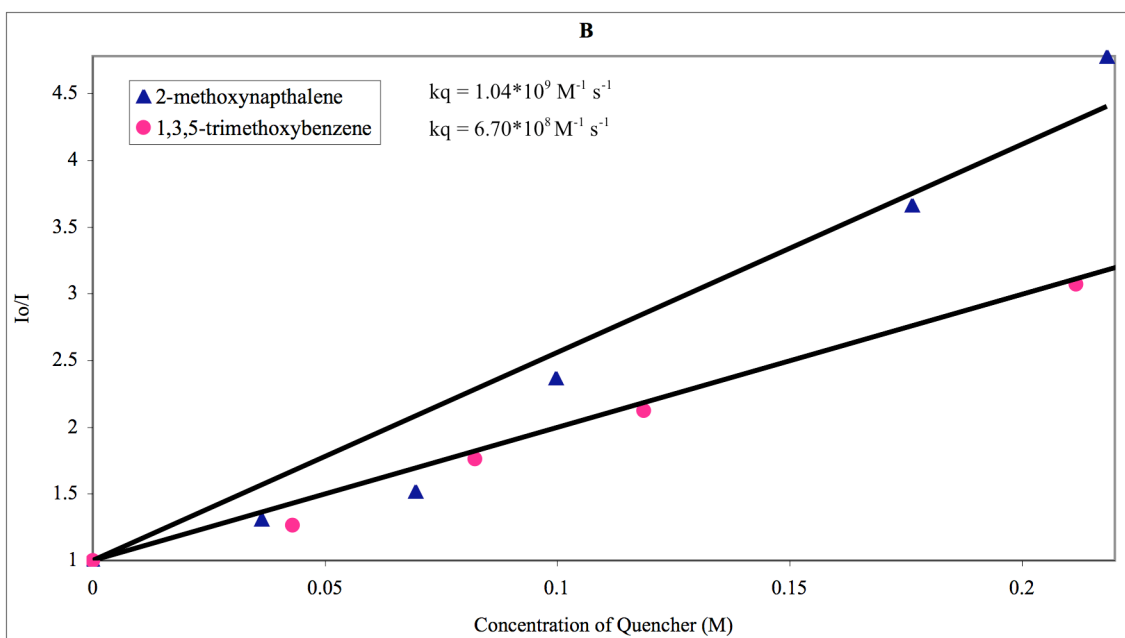


**Figure 2.4** Stern Volmer Analysis of Fluorescence Quenching Data From Two Amine Donors in 2.2.

**TABLE 2.2:** Oxidation Potentials ( $E_{ox}$ , V) and  $k_q$  ( $M^{-1} s^{-1}$ ) values for Fluorescence Quenching Experiments of DCA with Various Electron Donors in **2.1** and **2.2** measured at  $20 \pm 1^\circ C$ .

donor	$E_{ox}$ (V vs. SCE in MeCN)	$k_q$ ( $M^{-1} s^{-1}$ )/ $10^8$ using <b>2.1</b>	$k_q$ ( $M^{-1} s^{-1}$ )/ $10^8$ using <b>2.2</b>
N,N-dimethylaniline ( <b>2.4</b> )	0.53 <sup>a</sup>	43.7	12.0
N,N-diethylaniline ( <b>2.5</b> )	0.76 <sup>b</sup>	17.4	6.9
phenol ( <b>2.6</b> )	1.04 <sup>c</sup>	6.2	4.5
4-methoxyphenol ( <b>2.7</b> )	1.2 <sup>d</sup>	16.5	23.1
1,4-dimethoxybenzene ( <b>2.8</b> )	1.34 <sup>a</sup>	11.2	7.7
1-methoxynaphthalene ( <b>2.9</b> )	1.38 <sup>a</sup>	13.1	19.0
1,3-dimethoxybenzene ( <b>2.10</b> )	1.48 <sup>c</sup>	8.8	8.2
1,3,5-trimethoxybenzene ( <b>2.11</b> )	1.49 <sup>c</sup>	8.1	8.3
phenanthrene ( <b>2.12</b> )	1.5 <sup>a</sup>	13.7	4.7
naphthalene ( <b>2.13</b> )	1.54 <sup>a</sup>	8.0	3.5
2-methoxynaphthalene ( <b>2.14</b> )	1.52 <sup>a</sup>	9.7	13.0
fluorene ( <b>2.15</b> )	1.71 <sup>c</sup>	4.4	6.8
pentamethylbenzene ( <b>2.16</b> )	1.71 <sup>c</sup>	5.9	7.2
anisole ( <b>2.17</b> )	1.76 <sup>a</sup>	8.5	2.0
p-chloroanisole ( <b>2.18</b> )	1.84 <sup>f</sup>	9.8	6.6
biphenyl ( <b>2.19</b> )	1.92 <sup>c</sup>	5.6	1.9
p-xylene ( <b>2.20</b> )	2.01 <sup>c</sup>	3.8	0.8
p-methoxyacetophenone ( <b>2.21</b> )	2.05 <sup>g</sup>	4.4	0.61
m-xylene ( <b>2.22</b> )	2.11 <sup>c</sup>	0.30	0.20
o-xylene ( <b>2.23</b> )	2.16 <sup>c</sup>	0.24	0.26

<sup>a</sup> ref. 30 <sup>b</sup> Dileesh, S.; Gopidas, K. R. *J. Photochem. Photobiol., A* **2004**, *162*, 115-120. <sup>c</sup> Rathore, R.; Kochi, J. K. Donor/Acceptor Organizations and the Electron-Transfer Paradigm of Organic Reactivity *Adv. Phys. Org. Chem.*; Academic Press: New York, 2000; Vol. 35, pp 193-315. <sup>d</sup> Hammerich, O.; Parker, V. D.; Ronlan, A. *Acta Chem. Scand. B* **1976**, 89-90. <sup>e</sup> Gould, I. R.; Ege, D.; Moser, J. E.; Farid, S. *J. Am. Chem. Soc.* **1990**, *112*, 4290-4201. <sup>f</sup> Lutskii, A. E.; Beilis, Y. I.; Fedorchenko, V. I. *Zhurnal Obshchei Khimii* **1973**, *43*, 97-99. <sup>g</sup> Sasaki, K.; Kitani, A.; Tsuboi, M. *Nippon Kagaku Kaishi* **1973**, *12*, 2269-74.

Table 2.2 shows  $k_q$  values for **2.1** and **2.2** along with  $E_{ox}$  values for the associated donors. Two important qualitative observations are apparent from these data. First, as  $k_q$  decreases, the oxidation potential of the electron donor increases. The oxidation potential of the donor is directly related to  $\Delta G_{et}$ , which can be determined from the following equation:

$$\Delta G_{et} = 23.06 (E_{ox}^D - E_{red}^A) - E_{oo} - S \quad (3)$$

where  $E_{ox}^D$  is the oxidation potential of the donor,  $E_{red}^A$  is the reduction potential of the acceptor and  $E_{oo}$  is the excited state energy of the acceptor. The  $S$  term can be thought of as a solvation and coulombic interaction term for the radical ion pair as it occurs in the RTIL solvent. In common molecular liquids the  $S$  term can be estimated from  $q^2/\epsilon r$  (and is negligible in highly polar solvents.) For ionic liquids, however, the approximation which applies to molecular solvents is not valid. This is due to the fact that RTILs have no measurable dielectric constant.

Secondly,  $k_q$  values (Table 2) for the more easily oxidized donors were at least one order of magnitude higher than would be predicted by the Smoluchowski equation (equation 4).  $R$  is the ideal gas constant ( $J K^{-1} mol^{-1}$ ),  $T$  is temperature (K), and  $\eta$  is viscosity (Pa s)

$$k_{diff} = \frac{8000RT}{3\eta} \quad (4)$$

Using  $\eta$  values that had been experimentally determined (Table 1)  $k_{diff}$  values of approximately  $1.0 \times 10^7 \text{ M}^{-1}\text{s}^{-1}$  are predicted for **2.1** and **2.2**. Despite their high viscosities and predicted  $k_{diff}$  values, several accounts of reactions which occur at a rate higher than the predicted diffusion limit of the solvent in RTILs have been reported.<sup>29,30,70,71</sup> There have also been several cases of different electron transfer reactions in RTILs that occur at or above the calculated  $k_{diff}$ .<sup>30,31,65,66</sup> Thus it was thought that the observed  $k_q$  values would also be at or above the calculated  $k_{diff}$ . However, how high over the diffusion limit (for **2.2** and **2.1**) the rate of quenching would occur was unknown. (PET reactions occurring at the calculated  $k_{diff}$  has been well documented in less viscous solvents such as  $\text{CH}_3\text{CN}$ , in which  $k_q$  values for fluorescence quenching of DCA by various donors have been reported at  $10^6$ - $10^{10} \text{ M}^{-1}\text{s}^{-1}$ .<sup>80,81</sup>) In fact for the quenching experiments conducted with donors **2.4**, **2.7**, **2.9**, and **2.14** the rates of fluorescence quenching are two orders of magnitude greater than what was predicted by equation 3.

In order to determine if the observed quenching processes observed were static or dynamic a series of fluorescence lifetime measurements were made. Specifically, a solution of **2.3** in the desired RTIL (either **2.1** or **2.2**) was made and the fluorescence lifetime ( $\tau$ ) of the solution was then determined. The  $\tau$  for **2.3** in **2.1** was determined to be 13 ns, while the  $\tau$  for **2.3** in **2.2** was 12 ns. After this determination, a small aliquot of quencher (either **2.4** or **2.4**) was added to the solution and the lifetime measurement was repeated. This procedure was repeated at several different quencher concentrations. A modified version of equation 2 was used

to determine if the predominant quenching mechanism was dynamic or static. This equation:

$$\frac{\tau_0}{\tau} = 1 + k_q \tau_0 [Q] \quad (5)$$

where  $\tau_0$  is the fluorescence lifetime of the sample without quencher,  $\tau$  is the fluorescence lifetime of the sample in the presence of quencher,  $k_q$  is the fluorescence quenching rate constant of **2.3** with the desired donor, and  $[Q]$  is the concentration of quencher in molarity. If dynamic quenching was occurring for the donor-acceptor pair, then the data obtained would follow Stern-Volmer behavior. This is, in fact, the case. Our lifetime measurements confirm that the fluorescence quenching is predominantly dynamic.

The rate constant of fluorescence quenching ( $k_q$ ) is related to  $\Delta G_{et}$ , the rate constant for bimolecular diffusion ( $k_{diff}$ ), the diffusion equilibrium constant ( $K_{diff}$ ) and the rate of electron transfer of the encounter complex.  $k_q$  can be summarized as

$$k_q = \frac{k_{diff}}{1 + \frac{k_{diff}}{k_{max} K_{diff}} \exp\left(\frac{-\Delta G_{et}^\ddagger}{RT}\right)} \quad (6)$$

The free energy for the overall reaction can be predicted by:

$$\Delta G_{et}^{\ddagger} = \frac{\Delta G_{et}}{2} + \left[ \left( \frac{\Delta G_{et}}{2} \right)^2 + \left( \frac{\lambda}{2} \right)^2 \right]^{1/2} \quad (7)$$

This is known as the Rehm-Weller Equation, where  $\lambda$  represents the reorganization energy.

Reorganization energy ( $\lambda$ ) is a parameter that describes the ability of the solvent and the reactants to change their orientation as the electron transfer reaction progresses.<sup>6,7</sup> Total reorganization energy then can be summarized by the following:

$$\lambda = \lambda_s + \lambda_i \quad (8)$$

Internal reorganization energy ( $\lambda_i$ ) involves the energy required to change the geometries of the reactants. Solvent reorganization energy ( $\lambda_s$ ) involves the energy needed for the solvent to orient around a charged radical ion pair from its original neutral state. It is generally thought that the predominant contributor to  $\lambda$  is due to the  $\lambda_s$  term. Therefore it follows that the magnitude of  $\lambda$  depends on solvent polarity. To this effect, it is known that  $\lambda$  values for PET reactions in polar solvents are relatively high<sup>10-12</sup>, which would suggest that polar solvents undergo substantial changes to adjust to the newly generated charged state. On the other hand,  $\lambda$  values for electron transfer reactions in non-polar solvents are low<sup>10-12</sup> and would indicate that non-polar

solvents do not need to greatly realign to stabilize and accommodate the newly charged state generated during the reaction.

A quantitative Rehm-Weller analysis of the data presented in Table 2.3 involved the adjustment of three parameters with equations 6 and 7. These parameters were adjusted to obtain a best fit of the experimental data, from which the limiting  $k_{diff}$ , the  $S$  factor, as well as the  $\lambda$  for the solvent could be obtained. The three parameters that were chosen were  $k_{max}K_{diff}$  (qualitatively, the level at which the curve would plateau), the value of  $\lambda$  (which would determine the initial rise of the fitted curve), and the value for  $\Delta G_{et}$ .

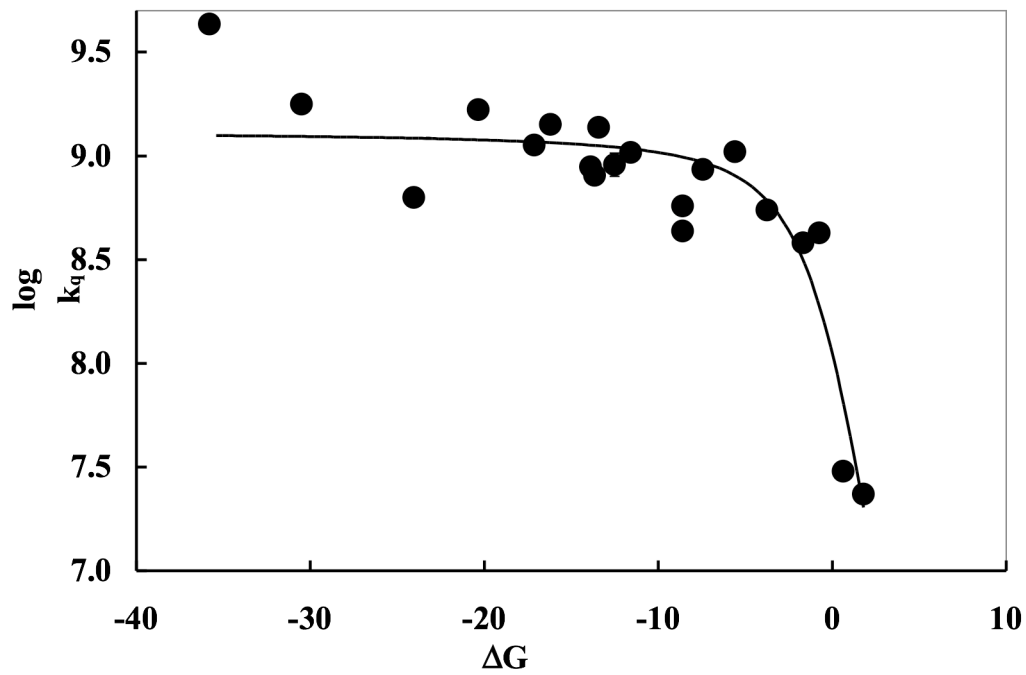


**Figure 2.5** Rehm-Weller Analysis of the experimental data with  $\Delta G$  offset for 2.1

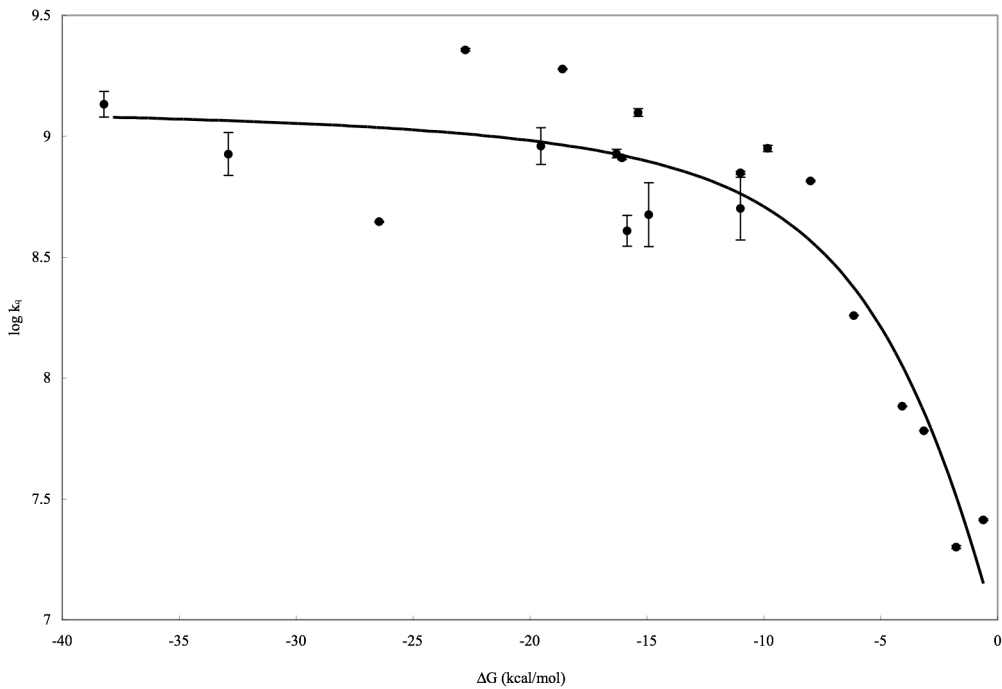


**Figure 2.6** Rehm-Weller Analysis of the experimental data with  $\Delta G$  offset for 2.2

The values that were obtained from the Rehm-Weller fit are detailed in Table 2.3

**TABLE 2.3** Electron Transfer Parameters Derived from Rehm-Weller Analysis of Fluorescence Quenching Data.

ionic liquid	$k_{diff}$ ( $M^{-1} s^{-1}$ )* $10^9$	$\lambda$ (kcal/mol)	$S$ (kcal/mol)
<b>2.1</b>	1.50	9.90	-5.32
<b>2.2</b>	1.65	17.6	-9.94

Several conclusions were gleaned from the data obtained from the Rehm-Weller analysis. First, the values obtained for  $k_{diff}$  are significantly larger than what had been predicted by the Smoluchowski equation (equation 4). This was not extremely surprising considering what has been discussed previously. However, the  $k_{diff}$  values that were obtained for **2.1** and **2.2** were two orders of magnitude greater than those predicted by equation 3.

Another observation from the qualitative fits was the magnitude of the  $S$  factor in equation 3. It is a valid concern whether the  $S$  term for PET reactions occurring in RTILs would enhance or diminish  $\Delta G_{et}$  values, and subsequently affect the overall rates of the PET reactions. It was assumed that the  $S$  term, while differing for each specific RTIL, would not differ for each specific donor-**2.3** pair tested. The general trend of decreasing  $k_q$  with increasing  $\Delta G$  values was expected, and overall the trend does not differ in each of the RTILs, while one would expect that the  $k_q$  values in **2.2**

would be less than the  $k_q$  values obtained in **2.1** due to the fact that **2.2** is more viscous than **2.1**. (Table 2.1)

The most interesting finding from the Rehm-Weller analysis is the  $\lambda$  values. Our initial expectation was that  $\lambda$  would be large, as we anticipated that the formation of ions from the neutral reactants would be coupled with large scale motions of the ions from the RTIL. The modest values obtained in this study imply the component ions of the RTIL do not strongly associate with the radical ion pair. This is qualitatively consistent with a number of solvatochromic studies of similar RTILs.<sup>34,36-38,82-86</sup> The latter suggest that the RTILs solvate organic probe molecules to about the same extent as moderately polar organic solvents such as ethanol or DMSO. Several recent molecular dynamics simulations suggest that RTILs are fairly ordered on the nanometer scale consisting of polar domains and in cases where the alkyl chains are C<sub>4</sub> and longer, a continuous 3-dimensional polar microdomain.<sup>87-89</sup>

While our PET studies cannot provide a direct measurement of these microdomains, they are clearly consistent with this picture. Specifically, we postulate that the relatively small, non-polar probe molecules reside in and diffuse through the non-polar microdomains and that excited state electron transfer occurs in these domains. Specific association of the radical ion pair with the polar components of the RTIL apparently occurs on a timescale that is long relative to the lifetime of the encounter complex (which we assume to be  $10^{-10}$  to  $10^{-9}$  s.<sup>90</sup>) In this regard, it is worth noting time dependent Stokes shift measurement of Samanta and Petrich et al. These

workers characterized two time regimes associated with solvation of fluorescence excited states; a fast relaxation of  $10^{-12}$  to  $10^{-10}$  s and a slower timescale of  $10^{-10}$  to  $10^{-8}$  s.<sup>36,37,82-84</sup> It is generally assumed that the latter corresponds to the large scale motions of the cations.

### 2.3 Conclusions

Fluorescence quenching kinetics and  $\lambda$  for two room temperature ionic liquids (RTILs), **2.1** and **2.2**, have herein been reported. These kinetic studies help elucidate the solvation dynamics and solution composition of a specific ionic liquid and will allow us to probe interesting properties of this new class of liquids. From the data, it was observed that the  $k_q$  values obtained for the steady state fluorescence quenching experiments were one to two orders of magnitude greater than the diffusion limited rate constant for **2.1** and **2.2**. This  $k_{diff}$  value was predicted by equation 8 to be  $1.0 \times 10^7$ . The  $\lambda$  values of 9.9 and 17.6 kcal/mol have been reported for **2.1** and **2.2** respectively. While reported  $\lambda$  values for polar molecular solvents tend to be very large, the values obtained for the two RTILs investigated were relatively small, especially if one considers that both the anion and cation portion of the RTIL must adjust to stabilize and solvate the radical ion pair generate during the electron transfer process. These results, especially in light of recent theoretical simulations, tend to suggest that electron transfer between the excited **2.3** and the donor molecule is occurring in the hydrophobic, non-polar alkyl chain region of the RTIL. These conclusions, however, are slightly contradicted by the overall trend seen in the data for  $\lambda$ . Thus, if in the future a trend is observed that  $\lambda$  increases with alkyl chain size

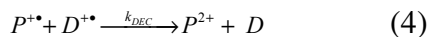
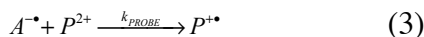
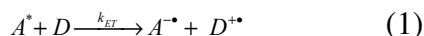
and as the hydrophobic region increases, then a new solvation model for RTILs will need to be proposed.

## Chapter 3: Solvent-Mediated Photoinduced Electron Transfer in a Pyridinium Ionic Liquid<sup>‡</sup>.

<sup>‡</sup>Excerpts from this chapter have previously been published as: Vieira, R.C.; Falvey, D.E. *J. Am. Chem. Soc.*, 2008, *130*, 1552-1553.

### 3.1 Introduction and Background

Photoinduced electron transfer (PET) is a fundamental process that is central to a variety of applications including solar energy conversion<sup>1</sup>, photolithography<sup>91</sup>, molecular photonics<sup>92</sup>, photo-triggering<sup>93</sup>, and the synthesis of complex molecules<sup>94</sup>. Equation 1 depicts a simple example of this wherein an excited state electron acceptor, A, abstracts an electron from a ground state donor, generating two radical species, A<sup>•-</sup> and D<sup>•+</sup>. Usually the net efficiency of PET reactions is determined by the rate of energy-wasting back electron transfer reactions (equation 2) relative to the completing chemical reactions or charge separation process (equation 3.)



Since the pioneering theoretical insights of Marcus<sup>95</sup>, experimentalists have sought to optimize the efficiency of PET reactions. Thus there have been extensive studies on the effects of the driving force, electronic coupling and the solvent medium on the rates of these reactions<sup>8,9,11,90,95</sup>.

Room temperature ionic liquids (ILs) have found many intriguing applications in synthetic chemistry<sup>96</sup>, electrochemistry<sup>54</sup> and separation science<sup>97</sup>. Their ionic nature implies that they might be able effect efficient charge separation in PET processes via specific ion-pairing interactions. On the other hand, typical ILs have high viscosities which tends to slow diffusion rates, and reduce the rate for cage escape. A recent study of PET rate constants in an imidazolium-based IL showed that the reorganization energies are not qualitatively different from what is observed in solvents of moderate polarity.<sup>1,98</sup> This observation is consistent with solvatochromic, simulation, and ET studies which indicate that imidazolium-based ionic liquids have polarities comparable to acetonitrile or ethanol.<sup>34,37,84,99-103</sup>

Several groups have studied reaction kinetics of electron transfer reactions in ionic liquids using pulse radiolysis. Gordon et al found that BMIM salts were an ideal solution with which to generate radical ions.<sup>104</sup> In this instance, using RTILS as a reaction medium, Gordon, for the first time, was able to observe radical cations generated from 1-methyl-1,3-dihydronicotinamide (a NADH analog.) This radical cation had previously been undetected due to the poor solubility of 1,3-dihydronicotinamide in conventional organic solvents in cryogenic matrix conditions. Neta et al. studied pulse radiolysis in methyltributylammonium bis(trifluoromethylsulfonyl)imide and observed solvated electrons generated by pulse radiolysis of the RTIL that persisted for hundreds of nanoseconds.<sup>105</sup> Once generated, these electrons proceed to react with aromatic solutes at diffusion limited rates. A pulse radiolysis study by Behar et al. suggested that in pyridinium ionic liquids,

through-solvent migration of the electron could facilitate rapid intermolecular electron transfer reactions.<sup>29,64</sup> We hypothesized that the proposed solvent-mediated pathway could be exploited as a means of segregating charges generated in PET reactions and that a rate acceleration could be realized relative to comparable processes that rely on the diffusion of photogenerated radical ions.

One application where the utilization of a RTIL solvent-mediated PET pathway would be beneficial is in the construction of solar cells. Dye-sensitized solar cells (DSSCs) or Grätzel cells, containing both organic and inorganic components, are based on a semiconductor formed between an anode and an electrolyte, and mimic the basic photosynthetic pathway. In DSSC, there are three basic layers; the anodic layer is a transparent anode which is fabricated from fluorine containing tin oxide compound. The second layer, which contains the dye sensitizer is comprised of TiO<sub>2</sub> which is coated with a dye that is highly absorbing (hence the sensitization.) An inorganic semiconductor provides a basis of electron transfer, and electrons are generated by a photoexcited small molecular weight dye which has been coated onto TiO<sub>2</sub> particles. Finally, the electrolytic layer is an I<sup>-</sup>/I<sub>3</sub><sup>-</sup> electrolytic layer flanked by a conductive metal sheet.

DSSCs work in the following manner. First, light is transmitted through the transparent anodic layer photoexcites the dye sensitizer. PET occurs from the photoexcited dye molecule to the TiO<sub>2</sub> which it coats, and subsequently those electrons move via diffusion to the anodic layer. The newly electron deficient dye

molecule will abstract an electron from  $I_2$  in the electrolytic layer causing the  $I^-/I_3^-$  redox couple to form.

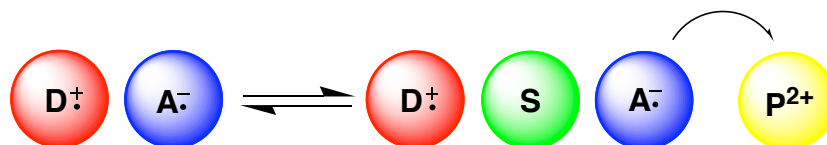
RTILs have been investigated as an electrolytic component in DSSCs. Using 1-ethyl-3-methylimidazolium bis(trifluoromethanesulfonyl)imide as a component of the electrolytic layer, Watanabe et al. were able to observe that the use of the RTIL promoted faster electron transfer from the  $I^-/I_3^-$  couple as compared to rates observed in conventional molecular solvents, despite the high viscosity of the RTIL.<sup>106</sup> They attributed this phenomenon to the high ionic strength of the RTIL. Grätzel et al. studied the use of a binary ionic liquid electrolyte in DSSC and found that in ionic liquid based electrolyte a high concentration of  $I_2$  was necessary to promote the reuse of the dye sensitizer.<sup>107</sup> Unfortunately, while DSSCs are relatively inexpensive when compared to traditional silicon based solar cells, they also have poor efficiencies, with the highest efficiencies of a commercial DSSC being at 10%.

To test our solvent mediated PET pathway we designed a series of donor-acceptor systems that could easily be monitored by laser flash photolysis. These systems would allow us to quantify to what degree a solvent mediated pathway can aid PET reactions.

### 3.2 Results and Discussion

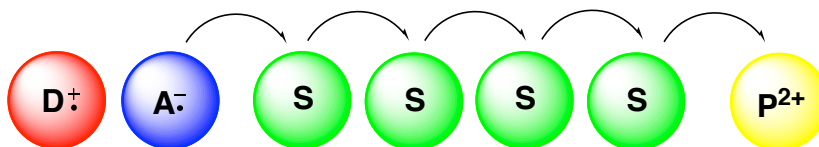
In most PET experiments, the solvent generally adopts a more passive role in the reaction. As was discussed in the previous chapter, the solvent acts solvate the radical ion products generated in a PET reaction.

**Scheme 3.1** The role of a conventional molecular solvent in PET



Unlike conventional molecular liquids, we envisioned that specific RTILs could act as more than just a vessel to stabilize charge. We hope that the correct choice of RTIL as well as donor and acceptor would facilitate a process in which the solvent would act as a charge mediator, effectively acting as an electron ferry to improve rates of electron transfer and facilitate greater yields of cage escape product.

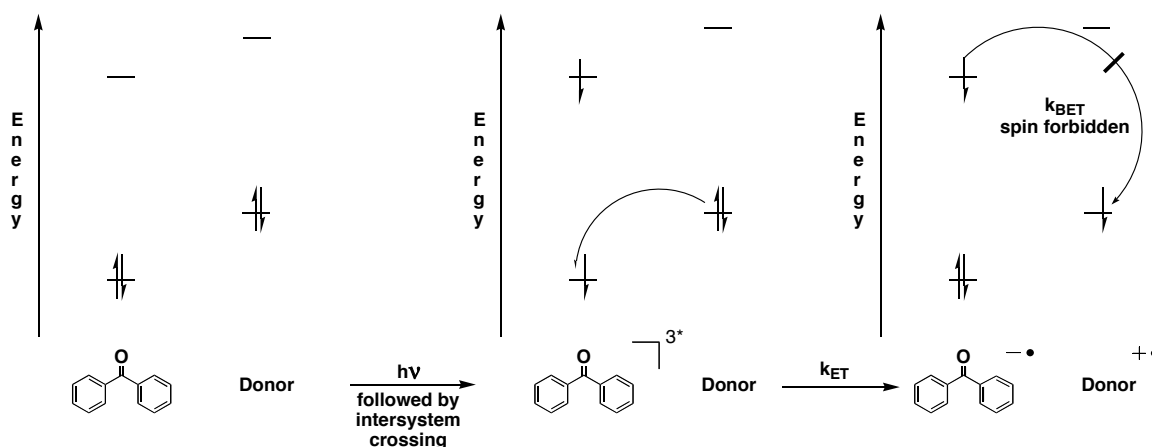
**Scheme 3.2** The potential role of an RTIL in PET



Based off of the results observed during the course of the experiments discussed in Chapter Two, we were cognizant of the fact that the imidazolium RTIL class would not be a good choice for solvent mediated (SM) PET. As an alternative to the imidazolium class we chose to use a RTIL that incorporated a cationic moiety that was more readily reduced, namely an RTIL that used a pyridinium core instead of an imidazolium core. As such, we used N-butyl pyridinium bis(trifluoromethanesulfonyl)imide (BuPyr-NTf<sub>2</sub>, **3.1**.)

To accomplish the goal of solvent-mediated PET, we designed two donor-acceptor PET systems, the first based on a triplet mediated system (using benzophenone, **3.2**, or duroquinone, **3.3**, as acceptors) and the second based off of a singlet mediated system (using 9-cyanoanthracene, **3.4**, as an acceptor.) The triplet system allowed us to demonstrate that rapid through solvent electron transfer can occur in cases where the electron donor (**3.2**) has a more negative potential than a pyridinium ionic solvent and diffusive electron transfer in cases where the donor (**3.3**) is less negative. Triplet mediate systems are excellent methods through which one can probe rate of electron transfer and quantum yield of cage escape product. This is due to the fact that using a triplet mediator, back electron transfer is initially a spin forbidden process (Scheme 3.3.)

**Scheme 3.3** Triplet Mediated PET using Benzophenone as a Triplet Acceptor.



In addition to the triplet mediated system, we employed a singlet mediated system. Using this singlet system with **3.4** as the electron acceptor we were able to validate that the solvent mediated pathway can greatly improve charge separation in a system, which previously displayed very low charge harvesting efficiency<sup>11</sup>. Poor charge separation is due to the fact back electron transfer, while spin forbidden in a triplet mediated system, is not forbidden in a singlet mediated system. This situation can lead to a greater yield of back electron transfer product and low efficiency of cage escape. Fast back electron transfer can also make it exceedingly difficult to monitor rates of electron transfer in singlet systems. This is due to the fact that rapid charge recombination of newly generated radical ion pairs back to ground state starting material can impede detection of the radical ions and impede solvent cage migration, which diminish cage escape yields.

**Scheme 3.4** Singlet Mediated PET using 9-Cyananthracene as a Singlet Acceptor.

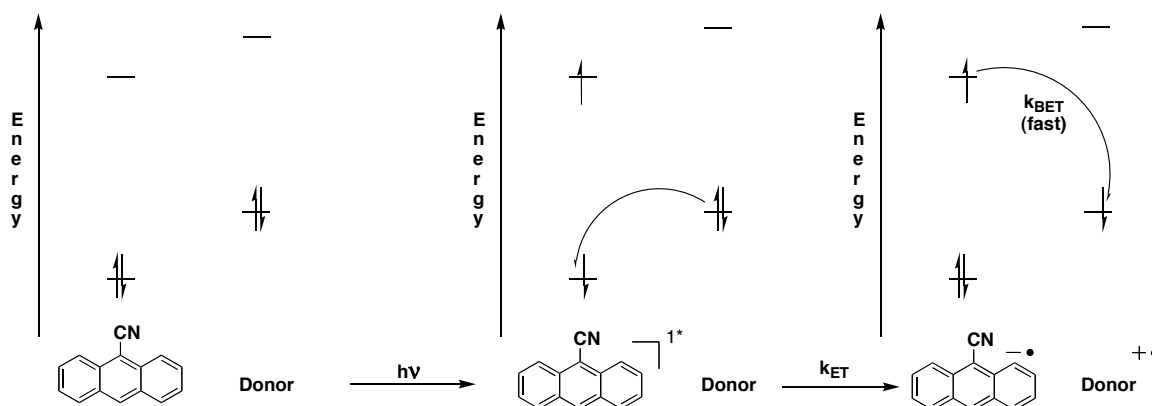
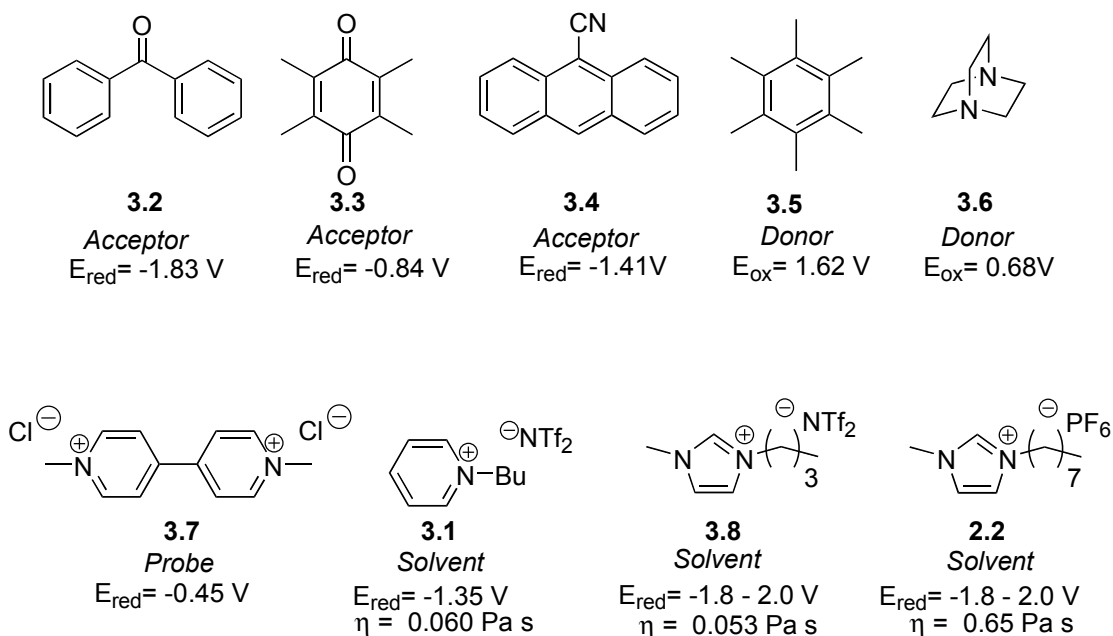


**Chart 3.1** Structures and Redox Properties of Donors, Acceptor, Probe Molecule, and IL Solvents



Both the triplet and singlet PET reactions were carried out in a mediated manner using laser flash photolysis wherein an excited electron acceptor ( $A = 3.3^{3*}$ ,  $3.2^{3*}$ ,  $3.4^{1*}$ ) abstracts an electron from a ground state donor ( $D = 3.6$ ,  $3.5$ ). The rates

and efficiencies for charge separation and intermolecular electron transfer are monitored by a subsequent reaction of  $A^{\bullet}$  with a probe ion ( $P = 3.7^{2+}$ ). These PET reactions were performed in one RTIL (**3.1**), which would facilitate solvent-mediated PET, and additionally in four solvents (MeCN, **2.2**, 3-butyl-1-methylimidazolium bis(trifluoromethanesulfonyl)imide (**3.8**) and Benzene for the singlet system) where PET is predicted to be solely a diffusive process. Rate constants  $k_{BET}$ ,  $k_{PROBE}$ , and  $k_{DEC}$  were determined from numerical simulations of LFP transient absorption signals for the  $3.7^{+\bullet}$  (at 610 nm) unless otherwise noted and assuming the mechanism in eq 2-4. The reported values each represent averages from at least five measurements on three different independently prepared solutions ( $\geq 15$  total.) In all cases independent measurements provided values within 10% of the mean. Additionally,  $\Phi_{SEP}$  was determined using the yield of  $3.7^{+\bullet}$  at saturating concentrations of  $3.7^{2+}$ .

In  $CH_3CN$ , the LFP showed PET behavior that is typical for such systems in conventional polar solvents. For example, LFP of **3.2** with **3.6** generates the transient spectra of the  $3.2^{\bullet}$  (545 nm) and the  $3.6^{+\bullet}$  (460 nm.) Addition of the  $3.7^{2+}$  quenches the  $3.2^{\bullet}$  and gives rise to the  $3.7^{+\bullet}$  signal at 610 nm. Similarly, LFP of **3.3/3.6** and **3.4/3.5** provide the corresponding ion radical transients and the inclusion of  $3.7^{2+}$  quenches the anion radicals and generates the probe ion radical,  $3.7^{+\bullet}$ . Qualitatively similar behavior was also observed for the two control RTILs, **2.2** and **3.8**.

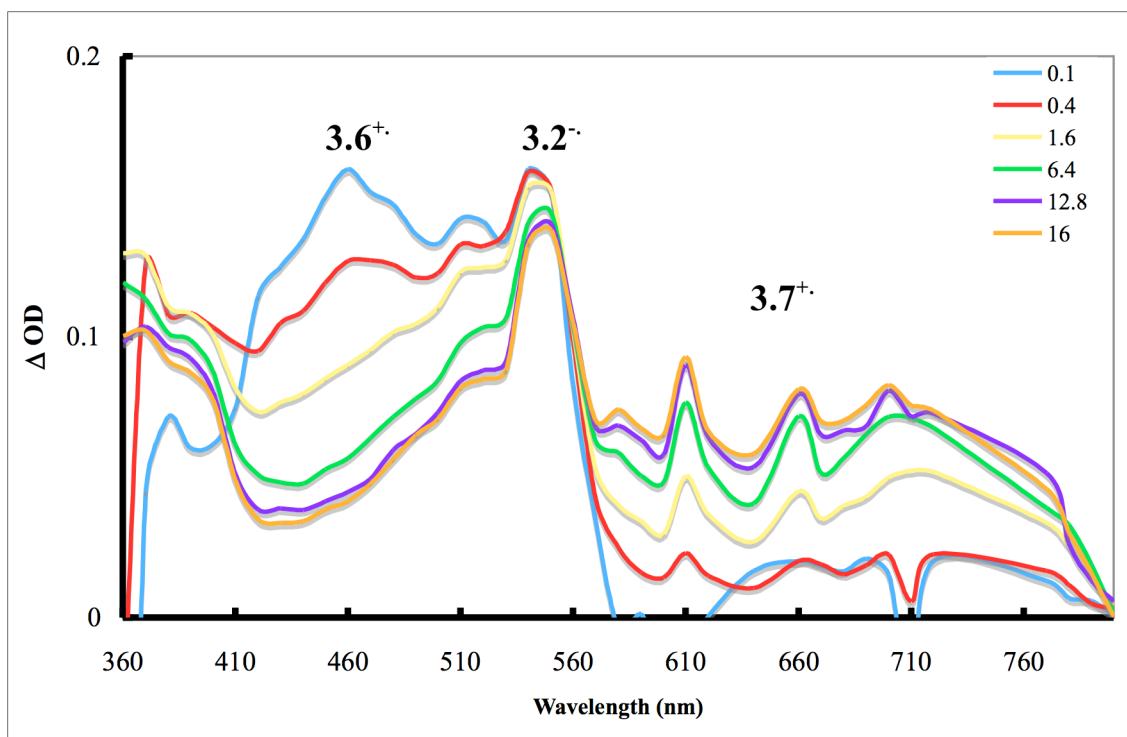


**Figure 3.1** Transient absorption spectra of **3.2•/3.6•/3.7<sup>2+</sup>** in CH<sub>3</sub>CN.

Rather different behavior is seen in **3.1**. In the case of **3.2•/3.6•**, no signal for **3.2•** is observed, even in the absence of **3.7<sup>2+</sup>**. This is consistent with the expected secondary electron transfer to the solvent cations, which is confirmed by the observation of the growth of **3.7<sup>2+</sup>** upon the addition of the probe (Figure 3.2). In contrast, **3.3•**, which is not expected to be capable of solvent reduction, is detected in the **3.3•/3.6•** LFP experiment (at 445 nm). Addition of the probe does result in formation of **3.7<sup>2+</sup>** but with lower efficiency (Figure 3.3).

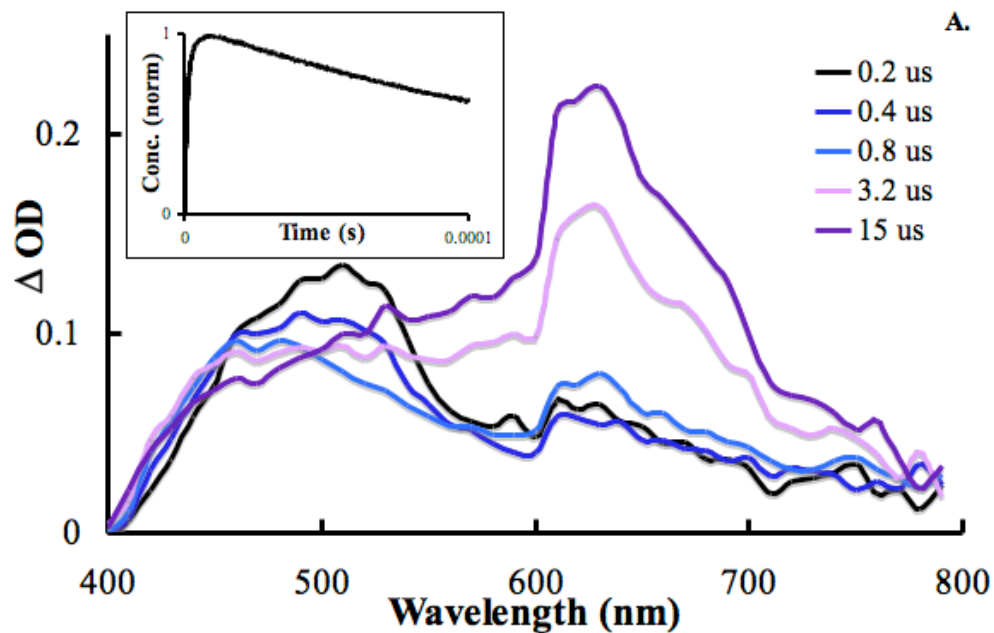


**Figure 3.2** Transient absorption spectra of  $3.2/3.6/ 3.7^{2+}$  in **3.1** with inset of waveform at 610 nm

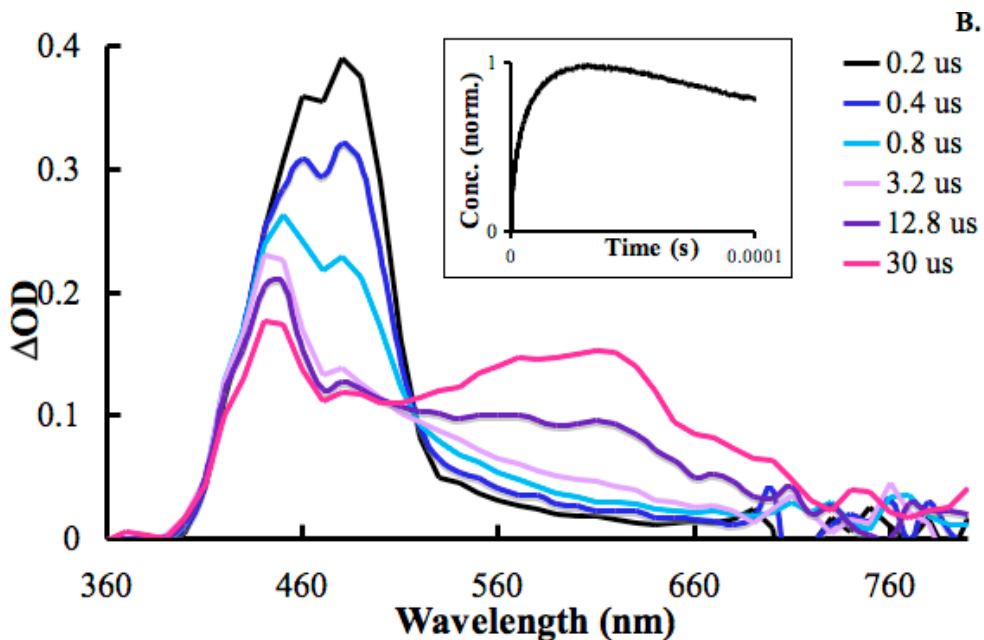


**Figure 3.3** Transient absorption spectra of  $3.3/3.6/ 3.7^{2+}$  in **3.1** with inset of waveform at 610 nm.

In addition to these qualitative observations in the transient spectra, we wanted to determine if **3.1** would directly quench the **3.2<sup>-</sup>** signal. To accomplish this, we added small aliquots of BuPyr-NTf<sub>2</sub> to a solution of **3.2/3.6** in CH<sub>3</sub>CN, and observed the effect of this addition of RTIL to the **3.2<sup>-</sup>** signal at 540 nm. Through this experiment we were able to directly confirm that **3.1** is able to quench the **3.2<sup>-</sup>**. (Figure 3.4)

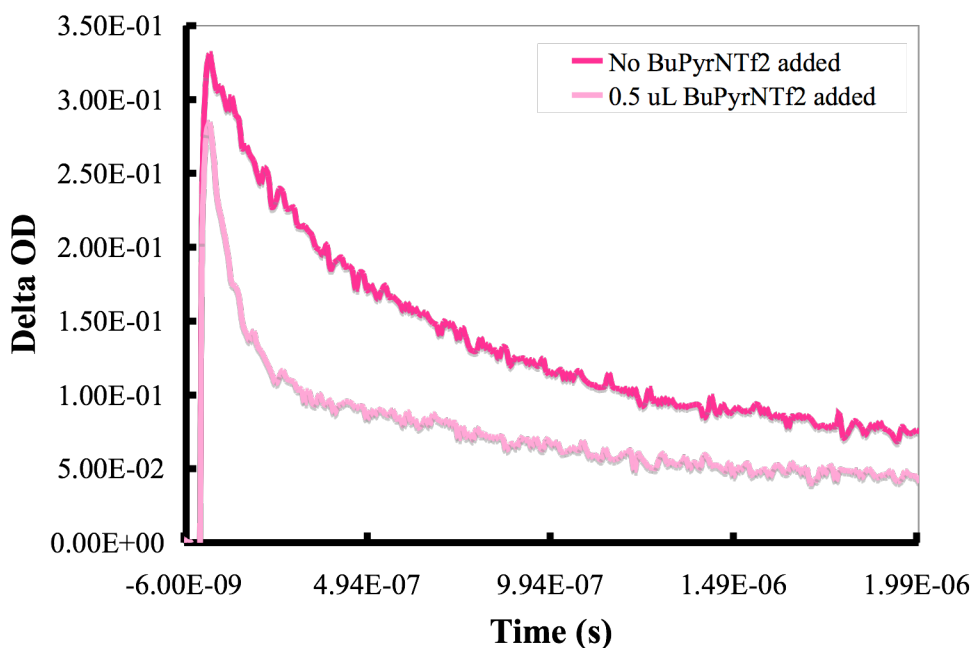
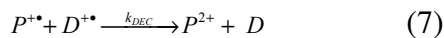
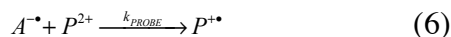
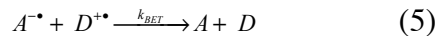


**Figure 3.4** Waveforms at 540 nm depicting the quenching of **3.2<sup>-</sup>** by **3.1**.

Copasi (Complex Pathway Simulator) is a freeware program designed to model and analyze data from a complex set of reaction conditions. The three equations used to model the reaction conditions and obtain the kinetic data are as follows:



From these three equations the following differential equations were derived and used to solve for  $k_{BET}$ ,  $k_{PROBE}$ , and  $k_{DEC}$ :

$$-\frac{dA^{\bullet}}{dt} = k_{BET} A^{\bullet} D^{+\bullet} + k_{PROBE} A^{\bullet} P^{2+} \quad (8)$$

$$\frac{dP^{2+}}{dt} = k_{DEC} P^{+\bullet} D^{+\bullet} - k_{PROBE} P^{2+} A^{\bullet} \quad (9)$$

$$\frac{dP^{+\bullet}}{dt} = k_{PROBE} P^{2+} A^{\bullet} - k_{DEC} P^{+\bullet} D^{+\bullet} \quad (10)$$

The concentration of **3.3<sup>•</sup>** (and subsequently **3.6<sup>+•</sup>**) was directly determined by obtaining the waveform at the  $\lambda_{max}$  of the **3.3<sup>•</sup>** and using the molar absorptivity of the **3.3<sup>•</sup>** at that wavelength ( $\epsilon_{3.3.} = 7.10 \times 10^3 \text{ g}^{-1} \text{ L cm}^{-1}$  at 455 nm.<sup>108</sup>) The concentration of **3.2<sup>•</sup>** was approximated by obtaining the waveform at the  $\lambda_{max}$  of the **3.2<sup>3\*</sup>** and using the molar absorptivity of the **3.2<sup>3\*</sup>** at that wavelength ( $\epsilon_{3.2*3} = 5.40 \times 10^3 \text{ g}^{-1} \text{ L cm}^{-1}$  at 525 nm.<sup>79</sup>) This approximation is assumed to be valid at high concentrations of **3.6**. The maximum concentration of **3.6** needed to validate this approximation was experimentally determined by adding aliquots of a solution of known concentration of **3.6** to a solution of **3.2** and **3.7<sup>2+</sup>** and observing the subsequent growth of **3.7<sup>+•</sup>**. Maximum concentration of **3.6** was defined to be when the concentration of **3.7<sup>+•</sup>**

reached a plateau and no longer increased with additional aliquots of **3.6**. This ideal concentration was found to be  $3 \times 10^{-3}$  M.

Concentration of **3.7<sup>+</sup>** was easily determined from subsequent addition of a stock solution of **3.7<sup>2+</sup>** to the experiment in progress, and was determined by obtaining the waveform at the  $\lambda_{\text{max}}$  of the **3.7<sup>+</sup>** and using the molar absorptivity of the **3.7<sup>+</sup>** at that wavelength ( $\epsilon_{3.7^+} = 10.7 \times 10^4 \text{ g}^{-1} \text{ L cm}^{-1}$  at 610 nm.<sup>109</sup>) Using this information and the experimental data obtained by monitoring the growth and decay of the **3.7<sup>+</sup>** signal at 610 nm, the three desired second order rate constants,  $k_{\text{BET}}$ ,  $k_{\text{PROBE}}$ , and  $k_{\text{DEC}}$  (in  $\text{M}^{-1} \text{ s}^{-1}$ ) were obtained using the parameter estimation function in Copasi. In the case of **3.2/3.6/3.7<sup>2+</sup>** in **2.2**,  $k_{\text{BET}}$  and  $k_{\text{PROBE}}$  were determined by monitoring the growth and decay of **3.2<sup>•</sup>** at 545 nm. This was done due to the overlapping absorbance of the **3.2<sup>•</sup>** and **3.7<sup>+</sup>** species at 610 nm. In cases where the results from fitting did not adequately match the experimental data, further simulation was needed to obtain accurate values for the three rate constants. This was not the case for the experiments performed in acetonitrile, but was done for the data obtain in either **2.2** or **3.1**.

For the **3.4** systems, due to low solubility of **3.5** in the RTILS,  $\Phi_{\text{SEP}}$  was determined in **2.2** and **3.1** by extrapolation of **3.7<sup>2+</sup>** to infinite concentrations using the equation supplied below.

$$\frac{1}{\Phi_{MV^{2+}}} = \frac{1}{\Phi_{A^{2+}}} + \frac{1}{\Phi_{A^{2+}}} \frac{k_{\text{BET}}}{k_{\text{PROBE}}} \frac{1}{[MV^{2+}]} \quad (11)$$

Additionally, as  $3.4^{\bullet}$  is difficult to detect via laser flash photolysis, the initial concentration of  $3.4^{\bullet}$  was approximated by the initial concentration of  $3.5^{+\bullet}$  ( $\epsilon_{3.5^{+\bullet}} = 3.2 \times 10^4 \text{ g}^{-1} \text{ L cm}^{-1}$  at 498 nm.<sup>108</sup>) A representative of the experimental data accompanied by either the curves obtained through fitting or simulation of that data are supplied as Figures 3.4-3.9.

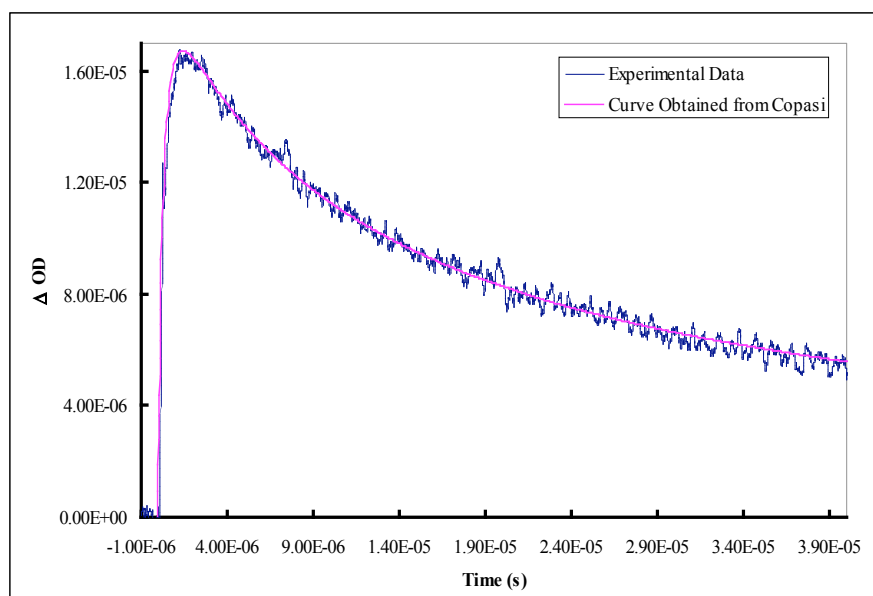


**Figure 3.4** . Waveform at 610 nm of  $3.2/3.6/3.7^{2+}$  in MeCN with corresponding fit from Copasi.

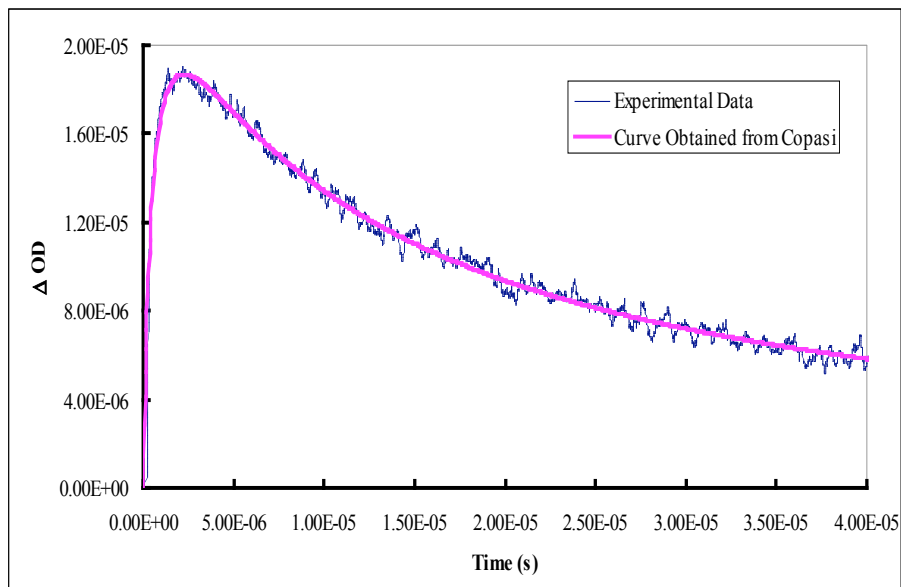


**Figure 3.5** . Waveform at 610 nm of **3.3/3.6/3.72+** in MeCN with corresponding fit from Copasi.

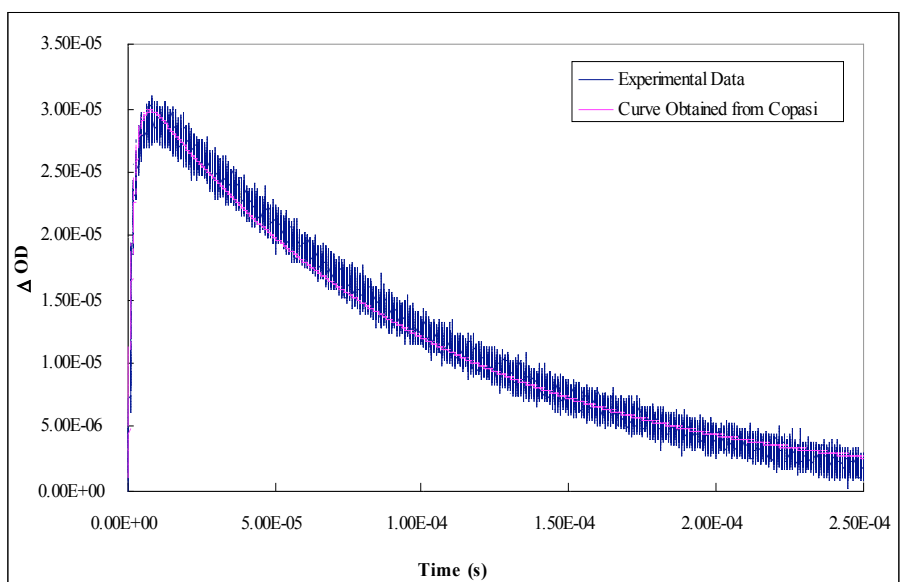


**Figure 3.6** Waveform at 610 nm of **3.2/3.6/3.72+** in **3.1** with corresponding fit from Copasi.

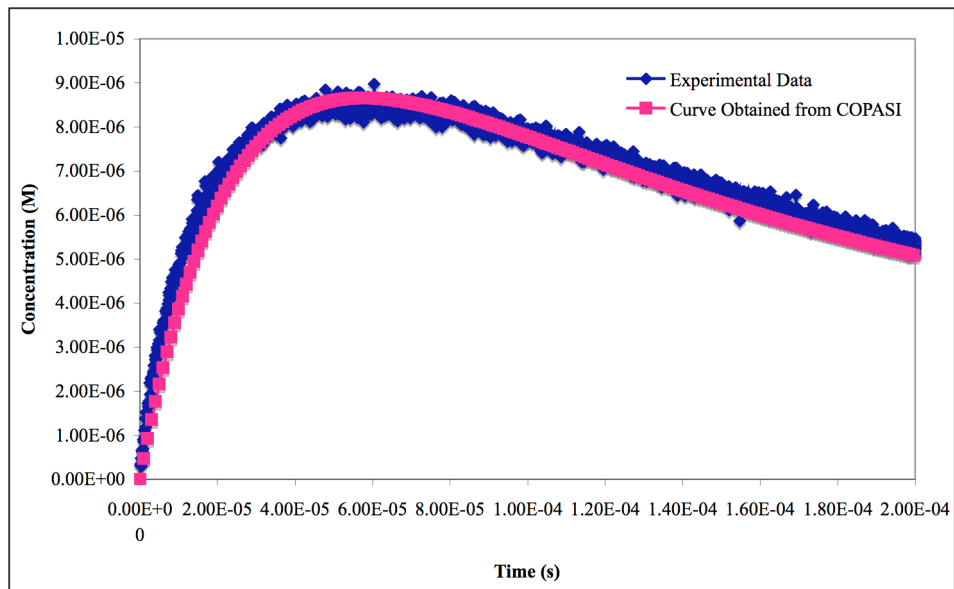


**Figure 3.7 .** Waveform at 610 nm of 3.3/3.6/3.72+ in 3.1 with corresponding fit from Copasi.

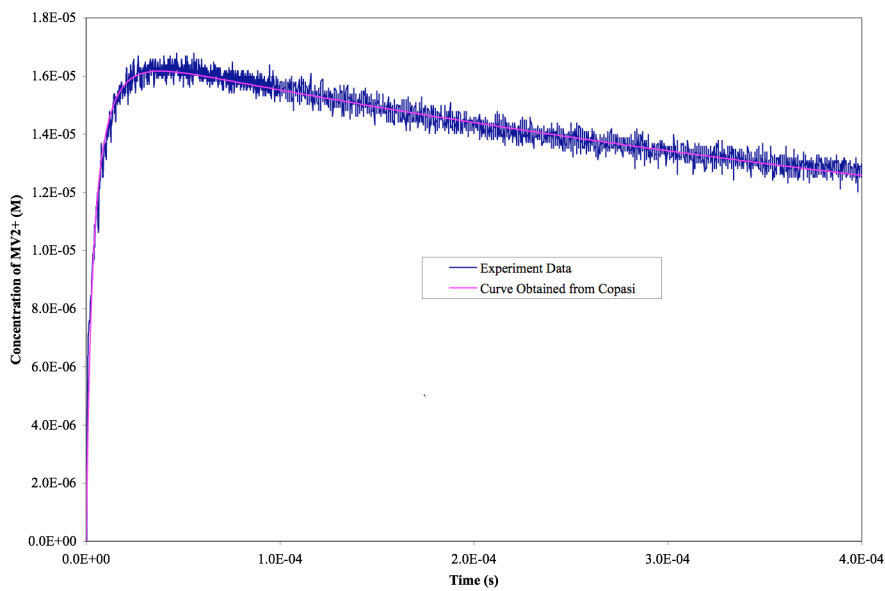


**Figure 3.8.** Waveform at 610 nm of 3.4/3.5/3.72+ in 3.1 with corresponding fit from Copasi.

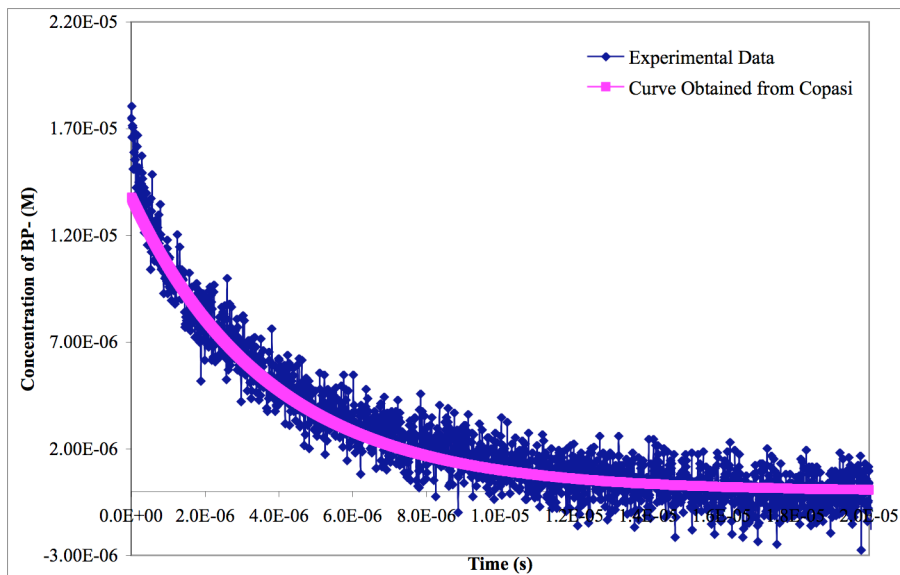


**Figure 3.9.** Waveform at 545 nm of 3.2/3.6/3.72+ in 2.2 with corresponding fit from Copasi.

**Table 3.1** Rate constants for PET Reactions

Entry	Solvent	Acceptor	$k_{BET}^a$	$k_{PROBE}^a$	$k_{DEC}^a$	$\Phi_{SEP}$
1	CH <sub>3</sub> CN	<b>3.3</b>	15.3	38.4	1.74	0.50
2	CH <sub>3</sub> CN	<b>3.2</b>	47.4	14.2	5.18	0.70
3	CH <sub>3</sub> CN	<b>3.4</b>	- <sup>b</sup>	- <sup>b</sup>	- <sup>b</sup>	0.25
4	Benzene	<b>3.4</b>	- <sup>b</sup>	- <sup>b</sup>	- <sup>b</sup>	0.05
5	<b>3.1</b>	<b>3.3</b>	0.45	0.15	0.59	0.90
6	<b>3.1</b>	<b>3.2</b>	1.03	1.00	0.12	0.89
7	<b>3.1</b>	<b>3.4</b>	3.64	0.49	0.05	0.65 <sup>c</sup>
8	<b>3.8</b>	<b>3.2</b>	0.10	0.21	0.15	0.85
9	<b>3.8</b>	<b>3.4</b>	- <sup>b</sup>	- <sup>b</sup>	- <sup>b</sup>	0.03
10	<b>2.2</b>	<b>3.2</b>	1.80	0.15	N/A <sup>d</sup>	N/A <sup>d</sup>
11	<b>2.2</b>	<b>3.4</b>	- <sup>b</sup>	- <sup>b</sup>	- <sup>b</sup>	0.20

<sup>a</sup> Rate constants are in units of M<sup>-1</sup>s<sup>-1</sup> and are x 10<sup>9</sup>. Measurements were made at 20 ± 1°C. Values determined are within ±10% error. <sup>b</sup>signal not sufficient enough to accurately determine rate <sup>c</sup>Determined within ±5% error <sup>d</sup>See supporting information for experimental detail.

Rate constants for the PET processes along with the quantum yields are compiled as entries 1-11 in Table 3.1. The **3.1** results (entries 5-7) were compared with two other ILs, **2.2** and **3.8**. These were chosen because their reduction potentials (-1.90 V vs. SCE)<sup>110</sup> are more negative than that of **3.2** (-1.83 V vs. SCE)<sup>110</sup> and **3.4**, thus through solvent electron transfer is not anticipated. Additionally, **3.8** was chosen as its viscosity (0.053 Pa s) is close to the viscosity of **3.1** (0.060 Pa s).

A direct comparison of entry 6, entry 8, and entry 10 demonstrate that electron transfer from **3.2**<sup>•</sup> to **3.7**<sup>2+</sup> ( $k_{\text{PROBE}}$ ) is an order of magnitude faster in **3.1** than the other ILs, which supports the solvent mediated ET pathway for **3.1**. A solely diffusive ET pathway is demonstrated by entries 5, 8, and 10. Electron transfer from the acceptor to the **3.7**<sup>2+</sup> is approximately  $1 \times 10^8 \text{ M}^{-1} \text{ s}^{-1}$  in these cases and solvents. This is remarkably slower for the **3.1** in comparison to the **3.2** case.

The **3.4/3.5** system shows very low charge separation yields in nonpolar solvents ( $\Phi_{\text{sep}} = 0.072$  in Benzene<sup>90</sup>) but in **3.1** we detect higher yields of **3.7**<sup>•</sup>, analysis of its' final intensity gives a  $\Phi_{\text{sep}} = 0.65$ . This is significant as **3.4/3.5** gives a singlet radical ion pair with a very low barrier to back electron transfer. Nonetheless, this system provides efficient charge separation in **3.1**.

### 3.3 Conclusions

The LFP experiments described above demonstrate that **3.1** can actively facilitate PET reactions by providing a through solvent pathway for electron transfer. However, further work will be necessary to fully elucidate this exact pathway. For example, the current experiments do not distinguish a pathway in which the electron hops sequentially from solvent molecule to solvent molecule from a pathway which a singular reduced solvent cation diffuses with the electron to the encounter the probe.

It is also possible that both of these pathways could occur during the course of a solvent-mediated PET reaction.

Additionally, it is known that while RTILs have microphase domains, their bulk nature is on the whole isotropic. This innate isotropic nature, which would be exploited if the diffusive single reduced solvent cation, could therefore hinder rates of electron transfer. If this were true, then greater rates might be realized in more organized media such as ionic liquid crystals<sup>55</sup>. This hypothesis will be fully explored in Chapter 4.

## **Chapter 4: A Continuation: Solvent-Mediated Photoinduced Electron Transfer in Ionic Liquid Crystals.**

### **4.1 Introduction and Background**

Chapter 3 discussed the use of a room temperature ionic liquid (RTIL) to improve rates of PET and quantum efficiencies. In this system, the solvent was designed to act as a charge carrier to shuttle electrons from their point of generation to a probe molecule via reduction of the one or more of the solvent cations. The RTIL systems capable of facilitating solvent mediated PET promote much faster rates of electron transfer and higher values of  $\Phi_{3,7^+}$ , than systems that could not undergo solvent mediated PET. However, as RTILs are still fairly isotropic on the macrophase level, there is still some component of solvent alignment is necessary to mediate electron transfer. There are two possible mechanisms for solvent mediated PET that can occur, one is a diffusive mechanism wherein one solvent cation is reduced and diffuses to  $3.7^{2+}$ . The alternative mechanism is a hopping mechanism where the electron moves through the solvent by hopping from one solvent cation to another until that electron reaches  $3.7^{2+}$ . We hypothesized that by using a solvent that already had a degree of bulk macrophase order, we would observe more rapid rates of PET and greater quantum efficiencies. Thus the objective of the studies described in this chapter is to determine to observe how rates of electron transfer and yields of free ions differed in molecular solvents, isotropic RTILS (both solvent mediated and not) and solvents that contained a specific mesophase, i.e. ILCs.

The chemical literature that encompasses PET in LCs is limited and does not involve any experiments performed in ILCs. Levanon et al studied intramolecular PET in a nematic liquid crystal and found that the anisotropic nature of the LC studied actually decreased the rate of intramolecular PET.<sup>111,112</sup> Wasielewski et al. also studied intramolecular PET in a nematic LC and determined that the kinetics of charge transfer were slow relative to the movements of the donor and acceptor within the aligned liquid crystal system.<sup>113-117</sup> While those studies seek to probe the effect of a liquid crystalline environment on the rates and efficiencies of PET reactions in LCs, there has been, to our knowledge, no investigations that demonstrates PET in an ILC that facilitates a solvent mediated pathway.

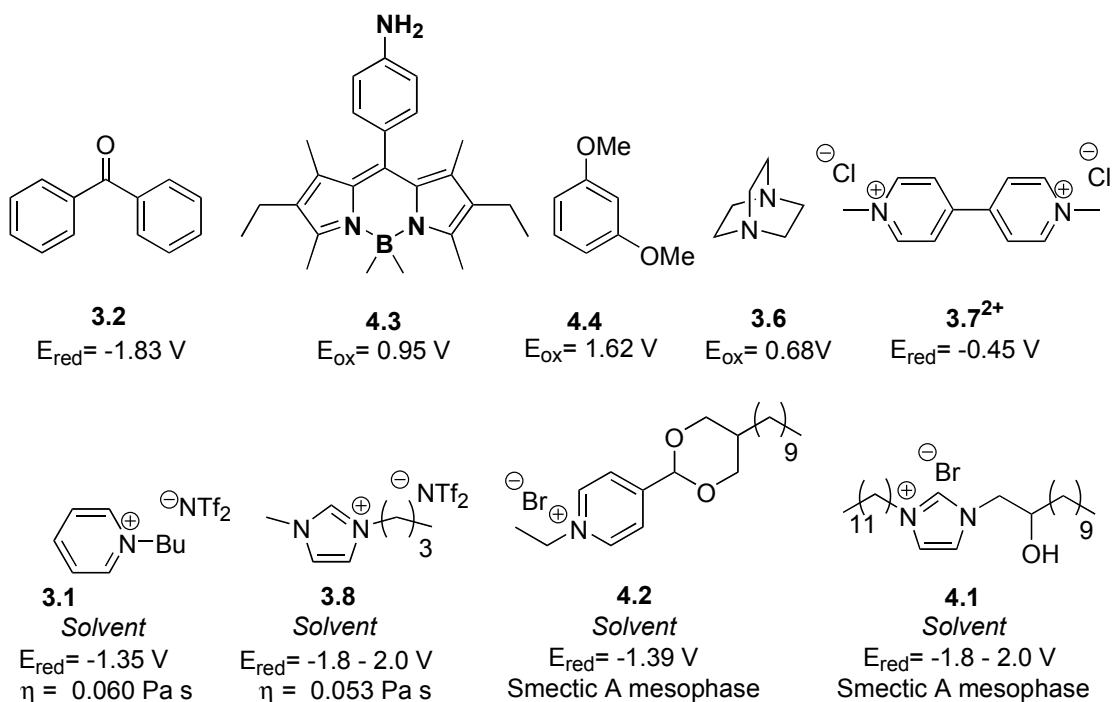


**Chart 4.1.** Donors, Acceptors, Probe Molecule and Solvents

To this end we chose to examine PET reactions in two ILCs, one based off of a cationic imidazolium core and another ILC based off of a cationic pyridinium core. We had several desired features necessary for ILCs; first that the ILCs possess the reduction potentials such that one ILC could facilitate solvent mediated PET and one would act as a control solvent. Secondly, both of these ILCs would be required to be in the same mesophase and that the phase be of a higher order than the nematic LC phase. (The nematic LC phase while generally being the most common LC phase has long-range molecular organization but lacks molecular positional order.<sup>55</sup> This makes the molecular organization of a nematic LC phase only slightly better than the ionic liquids.) Finally, both of the ILCs had to be liquid crystalline at room temperature.

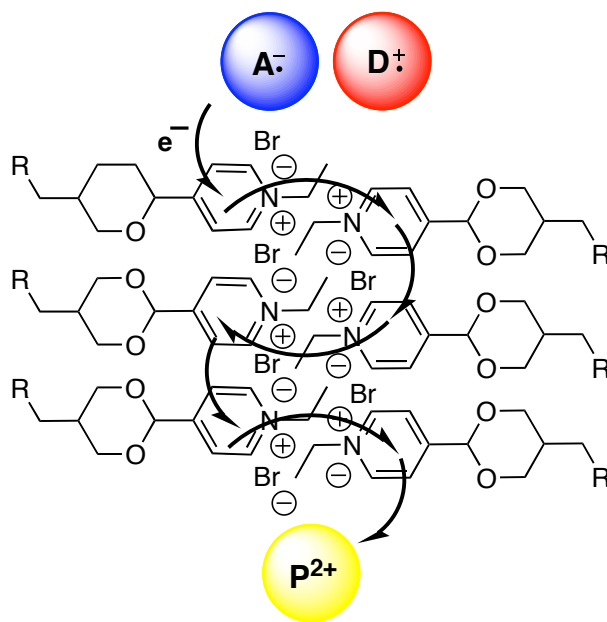


**Figure 4.1** Potential ILC mediated PET pathway.

The first ILC we chose uses a cationic imidazolium mesogen (**4.1**<sup>118</sup>) and has a reduction potential of -1.80 V. This ILC has a reduction potential that is more

negative than either of the donors. Thus it is expected that PET would occur through the diffusive mechanism. We also chose to use an ILC with a cationic pyridinium mesogen (**4.2**.<sup>119-121</sup>) In contrast to **4.1**, **4.2** has a reduction potential of -1.39V, which is less negative than the donors used, and thus it is capable of facilitating the solvent mediate hopping mechanism of PET. Furthermore, both **4.1** and **4.2** are in the the smectic A mesophase at room temperature.

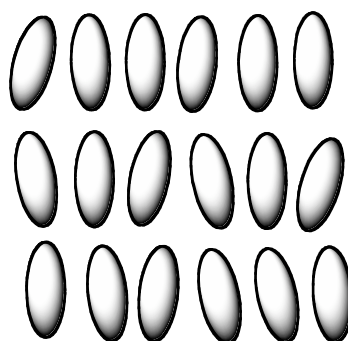


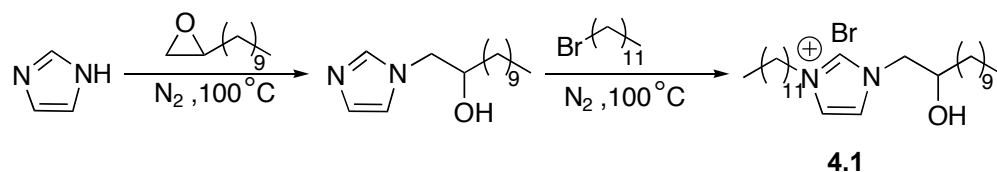
**Figure 4.2** Cartoon depiction of the S<sub>M</sub>A mesophase

Both ILCs have been investigated previously. **4.1** is was originally synthesized by Lin et al, who proposed that the new compound had potential application in the fabrication of electrical and optical devices.<sup>118</sup> **4.2** had previously been studied by Haramoto et al. as part of a series of acetal based pyridinium ILCs which had unique phase behaviors.<sup>119-121</sup> These ILCs had additionally previously been discussed as an electrolytic constituent for various applications including electrochemical cells, batteries, and sensors.

## 4.2 Results and Discussion

Our first task was to synthesis of both ILCs. While the synthesizes of both had previous been described, we were unsure if the proscribed synthesizes would yield ILC that was spectroscopically clean. Synthesis of **4.1** was very straightforward and did not deviate greatly from the literature procedure.<sup>118</sup> Recrystallized imidazole was dissolved in epoxydodecane and allowed to reflux for twelve hours. After the desired product was precipitated from hexane, it was subsequently submitted to a reaction with bromododecane under reflux. Purification by dissolving in hot methanol and adding decolorizing carbon yielded the ILC **4.1**. We took the same precautions (vigorous purification of starting material, moderate reaction conditions) that had been employed in the synthesis of the RTILs, and were able to obtain spectroscopically pure **4.1**.

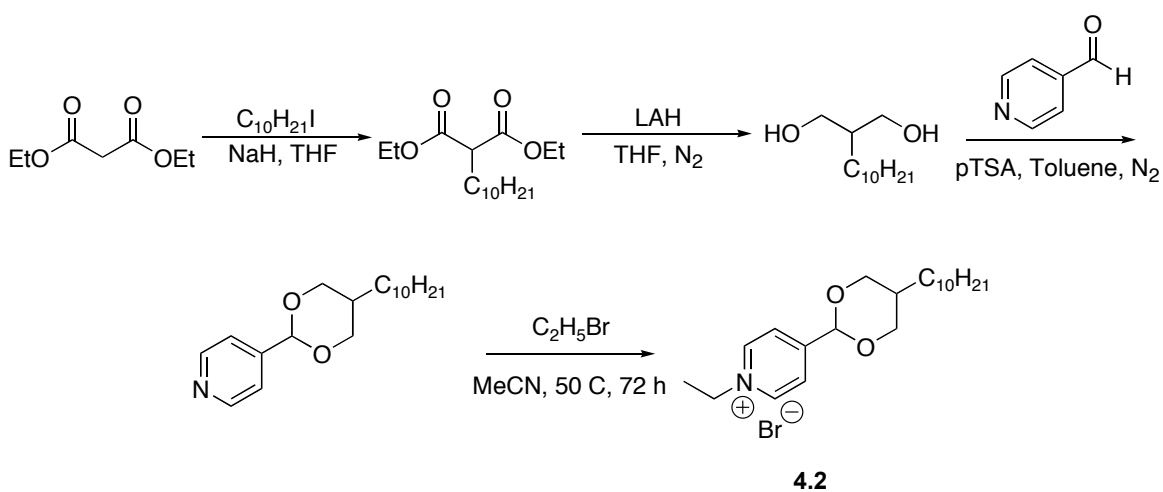
**Scheme 4.1** Synthesis of **4.1**



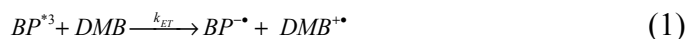
**4.2** was a more difficult target to arrive at. The synthetic procedure for this target was modified extensively. It was found that the literature procedure<sup>121</sup> was less than satisfactory as it produced ILCs in extremely low yields that were not spectroscopically pure. Here, diethyl malonate was alkylated under basic conditions with iodododecane. Reduction of the ester to the diol and subsequent condensation with

4-pyridylcarboxaldehyde gave the pyridine-acetal species. Finally, N-quaternization with bromoethane yields the pyridinium ILC, **4.2**. Careful modification of the procedure produced the pyridinium ILC in higher yields, in a five-step reaction sequence which required only one use of flash column chromatography, with spectroscopically pure material as the end result.

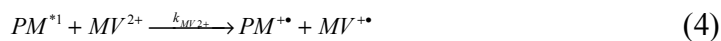
**Scheme 4.2** Synthesis of **4.2**



Experiments that monitored rates of PET as well as quantum yield of cage escape products were carried out using two chromophores with differing excitation wavelengths. Benzophenone ( $\lambda_{\text{ex}} = 355 \text{ nm}$ ) was used in a relay fashion with a ground state electron donor where the final electron transfer step that is monitored occurred from the benzophenone anion radical to methyl viologen dication (a ground state non-absorbing probe molecule which has strong monocation absorption bands at 390 nm and 610 nm.)



A non-commercially available pyrromethene dye<sup>122</sup> ( $\lambda_{ex} = 532$  nm) was used as a direct excited state electron donor (without the need of an additional ground state electron donor to generate the anion radical) to methyl viologen dication.



Results from experiments in the ILCs would then be contrasted with those found in conventional molecular solvents and the RTILs used in previous studies. .

The ILC samples were prepared in the following manner. First, the ILC was dissolved in minimal amounts of methanol. Then the desired mediator (**3.2** or **4.3**) as well as donor (if needed) was measured out and dissolved in the ILC/methanol mixture. The mixture was then placed in a 1 mL thick walled quartz cuvette, capped with a septum seal cap (NSG Precision Cells) with a disposable syringe needle. The cuvette was then placed in an Airfree drying chamber and connected to the house vacuum. The samples were placed under vacuum (1-2 days) until all of the methanol had evaporated and the samples passed the “inverted vial” test. Here, the cuvette containing the ILC was inverted for 45 seconds to make sure that no flow of the

solvent was present. This was an indication that all of the methanol had evaporated from the solution.

Unfortunately due to the fact that ILCs are extremely viscous gel-like compounds there are some limitations in addition of methyl viologen following sample preparation. To remedy this situation methyl viologen was dissolved in a combination of the ILC and methanol, and added to the premade ILC sample in small aliquots. The sample was then vortexed for 30 seconds and allowed to rest until all the bubbles generated by the vortexing had disappeared. At no time during the LFP experiments did the methanol content of the ILC sample exceed 1% by volume of the entire sample. This method ensured that a known concentration of methyl viologen was delivered to the sample, the molecular solvent composition of the sample was low, and that distribution of methyl viologen was homogeneous through the entire ILC sample.

### 3.2.1 355 nm Laser Flash Photolysis.



Benzophenone was chosen as a donor for much for the same reason that we chose **3.2** initially in the initial RTIL experiments. As an initial acceptor or relay

sensitizer, benzophenone reacts from its triplet state which makes it an ideal acceptor with which to monitor rates of PET as well as quantum yield of cage escape product. This is due to the fact that back electron transfer is initially a spin forbidden process in triplet initiated electron transfer. As immediate back electron transfer is spin forbidden, it allows for a greater percentage of cage escape of radical ion species and is beneficial for the determination of  $k_{3,7+}$ . (Scheme 3.3).

Benzophenone was used in conjunction with **3.6** (in the case of the molecular and RTILs) and **4.4** (in the case of the ILCs) as ground state electron donors. **3.6** was chosen due to the fact that while generally regarded as a good electron donor ( $E_{ox} = 0.68$  V), **3.6** is a very poor hydrogen atom donor given its lack of appreciably acidic protons. Unfortunately, when **3.6** was initially used in the ILCs, **3.6** formed a colored solution when combined with the pyridinium ILC. We attribute this color to a charge transfer complex formed via the electrostatic interactions between the electronically deficient pyridinium ILC and the electron rich **3.6**. In any case, the color change precludes spectroscopic observation. After sequential testing several other electron rich ground state donors, 1,3-dimethoxybenzene was chosen due to its oxidation potential ( $E_{ox} = 1.48$  V), its lack of colored complex with either the RTILs or the ILCs, and its inability to act as a hydrogen atom donor.

Laser flash photolysis experiments were performed using **4.1** and **4.2** and results from these experiments were compared to those obtained using RTILs and molecular solvents. (Results in entries 1, 2, and 3 of Table 4.1 have been discussed in

Chapter 3 and are presented here as a means of comparison to the results obtained using the ionic liquids crystals.) The transient spectra from LFP **3.2/4.4/3.7<sup>2+</sup>** in the **4.1** showed a distinct and long-lived absorption at 550 nm that corresponds to the anion radical of benzophenone. The weak and slow appearing band at 610 nm is assigned to **3.7<sup>+</sup>**. A low yield of **3.7<sup>+</sup>** indicates qualitatively that charge separation in **4.1** is inefficient due to slow diffusion of **3.2<sup>•</sup>** through **4.1** to **3.7<sup>2+</sup>**. This observation is further supported by the apparent slow growth of the 610 nm signal.

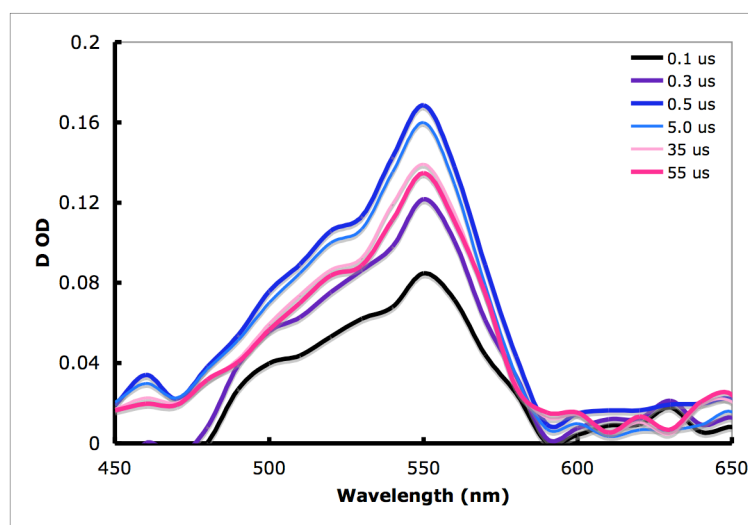


**Figure 4.2.** Transient absorption spectra of **3.2/4.4/3.7<sup>2+</sup>** in a **4.1**

The transient spectrum obtained in the **4.2** is in stark contrast to that obtained in the **4.1**. Whereas in the **4.1** the most prominent feature is the absorption of the **3.2<sup>•</sup>** at 550 nm, in the **4.2** the **3.7<sup>+</sup>** species at 610 nm is the most prominent and strongly absorption species. There is an initial weak absorption at 520 nm that we attribute to the triplet state of benzophenone. There is, however, no appreciable absorption at 550

nm. The distinct lack of  $3.2^{\bullet}$  but prominent presence of  $3.7^{+\bullet}$  at 610 nm suggests that  $3.2^{\bullet}$  is generated but is immediately consumed as it reacts with  $4.2$  cations in a subsequent electron transfer step to produce the ILC reduced cation species (which is not detected spectroscopically.) This newly generated reduced ILC species then goes on to react with  $3.7^{2+}$  to generate  $3.7^{+\bullet}$ . These results are similar to those obtained in **3.1**, which can also facilitate solvent mediate PET.

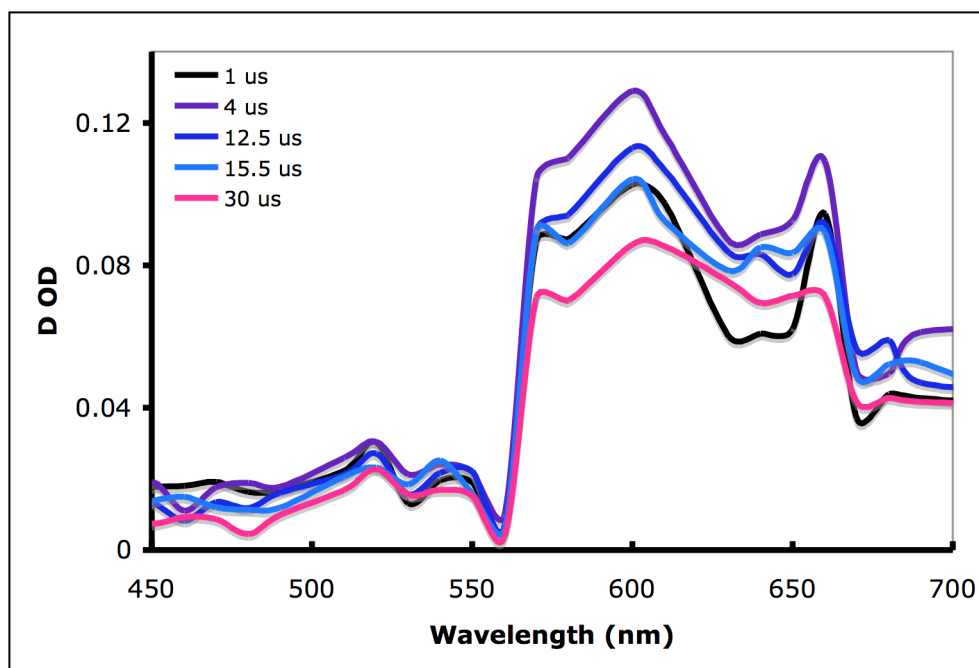


**Figure 4.3.** Transient absorption spectra of  $3.2/4.4/3.7^{2+}$  in  $4.2$

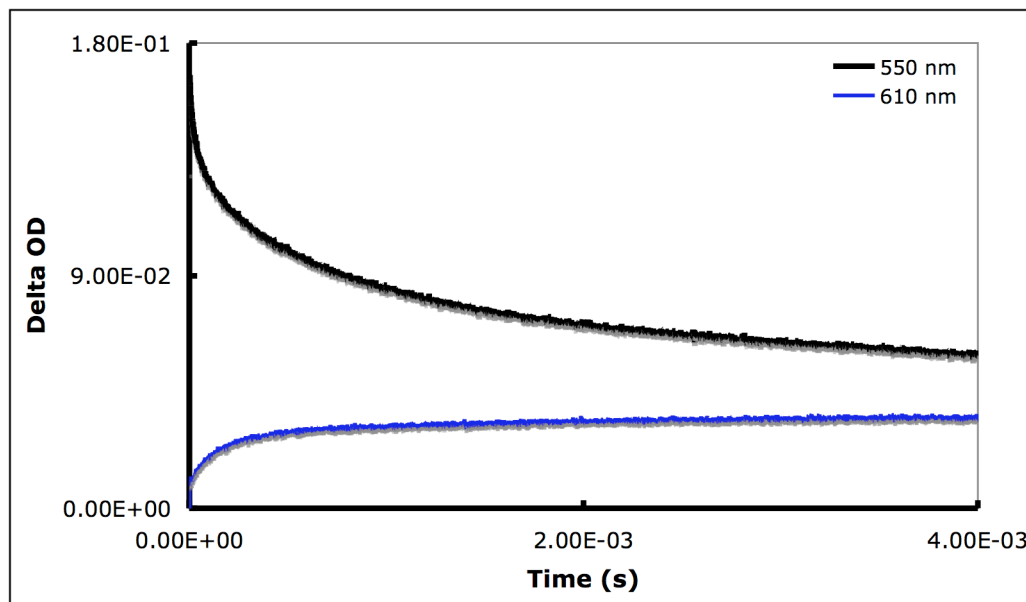


**Figure 4.4.** Selected waveforms from transient absorption spectra of  $3.2/4.4/3.7^{2+}$  in 4.1

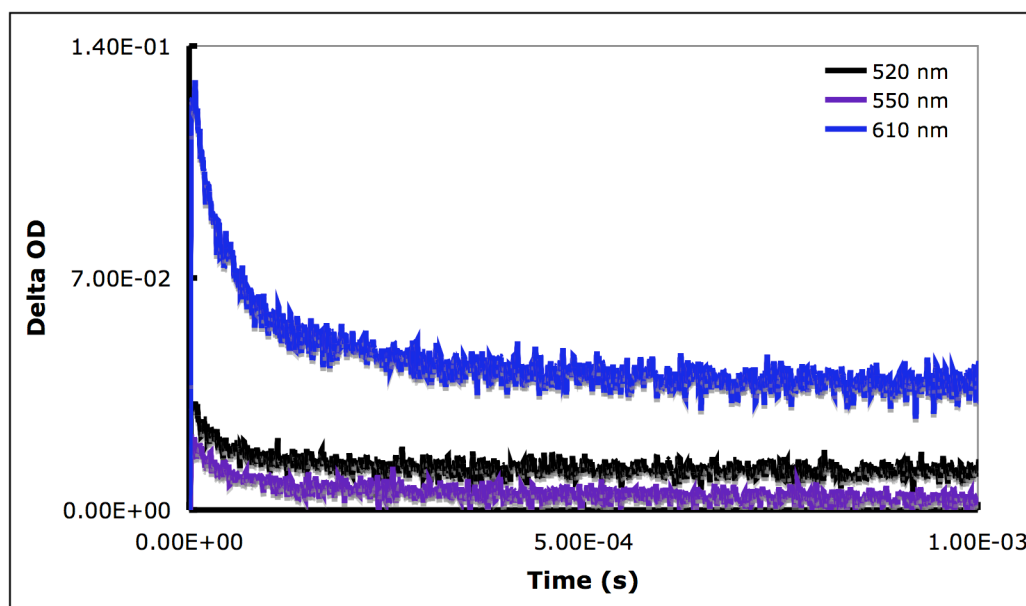


**Figure 4.5.** Selected waveforms transient absorption spectra of  $3.2/4.4/3.7^{2+}$  in 4.2

From a qualitative examination of the flash photolysis data, we find that the pyridinium ILC is an excellent medium with which to facilitate PET. The values for  $k_{\text{BET}}$ ,  $k_{3.72^+}$ ,  $k_{\text{DEC}}$  are derived from five to eight measurements (waveform at 610 nm with varying concentrations of  $3.7^{2+}$ ) from at least two individually prepared samples containing benzophenone and **4.4**. In the imidazolium ILC (entry 4, Table 2.1) one finds that while back electron transfer ( $k_{\text{BET}}$ , equation 9) is very rapid (an undesirable feature) and forward electron transfer to methyl viologen ( $k_{\text{MV}^{2+}}$ , equation 3) is very slow. Quantum yield of cage escape product is moderate and comparable to what is observed in the imidazolium RTIL (entry 2, Table 2.1).

We were able to use Copasi and the following system of equations to solve for the corresponding kinetic data:



From these three equations the following differential equations were derived and used to solve for  $k_{\text{BET}}$ ,  $k_{\text{MV}^{2+}}$ , and  $k_{\text{DEC}}$ :

$$-\frac{dA^{\bullet-}}{dt} = k_{\text{BET}} A^{\bullet-} D^{+\bullet} + k_{\text{MV}^{2+}} A^{\bullet-} P^{2+} \quad (12)$$

$$\frac{dP^{2+}}{dt} = k_{\text{DEC}} P^{+\bullet} D^{+\bullet} - k_{\text{MV}^{2+}} P^{2+} A^{\bullet-} \quad (13)$$

$$\frac{dP^{3+}}{dt} = k_{MV^{2+}} P^{2+} A^{-\bullet} - k_{DEC} P^{3+} D^{+\bullet} \quad (14)$$

The concentration of  $3.2^{\bullet}$  was approximated by obtaining the waveform at the  $\lambda_{\max}$  of the  $3.2^{3*}$  and using the molar absorptivity of the  $3.2^{3*}$  at that wavelength ( $\epsilon_{3.2^{3*}} = 5.40 \times 10^3 \text{ g}^{-1} \text{ L cm}^{-1}$  at 525 nm.<sup>79</sup>) Concentration of  $3.7^{+\bullet}$  was easily determined from subsequent addition of a stock solution of  $3.7^{2+}$  to the experiment in progress, and was determined by obtaining the waveform at the  $\lambda_{\max}$  of the  $3.7^{+\bullet}$  and using the molar absorptivity of the  $3.7^{+\bullet}$  at that wavelength ( $\epsilon_{3.7^{+\bullet}} = 10.7 \times 10^4 \text{ g}^{-1} \text{ L cm}^{-1}$  at 610 nm.<sup>109</sup>) Using this information and the experimental data obtained by monitoring the growth and decay of the  $3.7^{+\bullet}$  signal at 610 nm, the three desired second order rate constants,  $k_{BET}$ ,  $k_{MV^{2+}}$ , and  $k_{DEC}$  (in  $\text{M}^{-1} \text{ s}^{-1}$ ) were obtained using the parameter estimation function in Copasi.

**Table 4.1** Rate Constants and Quantum Yields for reactions using **3.2** measured at  $20 \pm 1^\circ \text{C}$ .

Entry	Phase Transition Temp <sup>a</sup>		Mediator	$\Phi_{MV^{+\bullet}}$	$k_{BET}$	$k_{MV^{2+}}$	$k_{DEC}$
	Solvent	116,117					
1	CH <sub>3</sub> CN	I	<b>3.2</b>	0.7	4.74E+10 <sup>b</sup>	1.42E+10 <sup>b</sup>	5.18E+09 <sup>b</sup>
2	<b>3.8</b>	I	<b>3.2</b>	0.85	1.00E+08 <sup>b</sup>	2.10E+08 <sup>c</sup>	1.50E+08 <sup>b</sup>
3	<b>3.1</b>	I	<b>3.2</b>	0.89	1.03E+09 <sup>b</sup>	1.00E+09 <sup>c</sup>	1.20E+08 <sup>b</sup>
4	<b>4.1</b>	Cr $\xrightleftharpoons[-20]{-8.4}$ SmA $\xrightleftharpoons[182.5]{184.5}$ I	<b>3.2</b>	0.75	3.87E+09 <sup>b</sup>	1.46E+07 <sup>c</sup>	1.03E+06 <sup>b</sup>
5	<b>4.2</b>	Cr $\xrightarrow{-24}$ SmA $\xrightarrow{152}$ I	<b>3.2</b>	0.98	1.17E+07 <sup>b</sup>	1.20E+09 <sup>c</sup>	1.14E+07 <sup>b</sup>

<sup>a</sup>. units are  $^\circ\text{C}$  <sup>b</sup>. units are  $\text{M}^{-1} \text{ s}^{-1}$  <sup>c</sup>. determined from equation 7 <sup>d</sup>. units are  $\text{s}^{-1}$  <sup>e</sup>.

$3.7^{+\bullet}$  signal in imidazolium LC using **4.3** was not appreciable enough to differentiate from noise and determine a value for  $\Phi_{3.7^{+\bullet}}$ .

From Copasi, we find that **4.2** is an excellent medium with which to facilitate PET. The values for  $k_{\text{BET}}$ ,  $k_{\text{MV}^{2+}}$ ,  $k_{\text{DEC}}$  are derived from five to eight measurements (waveform at 610 nm with varying concentrations of methyl viologen) from at least two individually prepared samples containing benzophenone and **4.4**. In **4.1** (entry 8, Table X) one finds that while back electron transfer ( $k_{\text{BET}}$ ) is very rapid ( $3.87 \times 10^9 \text{ M}^{-1} \text{ s}^{-1}$ .) Electron transfer to methyl viologen ( $k_{\text{MV}^{2+}}$ ) is very slow ( $1.46 \times 10^7 \text{ M}^{-1} \text{ s}^{-1}$ ) and  $\Phi_{3.7^+}$  (0.75) and comparable to what is observed in 3.8 (entry 4.) These results make sense in the context of previous experiments that demonstrate that the anisotropic nature of LCs can decrease rates of PET. As **4.1** cannot facilitate solvent mediated PET, all electron transfer events must occur under a diffusive pathway. The SmA mesophase of **4.1** therefore hinders successful electron transfer to  $3.7^{2+}$  and promotes rapid back electron transfer due to poor solvent cage escape of the radical ions.

The results obtained using **4.2** are quite remarkable. First, back electron transfer ( $k_{\text{BET}}$ ) is extremely slow,  $1.17 \times 10^7 \text{ M}^{-1} \text{ s}^{-1}$ , especially in comparison to what was observed with ImidC<sub>12</sub>C<sub>11</sub>OH and the RTILs including **3.1** which can facilitate solvent mediated PET. Forward electron transfer ( $k_{\text{MV}^{2+}}$ ) is  $1.20 \times 10^9 \text{ M}^{-1} \text{ s}^{-1}$  and is it is the most rapid rate of forward electron transfer that we have observed using ionic media. Finally, the value of  $\Phi_{\text{MV}^+}$  is quite high, 0.98, approaching unity. Both the rapid  $k_{3.72^+}$  and  $\Phi_{\text{MV}^+}$  would suggest that despite its nearly solid nature, **4.2** can easily facilitate solvent mediated PET and is an excellent medium with which to carry out PET reactions.

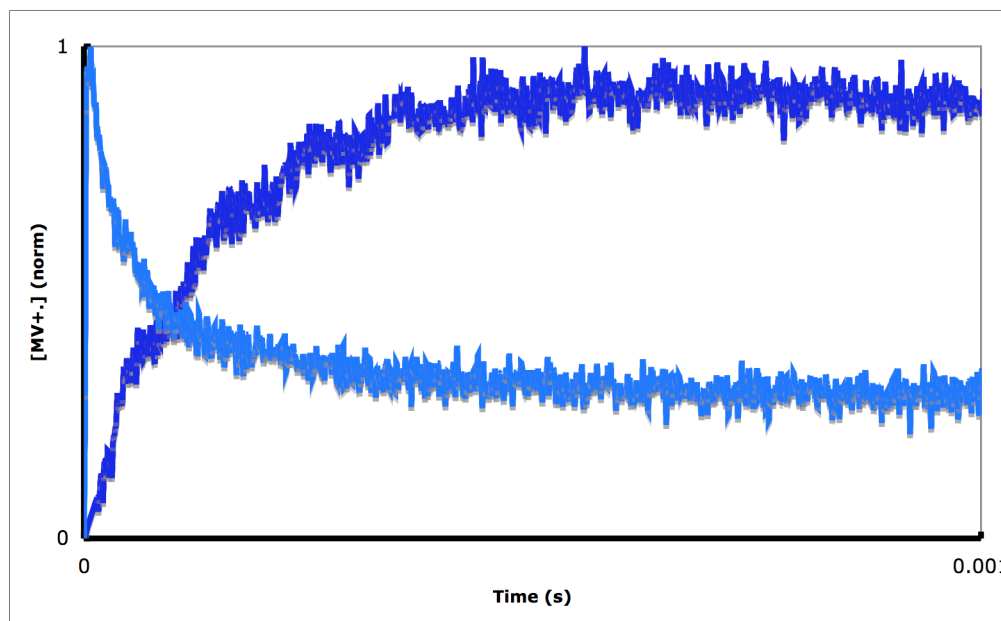


**Figure 4.6.** Waveform at 610 nm ( $3.7^{ps}$ ) in imidazolium ILC ( $\bullet$ ) and pyridinium ILC

( $\bullet$ )

### 3.2.2 532 nm Laser Flash Photolysis.



In addition to the work performed using benzophenone, we also wanted to use a chromophore for our PET experiments that a.) absorbed light in the visible region ( $\lambda_{ex} = 532 \text{ nm}$ ) b.) went through the singlet state instead of the triplet state and c.) had the correct oxidation potential to allow for solvent mediated PET. We desired a chromophore that absorbed in the visible region as we felt that this would better mimic a prototypical solar cell environment. We choose a singlet system because

back electron transfer is not spin forbidden (unlike the triplet system) thus electron transfer more energetically favorable which leads to the generation of a significantly lower yield of cage escape ion radical products ( $\Phi_{MV^+}$ ).

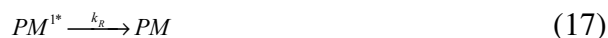
Pyrrromethene dyes are a class of high wavelength absorbing, robust compounds that are generally used as laser dyes. The pyrrromethene dye (**4.3**, Chart 4.1) we chose to use has previously been synthesized and characterized. It has a  $\lambda_{\text{max}}$  of 523 nm, is highly fluorescent and has an  $E_{\text{red}}$  of 0.95 V.<sup>122</sup> With this chromophore we were able to use it directly as an excited state donor with methyl viologen, instead of a relay manner, as described for case of benzophenone.

Unfortunately, there are some limitations inherent to using a pyrrromethene dye in electron transfer chemistry. In the case of some pyrrromethene dyes, the fluorescence intensity of the dye is highly solvent dependent.<sup>122,123</sup> This was a phenomenon that we experienced using our **4.3** dye. We found that in the non-polar solvent  $\text{CH}_2\text{Cl}_2$ , qualitatively and quantitatively, the fluorescence intensity of a sample was high, while a sample of the same concentration in a more polar solvent ( $\text{CH}_3\text{CN}$  and some of the RTILs) had lower fluorescence intensity. This may be a problem when monitoring rates of electron transfer via fluorescence measurements (i.e.: Stern-Volmer analysis) however for laser flash photolysis studies, this feature proves less of a burden.

Additionally, some pyrromethene dyes are known to have triplet states that can also be generated upon direct excitation of the dye. It was determined that triplet state low quantum yield of formation ( $\Phi_{\text{triplet}} < 0.03$ ) and thus a low contribution to the photochemistry that occurs with PM dyes.<sup>124</sup> While the triplet state has been characterized for PM 567, it has not been previously characterized for the PM dye we chose use. During the LFP experiments we were able to detect a small quantity of **4.3**<sup>\*3</sup> (at  $\sim 440$  nm) in some of the solvents used (CH<sub>3</sub>CN and as well as some of the ILs used) but chose to disregard it due to precedent of overall low **4.3**<sup>\*3</sup> contribution as compared to **4.3**<sup>\*1</sup> contribution.

We did obtain full transient spectra of the PM dye in each solvent before performing the kinetics measurements. However, we found that the large bleach due to dye fluorescence at 520-540 nm obscured any other additional transient species generated due chemistry that might be occurring between the dye and the solvent. Despite this we decided to continue on with the kinetics measurements. The values for  $\Phi_{3,7+}$  were determined from at least three individual runs measuring the  $\Delta\text{OD}$  at 610 nm under conditions of methyl viologen saturation. These values were then converted to concentration using the molar absorptivity of methyl viologen and the overall  $\Phi_{3,7+}$  was then determine using ZnTPP as an actinometer.<sup>79</sup>

Additionally, we were able to use Copasi and the following equations to determine the following kinetic data:





From these three equations the following differential equations were derived and used to solve for  $k_R$ ,  $k_{MV^{2+}}$ , and  $k_{DEC}$ :

$$-\frac{dPM^{1*}}{dt} = k_R PM^{1*} + k_{MV^{2+}} PM^{1*} P^{2+} \quad (20)$$

$$\frac{dP^{2+}}{dt} = k_{DEC} P^{+\bullet} - k_{MV^{2+}} P^{2+} PM^{1*} \quad (21)$$

$$\frac{dP^{+\bullet}}{dt} = k_{MV^{2+}} P^{2+} PM^{1*} - k_{DEC} P^{+\bullet} \quad (22)$$

We find that while  $k_{3,72+}$  is slow for the direct PET system in all of the molecular and ionic solvents,  $k_{3,72+}$  in **4.2** is rapid ( $5.65 \times 10^9 \text{ M}^{-1} \text{ s}^{-1}$ ) and that  $\Phi_{3,7+}$  is very efficient (0.98.) The  $k_{3,72+}$  in **4.2** is almost two orders of magnitude higher than in all of the other solvents, including **3.1**. (We expected rapid rates of PET in **3.1** as this solvent can facilitate solvent mediated electron transfer. However, as  $\Phi_{3,7+}$  is also low, 0.29, we hypothesis that in this case ET occurs through a diffusive pathway rather than a solvent mediated pathway.) High values for  $\Phi_{3,7+}$  in the pyridinium ILC suggest that this is an excellent media with which to perform PET with **4.3** dyes. In this the anisotropic environment of **4.2** promotes rapid and efficient electron transfer as this ILC is capable of facilitating solvent mediated PET.

**Table 4.2.** Rate Constants and Quantum Yields for all PET Reactions (measured at  $20 \pm 1^\circ \text{C}$ )

Entry	Solvent	Phase Transition Temp <sup>a</sup> 116,117	Mediator	$\Phi_{MV^+}$	$k_{\text{BET}}/k_r^c$	$k_{3.72^+}$	$k_{\text{DEC}}$
1	CH <sub>3</sub> CN	I	<b>3.2</b>	0.7	4.74E+10 <sup>b</sup>	1.42E+10 <sup>b</sup>	5.18E+09 <sup>b</sup>
2	CH <sub>3</sub> CN	I	<b>4.3</b>	0	-	-	-
3	CH <sub>2</sub> Cl <sub>2</sub>	I	<b>4.3</b>	0.18	1.00E+06 <sup>d</sup>	9.13E+07 <sup>b</sup>	1.20E+04 <sup>d</sup>
4	<b>3.8</b>	I	<b>3.2</b>	0.85	1.00E+08 <sup>b</sup>	2.10E+08 <sup>b</sup>	1.50E+08 <sup>b</sup>
5	<b>3.8</b>	I	<b>4.3</b>	0.39	1.83E+06 <sup>d</sup>	2.98E+07 <sup>b</sup>	330 <sup>d</sup>
6	<b>3.1</b>	I	<b>3.2</b>	0.89	1.03E+09 <sup>b</sup>	1.00E+09 <sup>b</sup>	1.20E+08 <sup>b</sup>
7	<b>3.1</b>	I	<b>4.3</b>	0.29	8.22E+04 <sup>d</sup>	3.18E+07 <sup>b</sup>	522 <sup>d</sup>
8	<b>4.1</b>	Cr $\xrightleftharpoons[<-20]{-8.4}$ SmA $\xrightleftharpoons[182.5]{184.5}$ I	<b>3.2</b>	0.75	3.87E+09 <sup>b</sup>	1.46E+07 <sup>b</sup>	1.03E+06 <sup>b</sup>
9	<b>4.1</b>	Cr $\xrightleftharpoons[<-20]{-8.4}$ SmA $\xrightleftharpoons[182.5]{184.5}$ I	<b>4.3</b>	0.00 <sup>b</sup>	-	-	-
10	<b>4.2</b>	Cr $\xrightarrow{-24}$ SmA $\xrightarrow{152}$ I	<b>3.2</b>	0.98	1.17E+07 <sup>b</sup>	1.20E+09 <sup>b</sup>	1.14E+07 <sup>b</sup>
11	<b>4.2</b>	Cr $\xrightarrow{-24}$ SmA $\xrightarrow{152}$ I	<b>4.3</b>	0.98	2.77E+07 <sup>d</sup>	5.65E+09 <sup>b</sup>	211 <sup>d</sup>

<sup>a</sup>. units are °C <sup>b</sup>. units are M<sup>-1</sup> s<sup>-1</sup> <sup>c</sup>. see equations 17-22 <sup>d</sup>. units are s<sup>-1</sup> <sup>e</sup>. **3.7<sup>+</sup>** signal in

imidazolium LC using **4.3** was not appreciable enough to differentiate from noise and

determine a value for  $\Phi_{MV^+}$ .

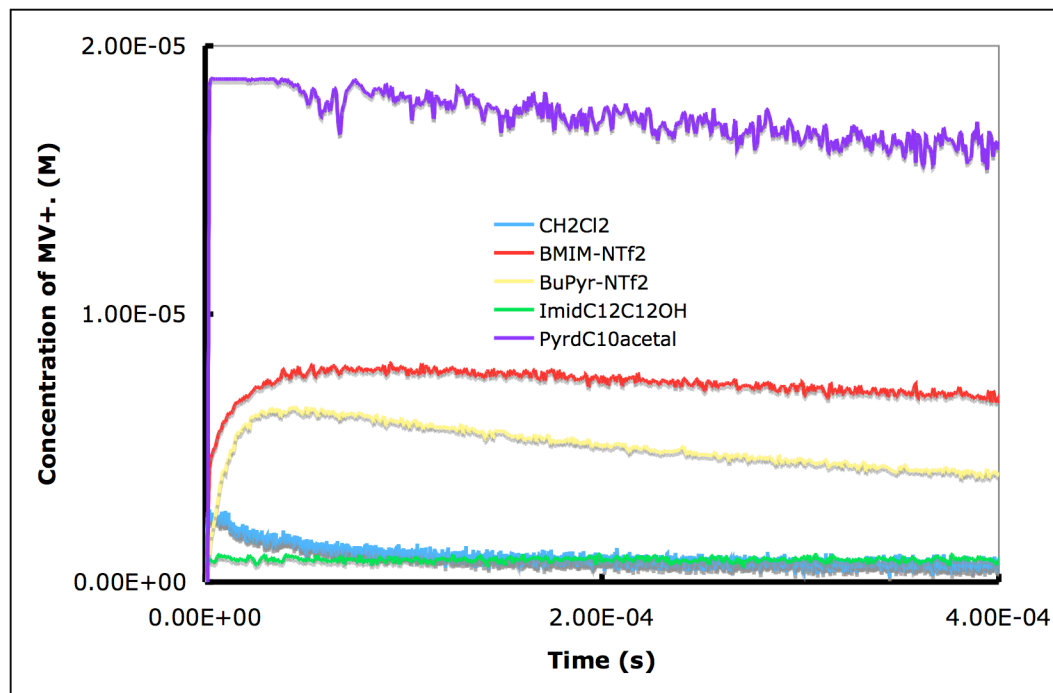


**Figure 4.7.** Waveforms at 610 nm for  $4.3/3.7^{2+}$  in various solvents.

### 4.3 Conclusions

From the flash photolysis data obtained indicates that the ionic liquid crystal **4.2** is an excellent solvent in which to do PET reactions. Rapid rates of  $k_{3,7^{2+}}$  and high  $\Phi_{3,7^{2+}}$  indicate that **4.2** is a medium which can easily facilitate a solvent mediated pathway for PET. Furthermore, given the anisotropic environment of **4.2**, we hypothesize that the mechanism of solvent mediation is occurring through a hopping pathway whereby the electron easily moves from one solvent cation to another without any additional diffusive processes occurring. This hypothesis is being further tested in our lab with the use of ILCs in the  $Col_H$  mesophase, which is more highly ordered than SmA.

## Chapter 5: Conclusions

The layman's paragraph: "This research involves the study of photoinduced electron transfer (PET) in ionic media which focuses on the use of ionic liquid and ionic liquid crystals as solvents in PET reactions as a means to improve various charge separation processes. Whereas many liquids such as water and alcohol are neutral and possess no charge, ionic liquids consist of a positively charged and negatively charged group. Photoinduced electron transfer is a major step in photosynthesis. The harvesting of light into energy, which is the goal of photosynthesis, is also a major working principle of solar cells, which are attractive conduits for renewable energy. We envision that the ionic materials we are studying, given their innate charged nature, will aid in the design and construction of more efficient solar cells."

RTILs are, perhaps, the first novel class of liquids to be conceived in the past 100 years. This fact coupled with unique properties of these new liquids (e.g. innate charged character, high thermostability, viscosity, low vapor pressure) mandates further study of this unique class of materials. While interest in RTILs as environmentally benign solvents for small scale and industrial scale synthesis was the most popular area of study, an effort that is still amazingly topical and impacting, the research field involving RTILs has broadened much beyond green chemistry.

Photoinduced electron transfer (PET) is a process that is important from everything to the common Xerox machine to lithographic processes and

photosynthesis. Given the fact that solar energy conversion and solar cells seek to mimic natural photosynthesis, understanding and manipulating these PET reactions are an integral part of the design and construction of solar cells. Specifically, improving the ability to harvest charge generate in a PET reaction is a fundamental step in understanding and improving the efficiencies of solar cells.

This dissertation has focused on using RTILs and the more highly ordered ILCs as media for PET reactions. We were able to demonstrate that while RTILs are highly viscous, there is the possibility for PET reactions to occur in RTILs at rates faster than one might predict given those viscosities. However, the discreet anionic and cationic portion of the RTILs may not interact with the charged intermediates as strongly as we initially predicted. More importantly, we were able to demonstrate that some RTILs and ILCs can act a charge shuttle during PET reactions, helping to improve rates of PET and most notably, yields of product generate via the charge harvesting process.

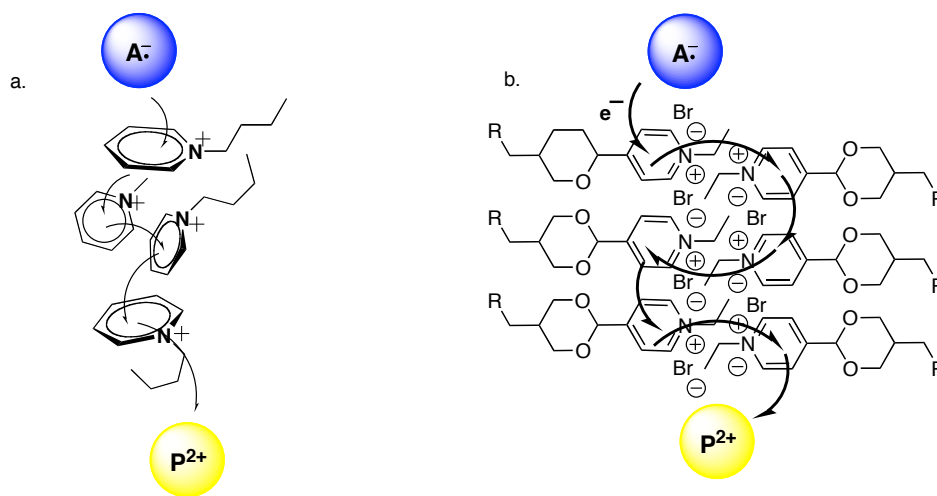


**Figure 5.1** An RTIL (a.) and ILC (b.) acting as charge shuttles in a PET reaction.

While these results have a huge impact on the future of RTILs and ILCs as potential components of solar cells, it is important to understand that they are the initial steps in a long chain of investigation. The fundamental research described herein helps elucidate the most basic and manageable PET reactions. These are not always analogous to the more sophisticated systems employed in solar cell fabrication.

Additionally, there are still many questions to be answered about the mechanism of solvent cation reduction during the PET process. The frequency of this solvent reduction process as it occurs during the course of PET and subsequent ET steps, along with the knowledge of how robust the solvent is to these reduction processes will have to be determined before RTILs and ILCs can be employed in solar cells. These studies are important ones, as the solvent used in this application should be able to shoulder the burden of an infinite number of PET reactions before degrading.

In conclusion, the results presented within this dissertation provide an excellent and substantial first step in understanding how ionic media can be employed to improve the harvesting of light into energy. These results suggest that while there are potential future applications for RTILs and ILCs as components of commercial solar cells, there is much work that needs to be done before this can come to fruition.

## Chapter 6: Experimental

### 6.1 General Experimental Information

All NMR experiments ( $^1\text{H}$ ,  $^{13}\text{C}$ ,  $^{31}\text{P}$  and 2D experiments) were performed on a Bruker 400 MHz NMR spectrometer. Chemical shifts ( $\delta$ ) are reported in ppm and coupling constants ( $J$ ) are reported in hertz (Hz.) Melting points were determined on a MelTemp melting point apparatus and are recorded in degrees Celsius ( $^{\circ}\text{C}$ .) Ultraviolet-visible spectra were recorded on a Perkin-Elmer Lambda 2S spectrophotometer. Column chromatography was performed using Silicycle SiliaFlash P60 silica. TLC plates were obtained from EMD Merck. Chemicals were obtained from Acros or other standard sources. Dry THF, DMF and  $\text{CH}_2\text{Cl}_2$  were obtained from a solvent purification system. Acetonitrile was distilled from calcium hydride under a  $\text{N}_2$  atmosphere. All other solvents and reagents were used as received. To prevent excess water from being absorbed by the RTILs, all samples and bulk solvent was purged with  $\text{N}_2$  and then stored under vacuum before use. Acetonitrile was distilled from calcium hydride under a  $\text{N}_2$  atmosphere.

### 6.2 Lifetime Measurements

Fluorescence lifetime measurements were made using time correlated single photon counting spectrometer (TCSPC). Fluorescence lifetime decays were collected using a home-built TCSPC spectrometer operated in reverse mode to avoid false start signals and capable of resolving lifetime components as short as 20 ps with

deconvolution of the instrument response function. The excitation source for this instrument was a mode-locked titanium sapphire laser with a repetition rate of 80 MHz and a tunable range from 920-710 nm (Wideband Mai Tai, Newport Corp.). A transverse field electro-optic modulator (Model 350-160, Conoptics) was used to reduce the excitation rate to 11.4 MHz. A beam splitter directed a portion of the excitation beam to a high speed photodiode (Model DET210, Thorlabs) the pulse passed through a nanosecond delay (Model 425A, Ortec) and a constant fraction discriminator (Model 935 Quad CFD, Ortec) to provide the stop pulse to the time-to-amplitude converter (TAC) (Model 567, Ortec). The remaining excitation light was frequency doubled by a barium borate crystal (Photop Technologies), vertically polarized and filtered to remove the remaining fundamental frequency light. Fluorescence emission was collected at a 90° angle relative to the excitation beam, passed through a linear polarizer oriented at 54.7° from vertical and imaged onto an adjustable slit which is used to insure single photon detection by a microchannel plate photomultiplier tube (MCP-PMT) (R3809U-50 Hamamatsu Photonics). The pulses from the MCP-PMT were passed to a pre-amplifier discriminator (model 9327 Ortec) and provided the start pulse to the TAC (model 567 Ortec). A multichannel analyzer card set in peak height analysis mode sorted the pulses from the TAC into a histogram of arrival times (TRUMP-PCI-8K, Ortec). Count rates for the emission detector were kept to less than 2000 counts per second by adjusting the excitation intensity and detection slit width. Typical instrument response functions have full width at half maximum of 45 ps. All decays were fit to an exponential with the

instrument response function and employing a least-squares fitting procedure using Spectra Solve™ software.

### **6.3 Viscosity Measurements**

The viscosities of the ionic liquids were determined experimentally using an AR2000 Rheometer from TA Instruments. A steady shear rheology test was run using cone and plate geometry with a 40 mm 2 deg steel cone, and was made at room temperature.

### **6.4 Fluorescence Quenching Experiments**

A stock solution of 9,10-dicyanoanthracene (DCA) in the desired RTIL was made such that the absorbance at the excitation wavelength (420 nm) was between 0.1 and 0.2. A 2 mL sample of the stock solution was then transferred into a quartz cuvette. A stock solution of quencher (if quencher was a solid) in RTIL was prepared by dissolving approximately 1 mmol of quencher in 1 mL of RTIL, followed by sonication and use of a vortexer until all of the quencher had dissolved. Neat quencher was added directly to the solution of DCA in the RTIL if the quencher was a liquid. The resulting solution was then degassed with N<sub>2</sub> for 15 minutes to eliminate the presence of dissolved O<sub>2</sub> in the RTIL, and to homogenize the sample. Finally, the solution was allowed to rest until all the bubbles had disappeared from the sample. The initial fluorescence of the stock sample was monitored and then the resulting fluorescence was recorded, this value would be regarded as  $\Phi_0$ . After the subsequent

addition of an aliquot of quencher solution, the fluorescence of the sample was recorded again. Several aliquots of quencher were added to obtain multiple data points, which were then utilized in determining the fluorescence quenching rate constant ( $k_q$ ).

The fluorescence quenching rate constant ( $k_q$ ) was calculated using the Stern-Volmer Equation:

$$\frac{\Phi_o}{\Phi} = 1 + k_q \tau [Q] \quad (1)$$

where  $\Phi_o$  is the fluorescence of the sample without quencher,  $\Phi$  is the fluorescence of the sample in the presence of quencher,  $\tau$  is the fluorescence lifetime of 9,10-dicyanoanthracene, and  $[Q]$  is the concentration of quencher in molarity.  $\tau$  was obtained from TCSPC measurement was determined to be 13 ns in BMIM-PF<sub>6</sub> and 12 ns in **2.2**. By plotting  $[Q]$  vs.  $\Phi_o/\Phi$ , the slope ( $k_q \tau$ ) can be determined, and from this  $k_q$  can easily be calculated. All of the Stern-Volmer plots obtained were linear with an average R<sup>2</sup> value of 0.95, indicating good linearity and Stern-Volmer behavior.

## 6.5 General Procedures for Laser Flash Photolysis Experiments

Laser flash photolysis experiments were performed using a Nd:YAG laser as the pump beam. The laser used was capable of 355 nm or 532 nm pulses between 4-6 ns duration. A 350 MHz digital oscilloscope was used to observe the waveforms. The samples were prepared in either dry acetonitrile or the ionic media such that the

optical density at the excitation wavelength of 355 nm or 532 nm was between 1.5 and 1.7. The samples were placed in 1 cm quartz cuvettes and N<sub>2</sub> purged for 15 min. (Solutions of MV<sup>2+</sup> were made up in the desired solvent such that the concentration of the solution was known.) The acetonitrile solutions were stirred continuously throughout the experiment. The RTIL solutions could not be mixed with a magnetic stir bar due to their viscosity, so these solutions were subject to a gentle, yet constant purge of N<sub>2</sub>, which effectively allowed for mixing of the solution.

The ILC samples were prepared by first dissolving the ILC in minimal amounts of methanol. Then the desired mediator (**3.2** or **4.3**) as well as donor (if needed) was measured out and dissolved in the ILC/methanol mixture. The mixture was then placed in a 1 mL thick walled quartz cuvette, capped with a septum seal cap (NSG Precision Cells) with a disposable syringe needle. The cuvette was then placed in an Airfree drying chamber and connected to the house vacuum. The samples were placed under vacuum (1-2 days) until all of the methanol had evaporated and the samples passed the “inverted vial” test. Methyl viologen was dissolved in a combination of the ILC and methanol, and added to the premade ILC sample in small aliquots. The sample was then vortexed for 30 seconds and allowed to rest until all the bubbles generated by the vortexing had disappeared. At no time during the LFP experiments did the methanol content of the ILC sample exceed 1% by volume of the entire sample. This method ensured that a known concentration of methyl viologen was delivered to the sample, the molecular solvent composition of the sample was

low, and that distribution of methyl viologen was homogeneous through the entire ILC sample.

## 6.6 Data Analysis

### 6.6.1 Methods used in Chapter 2

The method used to fit the fluorescence quenching data obtained from the fluorescence quenching studies was previously reported by Falvey and Scannell.<sup>125</sup> The basic program was an algorithm used to minimize the sum of squares difference of the experimentally obtained data as compared to the theoretical data generated by the fitting program, using a combination of equations 4 and 5 in Chapter 3. The final values were determined from using the value of  $k_{diff}$ ,  $\lambda$ , and  $\Delta G$  as variable parameters. The values that were obtained from the best fit of the data are  $\lambda$ ,  $k_{diff}$  for each of the RTILs.

### 6.6.2 Methods used in Chapter 3

Copasi (Complex Pathway Simulator) is a freeware program designed to model and analyze data from a complex set of reaction conditions. The three equations used to model the reaction conditions are as follows:



From these three equations the following differential equations were derived and used to solve for  $k_{\text{BET}}$ ,  $k_{\text{PROBE}}$ , and  $k_{\text{DEC}}$  :

$$-\frac{dA^{\bullet}}{dt} = k_{\text{BET}} A^{\bullet} D^{+\bullet} + k_{\text{PROBE}} A^{\bullet} P^{2+} \quad (5)$$

$$\frac{dP^{2+}}{dt} = k_{\text{DEC}} P^{2+} D^{+\bullet} - k_{\text{PROBE}} P^{2+} A^{\bullet} \quad (6)$$

$$\frac{dP^{+\bullet}}{dt} = k_{\text{PROBE}} P^{2+} A^{\bullet} - k_{\text{DEC}} P^{+\bullet} D^{+\bullet} \quad (7)$$

The concentration of **3.3<sup>•</sup>** (and subsequently **3.6<sup>+•</sup>**) was directly determined by obtaining the waveform at the  $\lambda_{\text{max}}$  of the **3.3<sup>•</sup>** and using the molar absorptivity of the **3.3<sup>•</sup>** at that wavelength ( $\epsilon_{\text{DQ}\cdot} = 7.10 \times 10^3 \text{ g}^{-1} \text{ L cm}^{-1}$  at 455 nm.) The concentration of **3.2<sup>•</sup>** was approximated by obtaining the waveform at the  $\lambda_{\text{max}}$  of the **3.2<sup>3\*</sup>** and using the molar absorptivity of the **3.2<sup>3\*</sup>** at that wavelength ( $\epsilon_{\text{BP}^*3} = 5.40 \times 10^3 \text{ g}^{-1} \text{ L cm}^{-1}$  at 525 nm.) This approximation is assumed to be valid at high concentrations of **3.6**. The maximum concentration of **3.6** needed to validate this approximation was experimentally determined by adding aliquots of a solution of known concentration of **3.6** to a solution of **3.2** and  $\text{MV}^{2+}$  and observing the subsequent growth of  $\text{MV}^{+\bullet}$ . Maximum concentration of **3.6** was defined to be when the concentration of  $\text{MV}^{+\bullet}$  reached a plateau and no longer increased with additional aliquots of **3.6**. This ideal concentration was found to be  $3 \times 10^{-3} \text{ M}$ .

Concentration of  $\text{MV}^{+\bullet}$  was easily determined from subsequent addition of a stock solution of  $\text{MV}^{2+}$  to the experiment in progress, and was determined by

obtaining the waveform at the  $\lambda_{\text{max}}$  of the  $MV^{2+}$  and using the molar absorptivity of the  $MV^{2+}$  at that wavelength ( $\epsilon_{MV^{2+}} = 10.7 \times 10^4 \text{ g}^{-1} \text{ L cm}^{-1}$  at 610 nm). Using this information and the experimental data obtained by monitoring the growth and decay of the  $MV^{2+}$  signal at 610 nm, the three desired second order rate constants,  $k_{\text{BET}}$ ,  $k_{\text{PROBE}}$ , and  $k_{\text{DEC}}$  (in  $\text{M}^{-1} \text{ s}^{-1}$ ) were obtained using the parameter estimation function in Copasi. In the case of **3.2/3.6/MV<sup>2+</sup>** in **2.2**,  $k_{\text{BET}}$  and  $k_{\text{PROBE}}$  were determined by monitoring the growth and decay of **3.2<sup>•</sup>** at 545 nm. This was done due to the overlapping absorbance of the **3.2<sup>•</sup>** and  $MV^{2+}$  species at 610 nm. In cases where the results from fitting did not adequately match the experimental data, further simulation was needed to obtain accurate values for the three rate constants. This was not the case for the experiments performed in acetonitrile, but was done on behalf of the data obtain in either **2.2** or **3.1**.

For the **3.4** systems, due to low solubility of **3.5** in the RTILS,  $\Phi_{\text{SEP}}$  was determined in **2.2** and **3.1** by extrapolation of  $MV^{2+}$  to infinite concentrations using the equation supplied below.

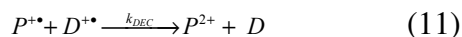
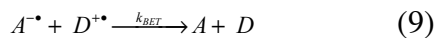
$$\frac{1}{\Phi_{MV^{2+}}} = \frac{1}{\Phi_{A^{\bullet}}} + \frac{1}{\Phi_{A^{\bullet}}} \frac{k_{\text{BET}}}{k_{\text{PROBE}}} \frac{1}{[MV^{2+}]} \quad (8)$$

Additionally, as **3.4<sup>•</sup>** is difficult to detect via laser flash photolysis, the initial concentration of **3.4<sup>•</sup>** was approximated by the initial concentration of **3.5<sup>•</sup>** ( $\epsilon_{\text{HMB}^{2+}} = 3.2 \times 10^4 \text{ g}^{-1} \text{ L cm}^{-1}$  at 498 nm). In cases where the waveform obtained at 610 nm for

the MV<sup>••</sup> species displayed a very short-time scale growth and decay subsequently followed by a long-time scale growth and decay, the short-time scale species was discounted in the simulation and fitting. This was due to the fact that this initial species can be attributed to the growth of the anion radical of the acceptor.

### 6.6.3 Methods used in Chapter 4

We were able to use Copasi and the following system of equations to solve for the corresponding kinetic data:



From these three equations the following differential equations were derived and used to solve for  $k_{BET}$ ,  $k_{PROBE}$ , and  $k_{DEC}$ :

$$-\frac{dA^{\bullet}}{dt} = k_{BET} A^{\bullet} D^{+\bullet} + k_{PROBE} A^{\bullet} P^{2+} \quad (12)$$

$$\frac{dP^{2+}}{dt} = k_{DEC} P^{+\bullet} D^{+\bullet} - k_{PROBE} P^{2+} A^{\bullet} \quad (13)$$

$$\frac{dP^{+\bullet}}{dt} = k_{PROBE} P^{2+} A^{\bullet} - k_{DEC} P^{+\bullet} D^{+\bullet} \quad (14)$$

The concentration of **3.2**<sup>•</sup> was approximated by obtaining the waveform at the  $\lambda_{max}$  of the **3.2**<sup>3\*</sup> and using the molar absorptivity of the **3.2**<sup>3\*</sup> at that wavelength ( $\epsilon_{3.2*3} = 5.40 \times 10^3 \text{ g}^{-1} \text{ L cm}^{-1}$  at 525 nm.) Concentration of **3.7**<sup>••</sup> was easily determined from subsequent addition of a stock solution of **3.7**<sup>2+</sup> to the experiment in progress, and was

determined by obtaining the waveform at the  $\lambda_{\text{max}}$  of the  $3.7^{+\bullet}$  and using the molar absorptivity of the  $3.7^{+\bullet}$  at that wavelength ( $\epsilon_{3.7^{+\bullet}} = 10.7 \times 10^4 \text{ g}^{-1} \text{ L cm}^{-1}$  at 610 nm). Using this information and the experimental data obtained by monitoring the growth and decay of the  $3.7^{+\bullet}$  signal at 610 nm, the three desired second order rate constants,  $k_{\text{BET}}$ ,  $k_{\text{PROBE}}$ , and  $k_{\text{DEC}}$  (in  $\text{M}^{-1} \text{ s}^{-1}$ ) were obtained using the parameter estimation function in Copasi.

For the singlet mediated system, the values for  $\Phi_{3.7^{+\bullet}}$  were determined from at least three individual runs measuring the  $\Delta\text{OD}$  at 610 nm under conditions of methyl viologen saturation. These values were then converted to concentration using the molar absorptivity of methyl viologen and the overall  $\Phi_{3.7^{+\bullet}}$  was then determined using ZnTPP as an actinometer.<sup>79</sup>

Additionally, we were able to use Copasi and the following equations to determine the following kinetic data:



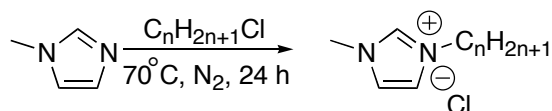
From these three equations the following differential equations were derived and used to solve for  $k_R$ ,  $k_{MV^{2+}}$ , and  $k_{\text{DEC}}$ :

$$-\frac{dPM^{1*}}{dt} = k_R PM^{1*} + k_{MV^{2+}} PM^{1*} P^{2+} \quad (18)$$

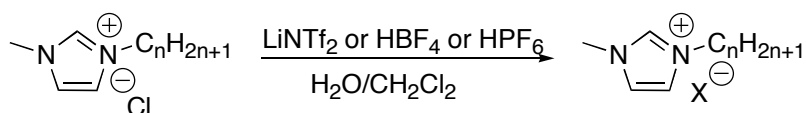
$$\frac{dP^{2+}}{dt} = k_{DEC} P^{2+} - k_{MV^{2+}} P^{2+} PM^{1*} \quad (19)$$

$$\frac{dP^{**}}{dt} = k_{MV^{2+}} P^{2+} PM^{1*} - k_{DEC} P^{**} \quad (20)$$

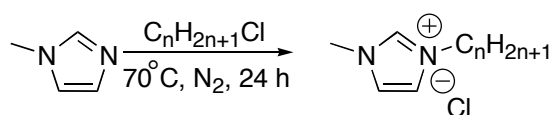
## 6.6 Synthesis



*1-Butyl-3-methylimidazolium chloride (BMIM-Cl)* Freshly distilled *N*-methylimidazole (76.3 mL, 0.957 mol) and *n*-butyl chloride (100 mL, 0.957 mol) were combined in a 250 mL round-bottomed flask equipped with a reflux condenser. The reaction mixture was heated at reflux (70°C) under a N<sub>2</sub> atmosphere for 24 hours, upon which two layers formed. The product (lower layer) was then washed repeatedly with ethyl acetate to remove excess starting material. Full removal of starting material was assured when 1-methylimidazole could no longer be observed in the ethyl acetate extract by UV absorption spectroscopy at 275 nm. The residual ethyl acetate was removed from the product under vacuum pressure affording the white solid BMIM-Cl (66.8 g, 39.9 % yield) <sup>1</sup>H NMR (400 MHz, CD<sub>3</sub>CN) δ: 10.10 (s, 1H), 7.73 (s, 1H) 7.68 (s, 1H) 4.24-4.20 (t, 2H, *J* = 7.2 Hz) 3.89 (s, 3H) 1.80-1.75 (m, 2H, *J* = 7.2 Hz), 1.24-1.20 (m, 2H, *J* = 7.6 Hz) 0.86-0.82 (t, 3H, *J* = 7.2 Hz) ; <sup>13</sup>C NMR (100 MHz, CD<sub>3</sub>CN) δ: 137.9, 128.9, 123.9, 49.3, 36.1, 32.2, 19.4, 13.2.

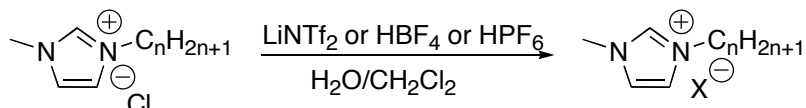


*1-Butyl-3-methylimidazolium hexafluorophosphate* (**2.1**) 1-Butyl-3-methylimidazolium chloride (66.8 g, 0.382 mol) was dissolved in 250 mL of distilled water, to which an equimolar amount of HPF<sub>6</sub> solution (60% wt/wt with water) was added dropwise via cannula to the solution over one hour. The reaction was then stirred for an additional hour, upon which the water insoluble **2.1** had formed in a viscous lower layer in the bottom of the flask. The resulting lower layer was then washed with 450 mL portions of distilled water until the aqueous washings were no longer acidic. The ionic liquid was then washed with equal portions of water, saturated NaHCO<sub>3</sub> solution and again water. The ionic liquid was then dried with stirring, under vacuum pressure for several hours. This yielded the clear, colorless **2.1** (97.2 g, 89.5% yield) <sup>1</sup>H NMR (400 MHz, CD<sub>3</sub>CN) δ: 8.39 (s, 1H), 7.37 (s, 1H) 7.33 (s, 1H), 4.14-4.10 (t, 2H, *J* = 7.2 Hz), 3.82 (s, 3H), 1.83-1.76 (m, 2H, *J* = 7.2 Hz), 1.33-1.27 (m, 2H, *J* = 7.6 Hz), 0.92-0.89 (t, 3H, *J* = 7.6 Hz) ; <sup>13</sup>C NMR (100 MHz, CD<sub>3</sub>CN) δ: 136.3, 124.4, 123.0, 50.1, 36.2, 31.9, 19.3, 13.1.

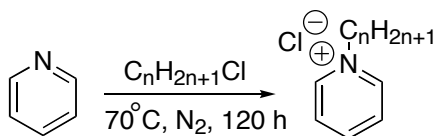


*1-Octyl-3-methylimidazolium chloride* (**OMIM-Cl**) OMIM-Cl was synthesized in the manner previously described for the synthesis of BMIM-Cl. The synthesis yielded the slightly yellow viscous liquid OMIM-Cl in 30.1 % yield (39.5 g, 0.171 mol) <sup>1</sup>H NMR (400 MHz, CD<sub>3</sub>CN, ppm) δ: 10.10 (s, 1H), 7.73 (s, 1H) 7.70 (s, 1H), 4.35-4.31 (t, 2H, *J* = 7.2 Hz), 4.02 (s, 3H), 1.85-1.78 (m, 2H, *J* = 6.8 Hz), 1.39-1.26 (m, 10H) 0.97-

0.93 (t, 3H,  $J = 6.8$  Hz) ;  $^{13}\text{C}$  NMR (100 MHz,  $\text{CD}_3\text{CN}$ , ppm)  $\delta$ : 138.4, 123.9, 122.3, 50.2, 36.7, 32.0, 30.6, 29.4, 29.3, 26.6, 22.9, 14.2.

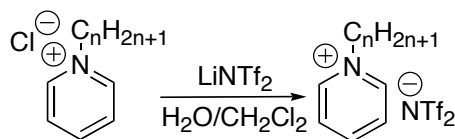


*1-Octyl-3-methylimidazolium hexafluorophosphate (2.2)* **2.2** was synthesized in the manner previously reported for the synthesis of **2.1**, and yielded the clear **2.2** (47.6 g, 0.139 mol, 85.6% yield)  $^1\text{H}$  NMR (400 MHz,  $\text{CH}_3\text{CN}$ , ppm)  $\delta$ : 8.39 (s, 1H), 7.36 (s, 1H) 7.33 (s, 1H), 4.12-4.08 (t, 2H,  $J = 7.6$  Hz), 3.82 (s, 3H), 1.82-1.79 (t, 2H,  $J = 6.8$  Hz), 1.29-1.26 (m, 10H), 0.88-0.85 (t, 3H,  $J = 6.8$  Hz) ;  $^{13}\text{C}$  NMR (100 MHz,  $\text{CD}_3\text{CN}$ , ppm)  $\delta$ : 136.7, 124.5, 123.1, 50.4, 36.6, 32.3, 30.4, 29.6, 29.4, 26.5, 23.2, 14.3.  $^{31}\text{P}$  NMR (161.8 MHz,  $\text{CD}_3\text{CN}$ )  $\delta$ : - 143.6 (septet).  $\eta = 0.65$  Pa s.



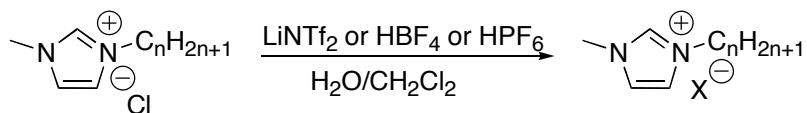
*Butyl pyridinium chloride (BuPyr-Cl)*. Pyridine (2.48 mol, 196.1 g) and n-butyl chloride (2.73 mol, 252.7 g) were added in a 1L round bottom flask equipped with a magnetic stir bar and was allowed to stir under an  $\text{N}_2$  atmosphere at  $70^\circ\text{C}$  for 5 to 7 days. After this time, the resulting white precipitate was isolated via vacuum filtration and recrystallized from a 50/50 ethyl acetate/acetonitrile mixture. (If after the 5-7 days the resulting precipitate contained trace amounts of color, a appropriate amount

of decolorizing carbon was added during the recrystallization process. This measure was satisfactory in removing all colored impurities from the pyridinium salt.) The white, plate-like crystals were isolated and washed with an additional ice cold portion of the recrystallization solvent, and were placed to dry on the vacuum for one hour. The resulting BuPyr-Cl was isolated in 65% yield.  $^1\text{H}$  NMR (400 MHz,  $\text{CDCl}_3$ , ppm) 9.12-9.10 (d, 2H,  $J = 5.7$  Hz), 8.54-8.50 (t, 1H,  $J = 7.6$  Hz), 8.08-8.04 (t, 2H,  $J = 6.8$  Hz), 4.72-4.69 (t, 2H,  $J = 6.8$  Hz), 1.98-1.92 (quintet, 2H), 1.42-1.33 (sextet, 2H), 0.97-0.94 (t, 3H,  $J = 7.6$  Hz).  $\delta$ : ;  $^{13}\text{C}$  NMR (100 MHz,  $\text{CD}_3\text{CN}$ , ppm)  $\delta$ : 13.58, 19.85, 33.75, 62.54, 129.32, 145.34, 146.62.

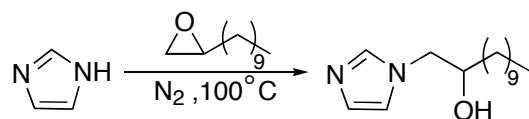


*Butyl pyridinium bis(trifluoromethanesulfonyl)imide (3.1)*. BuPyr-Cl (0.29 mol, 50.0 g) and  $\text{LiNTf}_2$  (0.29 mol, 83.6 g) were dissolved in 100 mL of deionized water and were allowed to stir at room temperature for one hour. This resulted in a biphasic mixture. The desired bottom layer was isolated and washed with several equal volume portions of deionized water. Excess water was removed by drying the ionic liquid under high vacuum at  $50^\circ\text{C}$  for several hours. A silver nitrate test was performed on the RTIL and indicated that a less than 10 ppm of chloride ion impurity existed in the RTIL. This yielded **3.1** in 90% yield.  $^1\text{H}$  NMR (400 MHz,  $\text{CDCl}_3$ , ppm)  $\delta$ : 8.75-8.74 (d, 2H,  $J = 5.6$  Hz), 8.47-8.43 (t, 1H,  $J = 7.6$  Hz), 7.99-7.95 (t, 2H,  $J = 6.8$  Hz), 4.53-4.49 (t, 2H,  $J = 7.6$  Hz), 1.95-1.87 (quintet, 2H), 1.36-1.27 (sextet, 2H),

0.89-0.86 (t, 3H,  $J = 7.5$  Hz).  $^{13}\text{C}$  NMR (100 MHz,  $\text{CD}_3\text{CN}$ , ppm)  $\delta$ : 13.65, 19.83, 33.96, 62.11, 129.15, 145.76, 146.41.  $\eta = 0.06$  Pa s.

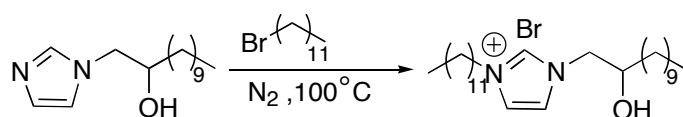


*1-Butyl-3-methylimidazolium bis(trifluoromethanesulfonyl)imide* (**3.8**) BMIM-Cl (0.43 mol, 75.0 g) and  $\text{LiNTf}_2$  (0.43 mol, 123.3 g) were dissolved in 100 mL of deionized water and were allowed to stir at room temperature for one hour. This resulted in a biphasic mixture. The desired bottom layer was isolated and washed with several equal volume portions of deionized water. Excess water was removed by drying the ionic liquid under high vacuum at  $50^\circ\text{C}$  for several hours. A silver nitrate test was performed on the RTIL and indicated that a less than 10 ppm of chloride ion impurity existed in the RTIL.  $^1\text{H}$  NMR (400 MHz,  $\text{CDCl}_3$ )  $\delta$ : 8.63 (s, 1H), 7.43-7.39 (d, 2H,  $J = 16$  Hz), 4.21-4.18 (t, 3H,  $J = 7.6$  Hz), 3.94 (s, 3H), 1.92-1.84 (m, 2H), 1.43-1.34 (m, 2H), 0.98-0.94 (t, 3H,  $J = 7.2$  Hz);  $^{13}\text{C}$  NMR (100 MHz,  $\text{CDCl}_3$ )  $\delta$ : 135.2, 124.2-114.6 (q,  $\text{CF}_3$ ), 123.3, 122.1, 49.3, 35.6, 31.4, 17.9, 10.77.

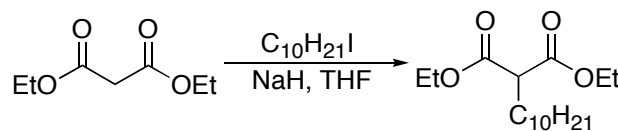


*1-(2-hydroxydodecyl)imidazole*. Imidazole (2.031g, 29.83 mmol) and 1,2-epoxydodecane (5.96 mL, 27.12 mmol) were combined in a 50 mL round bottom flask equipped with a reflux condenser and a  $\text{N}_2$  inlet. The reaction was allowed to stir at  $100^\circ\text{C}$  for 12 hours. After 12 hours, the now yellow viscous reaction mixture

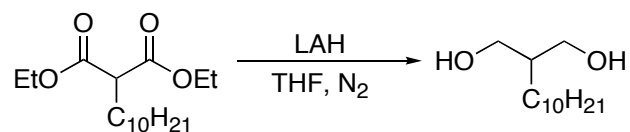
was allowed to cool and then dissolved in 125 mL of CH<sub>2</sub>Cl<sub>2</sub>. This was then washed two times with deionized water. The organic layer was then evaporate to 100 mL, to which hexanes was added. The mixture was then placed in the freezer, and after 12 hours white precipitate had formed. The precipitate was filtered yielding 5.30 g of white waxy solid. <sup>1</sup>H NMR (400 MHz, CDCl<sub>3</sub>) δ: 7.45 (s, 1H), 6.96 (s, 1H), 6.93 (s, 1H), 3.97 (m, 1H), 3.83 (m, 2H), 1.25-1.48 (m, 22H), 0.88 (t, 3H, *J* = 7 Hz)



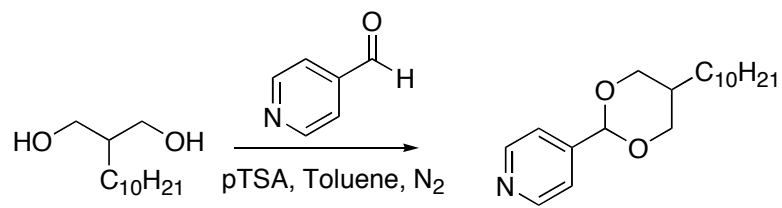
*1-(2-hydroxydodecyl)-3-dodecyl-imidazolium bromide. (4.1)* 1-(2-hydroxydodecyl)imidazole (1 g, 3.961 mmol) and bromododecane (0.958 mL, 3.961 mmol) were combined in a 5 mL round bottom flask equipped with a reflux condenser and a N<sub>2</sub> inlet. The resulting yellow mixture was stirred at 100°C for 12 hours. After cooling, the reaction mixture was dissolved in boiling MeOH to which decolorizing carbon was added. After stirring for 15 minute, the hot mixture was filter over Celite and the solvent evaporated to give a colorless gel like ionic liquid crystal in 90% yield. <sup>1</sup>H NMR (400 MHz, CDCl<sub>3</sub>) δ: 9.78 (s, 1H), 7.39 (s, 1H), 7.24 (s, 1H), 4.40 (m, 2H), 4.25 (m, 2H), 3.98 (m, 1H), 1.92 (m, 2H), 1.56-1.19 (m, 36H), 0.89 (t, 6H, *J* = 7 Hz)



*Diethyl 2-decylmalonate.* Diethyl malonate (9.46 mL, 62.14 mmol) was added via *cannula* to a slurry of NaH (2.858 g, 68.35 mol) in dry THF (100 mL) in a 250 mL round bottom flask fitted with a reflux condenser and a N<sub>2</sub> inlet at 0°C with stirring. The mixture was allowed to stir at 0°C for ten minutes and then at room temperature for one hour. During this time the evolution of H<sub>2</sub> gas was observed. The mixture was then cooled to 0°C and iododecane (20 mL, 93.21 mmol) was added via *cannula* and allowed to stir at 0°C for an hour. The resulting reaction mixture was then warmed to room temperature, during which time precipitate started to form, and stirred at reflux for twelve hours. After twelve hours, the reaction mixture was cooled to room temperature and the THF was stripped from the reaction mixture using rotary evaporation. The resulting viscous liquid was then dissolved in diethyl ether and washed with cold saturated aqueous NH<sub>4</sub>Cl. Aqueous extract was then washed with an equal volume of diethyl ether. The ether layers were then combined and washed with brine. The ether layer was dried (MgSO<sub>4</sub>) and evaporated to yield a light yellow viscous oil. Column chromatography (R<sub>f</sub> = 0.22, 19:1 hexanes/Et<sub>2</sub>O) yielded 13.96 g of clear liquid. <sup>1</sup>H NMR (400 MHz, CDCl<sub>3</sub>) δ: 4.14-4.09 (q, 4H, *J* = 8 Hz), 3.25-3.21 (t, 8H, *J* = 8 Hz), 1.82-1.80 (broad d, 2H, *J* = 8 Hz), 1.23-1.17 (m, 18H), 0.82-0.78 (t, 6H, *J* = 8 Hz); <sup>13</sup>C NMR (100 MHz, CDCl<sub>3</sub>) δ: 170.2, 66.0, 42.0, 32.4, 29.9, 29.8, 29.7, 29.6, 29.1, 27.7, 14.6.

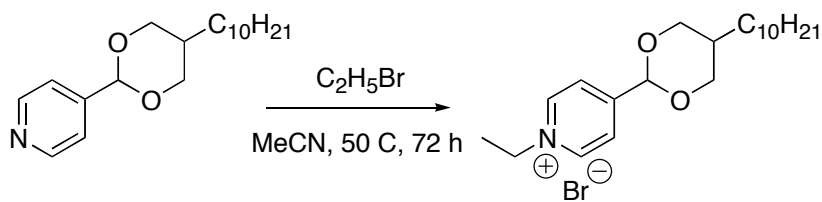


*2-decyl-propane-1,3-diol*. LAH (2.962g, 78.03 mol) was added to dry THF at 0°C. Diethyl 2-decylmalonate (4.686 g, 15.60 mol) was then added dropwise via cannula to the LAH/THF slurry. The reaction mixture was then warmed to room temperature and allowed to reflux for twelve hours. After this time, the reaction mixture was cool to 0°C and diluted with Et<sub>2</sub>O. The reaction was then quenched with 2.5 mL of deionized water, 2.5 mL of saturated aqueous NaOH, and 5 mL of deionized water. After all the LAH had turned into a white salt, MgSO<sub>4</sub> was added, and the reaction mixture was allowed to stir for an hour. The reaction mixture was then filtered over Celite and the solvent evaporated to yield a light yellow solid. Recrystallization from hexanes yielded 2.11 g of a fine white powder, mp 60°C. <sup>1</sup>H NMR (400 MHz, CDCl<sub>3</sub>) δ: 3.81-3.78 (dd, 2H, *J* = 4, 11 Hz), 3.65-3.63 (t, 2H, *J* = 8 Hz), 1.65 (m, 1H), 1.23 (m, 18H), 0.87-0.84 (t, 3H, *J* = 8Hz); <sup>13</sup>C NMR (100 MHz, CDCl<sub>3</sub>) δ: 67.2, 42.4, 32.3, 30.3, 30.0, 29.9, 29.8, 28.1, 27.6, 23.1, 14.5



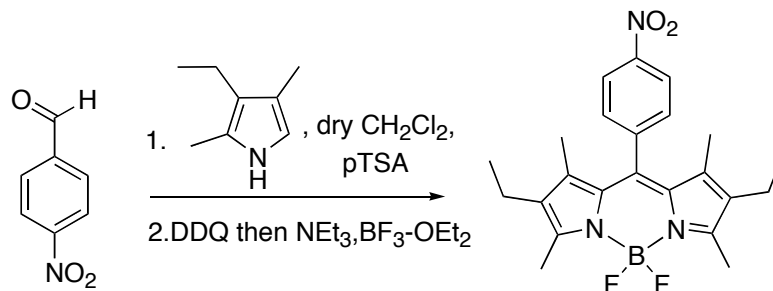
*4-(5-decyl-1,3-dioxan-2-yl)pyridine*. 4-pyridylcarboxaldehyde was freshly distilled via vacuum distillation. This (0.862 mL, 9.21 mmol) was then added to a 100 mL round bottom flask containing the 2-decyl-propane-1,3-diol (1.966g, 9.21 mmol) and pTSA (1.928g, 10.1 mmol) in dry toluene equipped with a Dean-Stark trap and an N<sub>2</sub> inlet. The mixture was then allowed to stir at reflux for 24 hours. After 24 hours, the reaction mixture was cooled to room temperature and washed with cold saturated

aqueous NaHCO<sub>3</sub>. The organic extract was dried (MgSO<sub>4</sub>) and evaporated to yield a light yellow solid. Recrystallization from 1% Et<sub>2</sub>O/Hexanes using decolorizing carbon yielded 2.11g of fluffy white powder, mp 60-61°C. <sup>1</sup>H NMR (400 MHz, CDCl<sub>3</sub>) δ: 8.61-8.59 (d, 2H, *J* = 5.5 Hz), 7.38-7.37 (d, 2H, *J* = 5.5 Hz), 5.37 (s, 1H), 4.25-4.21 (dd, 2H, *J* = 4.6, 11.7 Hz), 3.54-3.48 (t, 2H, *J* = 11.7 Hz), 2.10 (ddd, 1H, *J* = 4.6, 6.7, 11.7 Hz), 1.24 (m, 18H), 1.09-1.07 (d, 2H, *J* = 6.7 Hz), 0.88-0.84 (t, 3H, *J* = 6.7 Hz) ; <sup>13</sup>C NMR (100 MHz, CDCl<sub>3</sub>) δ: 150.1, 146.8, 121.1, 99.7, 72.9, 34.4, 32.1, 29.9, 29.8, 29.7, 29.6, 28.4, 26.5, 22.9, 14.4.



*4-(5-decyl-1,3-dioxan-2-yl-1-ethylpyridinium bromide. (4.2)* 4-(5-decyl-1,3-dioxan-2-yl)pyridine (1.135 g, 3.711 mmol) was dissolved in minimal amounts of dry CH<sub>3</sub>CN in a 50 mL round bottom flask equipped with a reflux condenser and a N<sub>2</sub> gas inlet. To this bromoethane (5.54 mL, 74.22 mmol) was added and the resulting mixture was stirred at 50°C for 72 hours. The reaction mixture was cooled and the solvent evaporated yielding an orange gel like solid. The crude ionic liquid crystal was then purified by reprecipitation by a hexanes/MeOH mixture, followed by addition of decolorizing carbon and heat. This yielded a virtually colorless ionic liquid crystal in 65% yield. <sup>1</sup>H NMR (400 MHz, CDCl<sub>3</sub>) δ: 9.50-9.48 (d, 2H, *J* = 8 Hz), 8.08-8.06 (d, 2H, *J* = 8 Hz), 5.64 (s, 0.3H) and 5.54 (s, 0.7H) due to two conformations of acetal, 5.10-5.05 (d, 2H, *J* = 4 Hz, 8 Hz), 4.25-4.21 (dd, 1.5H, *J* = 4 Hz, 8 Hz), 4.10-4.03

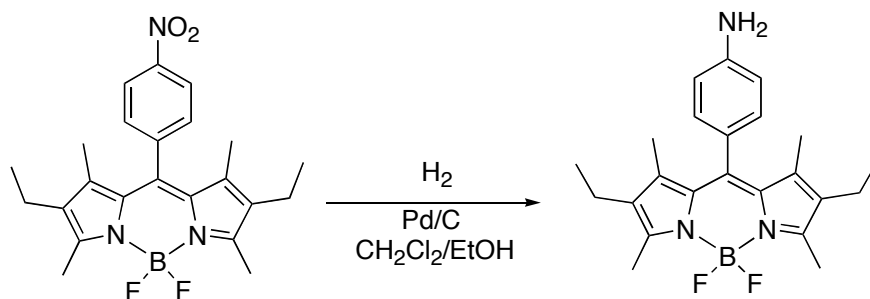
(dd, 1H,  $J = 4$  Hz, 8 Hz), 3.85-3.52 (t, 1.5H,  $J = 8$  Hz), 1.69-1.64 (q, 2H,  $J = 8$  Hz), 1.24 (m, 18H), 1.20 (t, 3H,  $J = 8$  Hz), 0.87-0.83 (t, 3H,  $J = 8$  Hz);  $^{13}\text{C}$  NMR (100 MHz,  $\text{CDCl}_3$ )  $\delta$ : 156.6, 145.2, 126.1, 97.6, 73.1, 71.3, 57.6, 34.5, 34.5, 30.0, 29.9, 29.8, 29.7, 29.6, 28.4, 26.6, 23.1, 14.5.



*8-(4-nitrophenyl)-1,3,5,7-tetramethyl-2,6-diethyl-3a,4a-diaza-s-indacene.* 4-

nitrobenzaldehyde (305.2 mg, 2.02 mmol) and 2,4-dimethyl-3-ethyl-1H-pyrrole (547  $\mu\text{L}$ , 4.05 mmol) were dissolved in dry  $\text{CH}_2\text{Cl}_2$  in a 100 mL round bottom flask equipped with a  $\text{N}_2$  inlet and allowed to stir under a  $\text{N}_2$  atmosphere for 1 hour. After 1 hr, TFA (15  $\mu\text{L}$ ) was added to the reaction mix and the resulting mixture was stirred at room temperature for 3 hours. Then the reaction mixture was washed with saturated aqueous  $\text{NaHCO}_3$ , deionized  $\text{H}_2\text{O}$ , and saturated aqueous  $\text{NaCl}$ . The organic layer was dried ( $\text{MgSO}_4$ ) and the solvent evaporated. The crude residue was then taken up in 5 mL of dry toluene and a slurry of DDQ (458.5 mg in 15 mL of dry toluene) was added to the solution dropwise, upon which the reaction mixture immediately turns purple. After stirring at room temperature for 1.25 hours,  $\text{NEt}_3$  (1.0 mL, 7.18 mmol) was added to the solution. Then after 10 minutes,  $\text{BF}_3\text{-OEt}_2$  (1.02 mL, 8.10 mmol) was added and the solution was allowed to stir for 30 minutes. After 30 minutes, the reaction mixture was subjected to a gentle reflux at  $50^\circ\text{C}$ . The

mixture allowed to stir for 2.5 hours, after which it was cooled and run through a silica plug. Column chromatography ( $R_f = 0.38$ , 1:1 cyclohexane/ $\text{CH}_2\text{Cl}_2$ ) yielded 570 mg of light red orange solid, mp 194-196°C.  $^1\text{H}$  NMR (400 MHz,  $\text{CDCl}_3$ )  $\delta$ : 8.39-8.36 (d, 2H,  $J = 8.8$  Hz), 7.54-7.52 (d, 2H,  $J = 8.8$  Hz), 2.54 (s, 6H), 2.33-2.27 (q, 4H,  $J = 7.6$  Hz), 1.43 (s, 6H), 1.26 (s, 6H), 0.98 (t, 3H,  $J = 7.6$  Hz);  $^{13}\text{C}$  NMR (100 MHz,  $\text{CDCl}_3$ )  $\delta$ : 154.98, 148.3, 142.8, 137.7, 136.9, 133.6, 129.9, 124.6, 78.2, 17.6, 14.9, 13.0, 12.4.



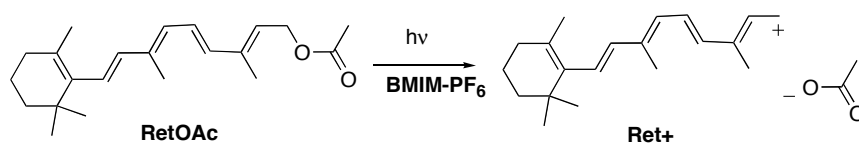
*4,4-Difluoro-8-(4-aminophenyl)-1,3,5,7-tetramethyl-2,6-diethyl-4-bora-3a,4a-diazas-indacene*. (**4.3**) Above (565 mg, 1.2 mmol) was dissolved in 1:1  $\text{CH}_2\text{Cl}_2/\text{EtOH}$  with stirring. The resulting mixture was then allowed to stir under a  $\text{H}_2$  atmosphere for 1 day. After this time the newly formed precipitated was collected and dried. Column chromatography ( $R_f = 0.1$ , 1:1 hexanes/ $\text{CH}_2\text{Cl}_2$  gradient to 100%  $\text{CH}_2\text{Cl}_2$ ) yields 530 mg of deep red powder, decomposes above 250°C.  $^1\text{H}$  NMR (400 MHz,  $\text{CDCl}_3$ )  $\delta$ : 7.02-7.00 (d, 2H,  $J = 8.4$  Hz), 6.79-6.77 (d, 2H,  $J = 8.4$  Hz), 2.52 (s, 3H), 2.33-2.27 (q, 2H,  $J = 8$  Hz), 1.39 (s, 6H), 1.00-0.96 (t, 3H, 8Hz);  $^{13}\text{C}$  NMR (100 MHz,  $\text{CDCl}_3$ ) 153.3, 146.8, 141.2, 138.7, 133.2, 131.5, 129.2, 125.8, 115.6, 17.2, 15.0, 12.9, 12.3

## Appendices

### Appendix I. Laser Flash Photolysis Experiments of Retinyl Acetate in Ionic Liquids.

These experiments were completed as part of a Petroleum Research Fund grant application. Although they were never picked up, these experiments are intriguing and provide a potential platform for a future project. Photolysis of retinyl acetate (RetOAc) produces the retinyl cation (Ret<sup>+</sup>) through photoheterolysis of the C-O bond. The resulting, highly conjugated cation reacts rapidly with water as well as with various anionic nucleophiles (N<sub>3</sub><sup>-</sup>, Cl<sup>-</sup> etc.) with rates that depend on the water content of the co-solvent mixture. Preliminary LFP experiments show that photolysis of RetOAc in **2.1** produces relatively high yields of Ret<sup>+</sup> which has a lifetime of >100 ms. This result would suggest that it would be feasible to use this reaction to examine properties of RTILs. For instance, the relationship between the quantum yield for Ret<sup>+</sup> formation could be studied as a function of the Et values for the RTIL. Additionally, one could determine how the properties of the RTIL correlate with rate constants for trapping of the Ret<sup>+</sup> by various nucleophiles.

#### Scheme 1. Photolysis of RetOAc



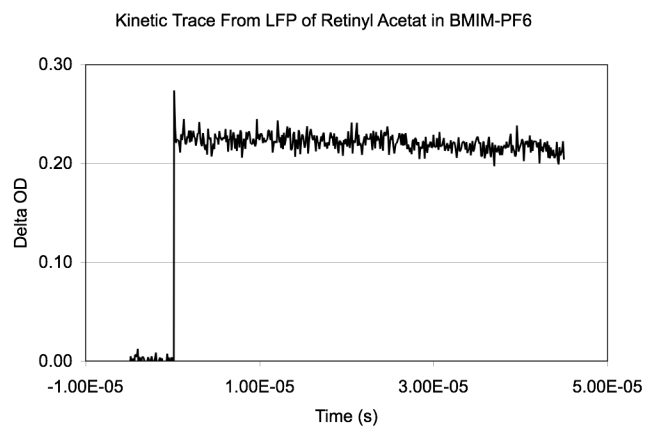


**Figure 1.** Photoheterolysis of Retinyl Acetate in **2.1** and a kinetic waveform from a preliminary experiment.

## Appendix II. Fluorescence Correlation Spectroscopy using Ionic Liquids as Solvents.

These experiments were conducted as collaboration between the Falvey lab and the English lab. The impetus for this project came from paper out of the Baker lab that described a similar experiment.<sup>126</sup> It was our goal to determine if the lipophilicity and molecular weight of the fluorescent probes studied and ionic liquid used would affect the diffusion coefficient of the fluorescent probe. Although this project was never published, it did provide some intriguing data that should be reported.

**Chart 1.** Structures of Fluorescent Dyes Used.

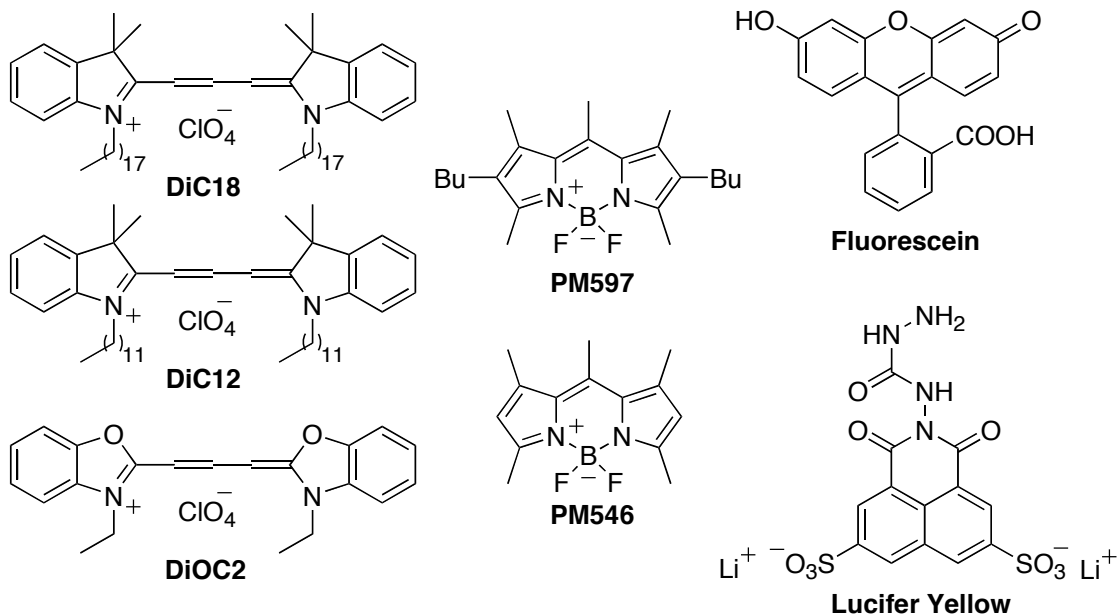


**Table 1.** Results from the FCS Experiments.

<b>Fluorophore</b>	<b>D (<math>\mu\text{m}^2/\text{s}</math>)</b>
DiIC18	1.0
DiIC12	1.4
DiOC2	3.5
PM597	1.7
PM546	3.0
Lucifer Yellow	3.3
Fluorescein	2.14

## Bibliography

- (1) Wasielewski, M. R. *Chem. Rev.* **1992**, *92*, 435-461.
- (2) Tour, J. M. *Acc. Chem. Res.* **2000**, *33*, 791-804.
- (3) Di Ventra, M.; Lang, N. D.; Pantelides, S. T. *ACS Symp. Ser.* **2003**, *844*, 219-229.
- (4) Marcus, R. A. *J. Chem. Phys.* **1956**, *24*, 966-78.
- (5) Marcus, R. A.; Siders, P. *J. Phys. Chem.* **1982**, *86*, 622-30.
- (6) Swiderski, K.; McLean, A.; Gordon, C. M.; Vaughan, D. H. *Chem. Commun. (Cambridge, U. K.)* **2004**, 2178-2179.
- (7) Richoux, M. C.; Neta, P.; Christensen, P. A.; Harriman, A. *J. Chem. Soc., Faraday Trans. 2* **1986**, *82*, 235-49.
- (8) Rehm, D.; Weller, A. *Ber. Bunsenges. Phys. Chem.* **1969**, *73*, 834-9.
- (9) Rehm, D.; Weller, A. *Isr. J. Chem.* **1970**, *8*, 259-71.
- (10) Closs, G. L.; Miller, J. R. *Science (Washington, D. C., 1883-)* **1988**, *240*, 440-7.
- (11) Gould, I. R.; Ege, D.; Moser, J. E.; Farid, S. *J. Am. Chem. Soc.* **1990**, *112*, 4290-301.
- (12) Gould, I. R.; Noukakis, D.; Gomez-Jahn, L.; Goodman, J. L.; Farid, S. *J. Am. Chem. Soc.* **1993**, *115*, 4405-6.
- (13) Gould, I. R.; Farid, S. *Acc. Chem. Res.* **1996**, *29*, 522-528.
- (14) Hurley, F. H.; Wier, T. P. *J. Electrochem. Soc.* **1951**, *98*, 207-212.
- (15) Chum, H. L.; Koch, V. R.; Miller, L. L.; Osteryoung, R. *J. Am. Chem. Soc.* **1975**, *97*.
- (16) Robinson, J.; Osteryoung, R. *J. Am. Chem. Soc.* **1979**, *101*, 323-327.
- (17) Wilkes, J. S.; Levisky, J. A.; Wilson, R. A.; Hussey, C. L. *Inorg. Chem.* **1982**, *21*, 1263-1264.
- (18) Dupont, J.; Consorti, C. S.; Suarez, P. A. Z.; De Souza, R. F.; Dupont, J. *J. Chim. Phys. Phys.-Chim. Biol.* **1998**, *95*, 1626-1639.
- (19) Suarez, P. A. Z.; Einloft, S.; Dullius, J. E. L.; De Souza, R. F.; Dupont, J. *J. Chim. Phys. Phys.-Chim. Biol.* **1998**, *95*, 1626-1639.
- (20) Xu, D. Q.; Liu, B. Y.; Luo, S. P.; Xu, Z. Y.; Shen, Y. C. *Synthesis* **2003**, *17*, 2626-2628.

- (21) Behar, D.; Gonzalez, C.; Neta, P. *J. Phys. Chem. A* **2001**, *105*, 7607-7614.
- (22) Kosmulski, M.; Gustafsson, J.; Rosenholm, J. B. *Thermochim. Acta* **2004**, *412*, 47-53.
- (23) Huddleston, J. G.; Visser, A. E.; Reichert, W. M.; Willauer, H. D.; Broker, G. A.; Rogers, R. D. *Green Chem.* **2001**, *3*, 156-164.
- (24) Xu, W.; Cooper, E. I.; Angell, C. A. *J. Phys. Chem. B* **2003**, *107*, 6170-6178.
- (25) Pringle, J. M.; Golding, J.; Baranyai, K.; Forsyth, C. M.; Deacon, G. B.; Scott, J. L.; MacFarlane, D. R. *New J. Chem.* **2003**, *27*, 1504-1510.
- (26) Dzyuba, S. V.; Bartsch, R. A. *ChemPhysChem* **2002**, *3*, 161-166.
- (27) Carda-Broch, S.; Berthod, A.; Armstrong, D. W. *Anal. Bioanal. Chem.* **2003**, *375*, 191-199.
- (28) McLean, A. J.; Muldoon, M. J.; Gordon, C. M.; Dunkin, I. R. *Chem. Commun. (Cambridge, U. K.)* **2002**, 1880-1881.
- (29) Skrzypczak, A.; Neta, P. *J. Phys. Chem. A* **2003**, *107*, 7800-7803.
- (30) Grodkowski, J.; Neta, P.; Wishart, J. F. *J. Phys. Chem. A* **2003**, *107*, 9794-9799.
- (31) Grodkowski, J.; Neta, P. *J. Phys. Chem. A* **2002**, *106*, 9030-9035.
- (32) Grodkowski, J.; Neta, P. *J. Phys. Chem. A* **2002**, *106*, 11130-11134.
- (33) Carmichael, A. J.; Seddon, K. R. *J. Phys. Org. Chem.* **2000**, *13*, 591-595.
- (34) Fletcher, K. A.; Storey, I. A.; Hendricks, A. E.; Pandey, S.; Pandey, S. *Green Chem.* **2001**, *3*, 210-215.
- (35) Kawai, A.; Hidemori, T.; Kazuhiko, S. *Chem. Lett.* **2004**, *33*, 1464-1465.
- (36) Karmakar, R.; Samanta, A. *J. Phys. Chem. A* **2003**, *107*, 7340-7346.
- (37) Karmakar, R.; Samanta, A. *J. Phys. Chem. A* **2002**, *106*, 6670-6675.
- (38) Karmakar, R.; Samanta, A. *J. Phys. Chem. A* **2002**, *106*, 4447-4452.
- (39) Ingram, J. A.; Moog, R. S.; Ito, N.; Biswas, R.; Maroncelli, M. *J. Phys. Chem. B* **2003**, *107*, 5926-5932.
- (40) Arzhantsev, S.; Ito, N.; Heitz, M.; Maroncelli, M. *Chem. Phys. Lett.* **2003**, *381*, 278-286.
- (41) Arzhantsev, S.; Jin, H.; Ito, N.; Maroncelli, M. *Chem. Phys. Lett.* **2006**, *417*, 524-529.
- (42) Laali, K. K.; Gettwert, V. J. *J. Org. Chem.* **2001**, *66*, 35-40.

- (43) Xie, Y.-Y. *Synth. Commun.* **2005**, *35*, 1741-1746.
- (44) Siddiqui, S. A.; Narkhede, U. C.; Palimkar, S. S.; Daniel, T.; Lahoti, R. J.; Srinivasan, K. V. *Tetrahedron* **2005**, *61*, 3539-3546.
- (45) Shen, Z.-L.; Ji, S.-J.; Loh, T.-P. *Tetrahedron Lett.* **2005**, *46*, 3137-3139.
- (46) Ranu, B. C.; Banerjee, S. *J. Org. Chem.* **2005**, *70*, 4517-4519.
- (47) Lancaster, N. L.; Salter, P. A.; Welton, T.; Young, G. B. *J. Org. Chem.* **2002**, *67*, 8855-8861.
- (48) Chiappe, C.; Pieraccini, D.; Saullo, P. *J. Org. Chem.* **2003**, *68*, 6710-6715.
- (49) Aggarwal, A.; Lancaster, N. L.; Sethi, A. R.; Welton, T. *Green Chem.* **2002**, *4*, 517-520.
- (50) Huddleston, J. G.; Rogers, R. D. *Chem. Commun. (Cambridge)* **1998**, 1765-1766.
- (51) Visser, A. E.; Swatloski, R. P.; Reichert, W. M.; Mayton, R.; Sheff, S.; Wierzbicki, A.; Davis, J. H., Jr.; Rogers, R. D. *Environ. Sci. Technol.* **2002**, *36*, 2523-2529.
- (52) Stalcup, A. M.; Cabovska, B. *J. Liq. Chromatogr. Relat. Technol.* **2004**, *27*, 1443-1459.
- (53) Anderson, J. L.; Armstrong, D. W. *Anal. Chem.* **2003**, *75*, 827-838.
- (54) Buzzeo, M. C.; Evans, R. G.; Compton, R. G. *ChemPhysChem* **2004**, *5*, 1106-1120.
- (55) Binnemans, K. *Chem. Rev.* **2005**, *105*, 4148-4204.
- (56) Yoshio, M.; Kato, T.; Mukai, T.; Yoshizawa, M.; Ohno, H. *Mol. Cryst. Liq. Cryst.* **2004**, *423*, 99.
- (57) Yoshio, M.; Mukai, T.; Ohno, H.; Kato, T. *J. Am. Chem. Soc.* **2004**, *126*, 994.
- (58) Yoshio, M.; Mukai, T.; Kanie, K.; Yoshizawa, M.; Ohno, H.; Kato, T. *Adv. Mater.* **2002**, *14*, 351.
- (59) Hoshino, K.; Yoshio, M.; Mukai, T.; Kishimoto, K.; Ohno, H.; Kato, T. *Polym. Sci. A.* **2003**, 3486.
- (60) Kishimoto, K.; Yoshio, M.; Mukai, T.; Yoshio, M.; Ohno, H.; Kato, T. *J. Am. Chem. Soc.* **2003**, *125*, 3196.

- (61) Lee, C. K.; Huang, H. W.; Lin, I. J. B. *Chem. Commun. (Cambridge, U. K.)* **2000**, 1911.
- (62) Howarth, J.; James, P.; Dai, J. *Tetrahedron Lett.* **2000**, *41*, 10319-10321.
- (63) Marcus, R. A.; Eyring, H. *Annu. Rev. Phys. Chem.* **1964**, *15*, 155-96.
- (64) Behar, D.; Neta, P.; Schultheisz, C. *J. Phys. Chem. A* **2002**, *106*, 3139-3147.
- (65) Grodkowski, J.; Neta, P. *J. Phys. Chem. A* **2002**, *106*, 5468-5473.
- (66) Fletcher, K. A.; Pandey, S.; Storey, I. K.; Hendricks, A. E.; Pandey, S. *Anal. Chim. Acta* **2002**, *453*, 89-96.
- (67) Alvaro, M.; Ferrer, B.; Garcia, H.; Narayana, M. *Chem. Phys. Lett.* **2002**, *362*, 435-440.
- (68) Gordon, C. M.; McLean, A. *Chem. Commun. (Cambridge, U. K.)* **2000**, 1395-1396.
- (69) Marquis, S.; Ferrer, B.; Alvaro, M.; Garcia, H.; Roth, H. *J. Phys. Chem. B* **2006**, *110*, 14956-14960.
- (70) Gordon, C. M.; McLean, A. J.; Muldoon, M. J.; Dunkin, I. R. *ACS Symp. Ser.* **2002**, *818*, 428-443.
- (71) Neta, P.; Behar, D.; Grodkowski, J. *ACS Symp. Ser.* **2003**, *856*, 397-409.
- (72) Seddon, K. R.; Stark, A.; Torres, M.-J. *Pure Appl. Chem.* **2000**, *72*, 2275-2287.
- (73) Paul, A.; Mandal, P. K.; Samanta, A. *Chem. Phys. Lett.* **2005**, *402*, 375-379.
- (74) Paul, A.; Mandal, P. K.; Samanta, A. *J. Phys. Chem. B* **2005**, *109*, 9148-9153.
- (75) Swatloski, R. P.; Holbrey, J. D.; Rogers, R. D. *Green Chem.* **2003**, *5*, 361-363.
- (76) Widegren, J. A.; Laesecke, A.; Magee, J. W. *Chem. Commun. (Cambridge, U. K.)* **2005**, 1610-1612.
- (77) Baker, S. N.; Baker, G. A.; Munson, C. A.; Chen, F.; Bukowski, E. J.; Cartwright, A. N.; Bright, F. V. *Ind. Eng. Chem. Res.* **2003**, *42*, 6457-6463.
- (78) Branco, L. C.; Rosa, J. N.; Ramos, J. J. M.; Afonso, C. A. M. *Chem.--Eur. J.* **2002**, *8*, 3671-3677.
- (79) Murov, S. L.; Carmichael, I.; Hug, G. L. *Handbook of Photochemistry* 2nd ed. ed.; Marcel Dekker Inc.: New York, 1993.
- (80) Eriksen, J.; Lund, H.; Nyvad, A. *Acta Chem. Scand. B.* **1983**, *37*, 59-66.

- (81) Ghoneim, N.; Hammer, C.; Haselbach, E.; Pilloud, D.; Suppan, P.; Jacques, P. *J. Chem. Soc., Faraday Trans.* **1993**, *89*, 4271-3.
- (82) Bart, E.; Meltsin, A.; Huppert, D. *J. Phys. Chem.* **1994**, *98*, 3295-9.
- (83) Bart, E.; Meltsin, A.; Huppert, D. *J. Phys. Chem.* **1994**, *98*, 10819-23.
- (84) Chowdhury, P. K.; Halder, M.; Sanders, L.; Calhoun, T.; Anderson, J. L.; Armstrong, D. W.; Song, X.; Petrich, J. W. *J. Phys. Chem. B* **2004**, *108*, 10245-10255.
- (85) Mandal, P. K.; Samanta, A. *J. Phys. Chem. B* **2005**, *109*, 15172-15177.
- (86) Mandal, P. K.; Paul, A.; Samanta, A. *Res. Chem. Intermed.* **2005**, *31*, 575-583.
- (87) Wang, Y.; Voth, G. A. *J. Am. Chem. Soc.* **2005**, *127*, 12192-12193.
- (88) Canongia Lopes, J. N.; Padua, A. A. H. *J. Phys. Chem. B* **2006**, *110*, 3330-35.
- (89) Wang, Y.; Izvekov, S.; Yan, T.; Voth, G. A. *J. Phys. Chem. B* **2006**, *110*, 3564-3575.
- (90) Gould, I. R.; Young, R. H.; Moody, R. E.; Farid, S. *J. Phys. Chem.* **1991**, *95*, 2068-80.
- (91) DeFranco, J. A.; Schmidt, B. S.; Lipson, M.; Malliaras, G. G. *Organic Electronics* **2006**, *7*, 22-28.
- (92) Lewis, F. D. *Photochem. Photobio.* **2005**, *81*, 65-72.
- (93) Tang, X.; Dmochowski, I. *J. Organic Letters* **2005**, *7*, 279-282.
- (94) Griesbeck, A. G.; Hoffmann, N.; Warzecha, K.-d. *Accounts of Chemical Research* **2007**, *40*, 128-140.
- (95) Marcus, R. A. *J. Chem. Phys.* **1965**, *43*, 2654-2657.
- (96) Wasserscheid, P.; Welton, T. *Ionic Liquids in Synthesis*; Wiley-VCH: Weinheim, 2003.
- (97) Baker, G. A.; Baker, S. N.; Pandey, S.; Bright, F. V. *Analyst* **2005**, *130*, 800-808.
- (98) Vieira, R. C.; Falvey, D. F. *J. Phys. Chem B* **2007**, *111*, 5023-5029.
- (99) Shim, Y.; Kim, H. J. *J. Phys. Chem B* **2007**, *111*, 4510-4519.
- (100) Lynden-Bell, R. M. *J. Phys. Chem B* **2007**, *111*, 10800-10806.
- (101) Lockard, J. V.; Wasielewski, M. R. *J. Phys. Chem B* **2007**.
- (102) Samanta, A. *J. Phys. Chem. B* **2006**, *110*, 13704-13716.
- (103) Paul, A.; Samanta, A. *Journal of Physical Chemistry B* **2007**, *111*, 1957-1962.

- (104) Marcinek, A.; Zielonka, J.; Gebicki, J.; Gordon, C. M.; Dunkin, I. R. *J. Phys. Chem. A* **2001**, *105*, 9305-9309.
- (105) Wishart, J. F.; Neta, P. *J. Phys. Chem. B* **2003**, *107*, 7261-7267.
- (106) Kawano, R.; Wantanabe, M. *Chem. Commun. (Cambridge, U. K.)* **2005**, 2107-2109.
- (107) Wang, P.; Wenger, B.; Humphry-Baker, R.; Moser, J. E.; Teuscher, J.; Kantlehner, W.; Mezger, J.; Stoyanov, E. V.; Zakeeruddin, S. M.; Graetzel, M. *J. Am. Chem. Soc.* **2005**, *127*, 6850-6856.
- (108) Shida, T. *Electronic Absorption Spectra of Radical Ions (Physical Science Data 34)*; Elsevier, 1988.
- (109) Haupl, T.; Lomoth, R.; Hammarstrom, L. *J. Phys. Chem. A* **2003**, *107*, 435-438.
- (110) Rathore, R.; Kochi, J. K. In *Advances in Physical Organic Chemistry*; Tidwell, T. T., Ed.; Academic Press: 2000; Vol. 35, p 193-315.
- (111) Hasharoni, K.; Levanon, H. *J. Phys. Chem.* **1995**, *99*, 4875-4878.
- (112) Berg, A.; Shuali, Z.; Levanon, H.; Wiche, A.; Kurreck, H. *J. Phys. Chem. A* **2001**, *105*, 10060-10064.
- (113) Hasharoni, K.; Levanon, H.; Greenfield, S. R.; Gosztola, D. J.; Svec, W. A.; Wasielewski, M. R. *J. Am. Chem. Soc.* **1996**, *118*, 10228-10235.
- (114) Wiederrecht, G. P.; Svec, W. A.; Wasielewski, M. R. *J. Am. Chem. Soc.* **1997**, *119*, 6199-6200.
- (115) Wiederrecht, G. P.; Svec, W. A.; Wasielewski, M. R. *J. Phys. Chem. B* **1999**, *103*, 1386-1389.
- (116) Sinks, L.; Wasielewski, M. R. *J. Phys. Chem. A* **2003**, *107*, 611-620.
- (117) Sinks, L.; Fuller, M. J.; Liu, W.; Ahrens, M. J.; Wasielewski, M. R. *Chemical Physics* **2005**, *319*, 226-234.
- (118) Chiou, J. Y. Z.; Chen, J. N.; Lei, J. S.; Lin, I. J. B. *J. Mater. Chem.* **2006**, *16*, 2972-2977.
- (119) Haramoto, Y.; Akiyama, Y.; Segawa, R.; Ujiie, S.; Nansawa, M. *J. Mater. Chem.* **1998**, *8*, 275-276.
- (120) Haramoto, Y.; Akiyama, Y.; Segawa, R.; Nansawa, M.; Ujiie, S.; Holmes, A. B. *Bull. Chem. Soc. Jpn.* **1999**, *72*, 875-878.

- (121) Haramoto, Y.; Nansawa, M. *Liquid Crystals* **2001**, *28*, 557-560.
- (122) Ziessel, R.; Bonardi, L.; Retailleau, P.; Ulrich, G. *J. Org. Chem.* **2006**, *2006*, 3093-3102.
- (123) Jones II, G.; Kumar, S.; Klueva, O.; Pacheco, D. *J. Phys. Chem. A* **2003**, *107*, 8429-8434.
- (124) Gorman, A. A.; Hamblett, I.; King, T. A.; Rahn, M. D. *J. Photochem. Photobio. A* **2000**, *130*, 127-132.
- (125) Scannell, M. P.; Fenick, D. J.; Yeh, S.-R.; Falvey, D. E. *J. Am. Chem. Soc.* **1997**, *119*, 1971-1977.
- (126) Werner, J. H.; Baker, S. N.; Baker, G. A. *The Analyst* **2003**, *128*, 786-789.